AD-A150 430 DETERMINATION OF STRUCTURE AND REACTION KINETICS OF EPOXY/AMINE SYSTEMS U.. (U) MCDONNELL DOUGLAS RESEARCH LABS ST LOUIS MO I M BROWN ET AL. 07 OCT 83 MDC-Q1209 1/1

UNCLASSIFIED N00019-82-C-0244 F/G 7/4 NL

END

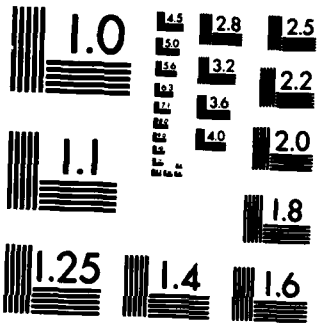

MICROCOPY RESOLUTION TEST CHART
NATIONAL BUREAU OF STANDARDS-1963-A

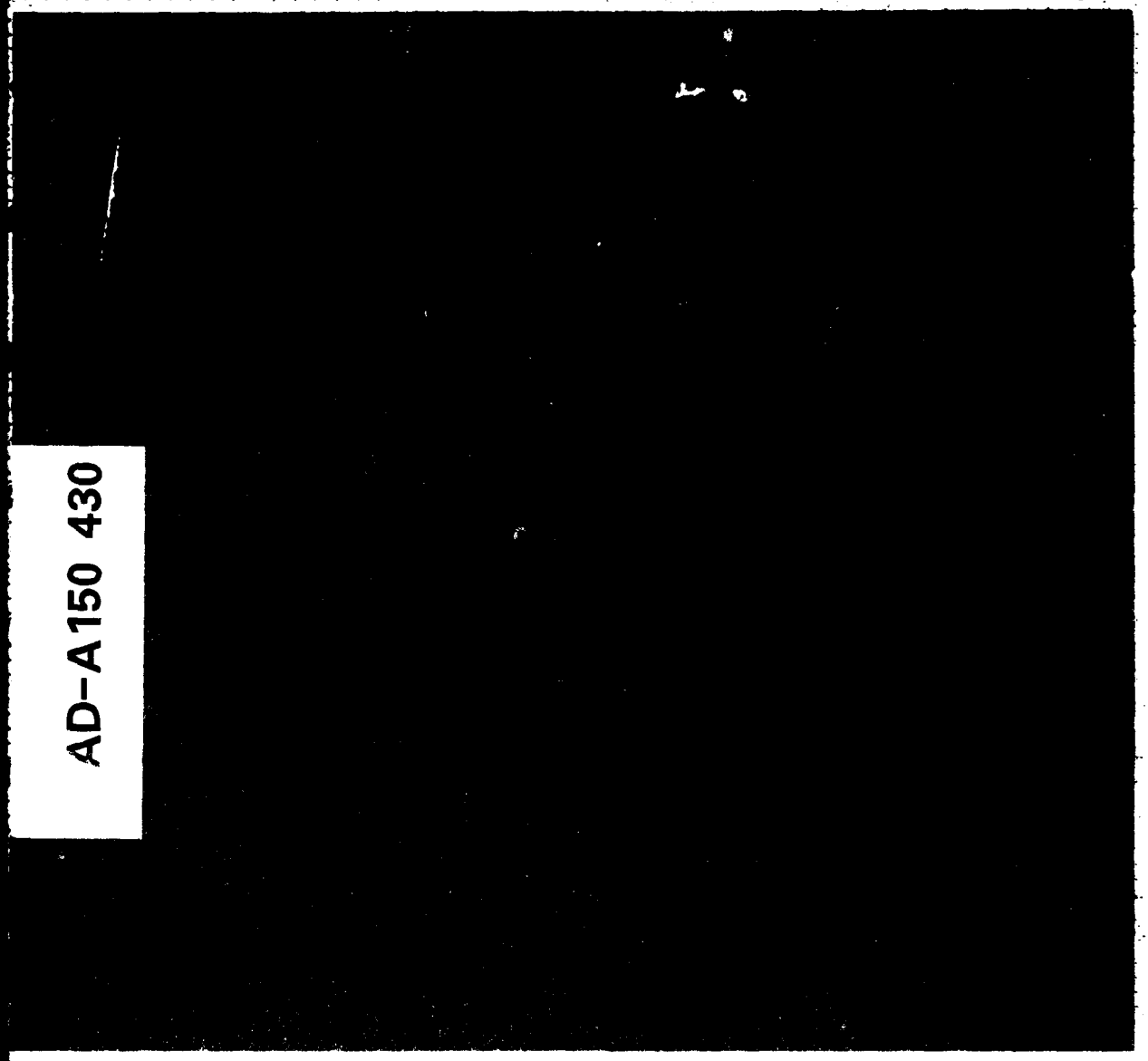

MCDONNELL DOUGLAS RESEARCH LABORATORIES

MCDONNELL DOUGLAS CORPORATION

UNCLASSIFIED

SECURITY CLASSIFICATION OF THIS PAGE

REPORT DOCUMENTATION PAGE

1a. REPORT SECURITY CLASSIFICATION: Unclassified	1b. RESTRICTIVE MARKINGS
2a. SECURITY CLASSIFICATION AUTHORITY	3. DISTRIBUTION/AVAILABILITY OF REPORT: Approved for public release; distribution unlimited
2b. DECLASSIFICATION/DOWNGRADING SCHEDULE	
4. PERFORMING ORGANIZATION REPORT NUMBER(S): MDC Q1209	5. MONITORING ORGANIZATION REPORT NUMBER(S)
6a. NAME OF PERFORMING ORGANIZATION: McDonnell Douglas Research Laboratories; 6b. OFFICE SYMBOL (If applicable)	7a. NAME OF MONITORING ORGANIZATION
6c. ADDRESS (City, State and ZIP Code): P.O. Box 516, St. Louis, MO 63166	7b. ADDRESS (City, State and ZIP Code)
8a. NAME OF FUNDING/SPONSORING ORGANIZATION: Department of the Navy; 8b. OFFICE SYMBOL (If applicable)	9. PROCUREMENT INSTRUMENT IDENTIFICATION NUMBER: N00019-82-C-0244
8c. ADDRESS (City, State and ZIP Code): Naval Air Systems Command, Washington, DC 20361	10. SOURCE OF FUNDING NOS. — PROGRAM ELEMENT NO. / PROJECT NO. / TASK NO. / WORK UNIT NO.
11. TITLE (Include Security Classification) DETERMINATION OF STRUCTURE AND REACTION KINETICS OF EPOXY/AMINE SYSTEMS USING MAGNETIC RESONANCE	
12. PERSONAL AUTHOR(S) Brown, Ian M., Lind, Arthur C., Sandreczki, Thomas C.	
13a. TYPE OF REPORT: Final Report; 13b. TIME COVERED: FROM 82 Jul 9 TO 83 Oct 7; 14. DATE OF REPORT (Yr., Mo., Day): 1983 October 7; 15. PAGE COUNT: 85	
16. SUPPLEMENTARY NOTATION	

17. COSATI CODES		
FIELD	GROUP	SUB. GR.

18. SUBJECT TERMS (Continue on reverse if necessary and identify by block number)
Amines, Spin labels, Nuclear magnetic resonance, Epoxy resins, Reaction kinetics, Glass transition temperature, Spin probes, Electron paramagnetic resonance

19. ABSTRACT (Continue on reverse if necessary and identify by block number)

Electron paramagnetic resonance (EPR) and nuclear magnetic resonance (NMR) were used to investigate: (1) the kinetics of the reactions between amines and epoxies; (2) the dependence of molecular mobility on temperature and crosslink density of the host epoxy matrix; (3) the number of unreacted amine and epoxy functional groups trapped in amine-cured epoxy samples; (4) the measurement of the composition of amine-cured epoxies, and (5) the utility of two-dimensional ^{13}C NMR to characterize slow molecular motion in cured epoxies. In the EPR experiments, stable nitroxide free radicals were used as spin labels and spin probes. The changes in EPR line shapes were used to monitor the rates of formation of the initial addition products in the reactions between the epoxy tetraglycidyl-4,4'-diaminodiphenylmethane

20. DISTRIBUTION/AVAILABILITY OF ABSTRACT: UNCLASSIFIED/UNLIMITED ☒ SAME AS RPT ☐ OTIC USERS ☐	21. ABSTRACT SECURITY CLASSIFICATION: Unclassified
22a. NAME OF RESPONSIBLE INDIVIDUAL	22b. TELEPHONE NUMBER (Include Area Code); 22c. OFFICE SYMBOL

DD FORM 1473, 83 APR — EDITION OF 1 JAN 73 IS OBSOLETE.

UNCLASSIFIED

SECURITY CLASSIFICATION OF THIS PAGE

18. Subject terms (continued)

Motional correlation time, Quaternary amines,
Crosslink density, Relaxation times,
Unreacted groups Free volume

20. Abstract (continued)

(TGDDM) and two model compounds, a secondary amine nitroxide and a tertiary amine nitroxide. The temperature dependence for the rate constants for both reactions (k_1, k_2, respectively) can be written as $k_{1,2} = k_{01,02} \exp(-\Delta E/RT)$, where $k_{01} = 1.3 \times 10^4$ s^{-1} and $\Delta E = 55$ kJ mol^{-1} for the secondary amine; and $k_{02} = 4 \times 10^3$ s^{-1}, $\Delta E = 55$ kJ mol^{-1} at 333 K and $k_{02} = 1.7 \times 10^{-2}$ s^{-1} $\Delta E = 18.5$ kJ mol^{-1} at 373 K for the tertiary amine. The results are tentatively explained in terms of two or more impurities in the resin and a difference in activation entropy, which is the result of steric hindrance around the quaternary nitrogen.

In amine-cured epoxy host matrices at all temperatures, the EPR line shape of the spin probe can be characterized by one value of the rotational correlation time. Above the glass transition temperature of the host matrix, the values of the rotational correlation times depend on the average crosslink density and obey a modified form of the WLF equation. The expression for the temperature dependence of the rotational correlation time contains a contribution from the fractional free volume content (Doolittle term) and one from the explicit temperature dependence (Arrhenius term).

Both unreacted amine groups and unreacted epoxy groups were detected in the same samples of amine-cured TGDDM.

Hydrogen NMR measurements of the spin-spin relaxation times and spin-lattice relaxation times were obtained during the cure of the epoxy MY720 (Ciba Geigy) with the amine Eporal (Ciba Geigy). The activation energy for the curing process appeared to increase from 45 to 55 kJ/mol as the curing proceeded. During most of the cure, two components were observed, one more mobile than the other. The two components were interpreted in terms of the formation of regions having different crosslink densitites.

Solid-state ^{13}C NMR was used to measure the composition of a series of different amine-cured epoxies, and preliminary two-dimensional ^{13}C NMR spectra were obtained to characterize slow molecular motion in cured epoxies. Originator furnished Keywords include:-

PREFACE

This report is an account of the work performed by the McDonnell Douglas Research Laboratories on the Magnetic Resonance Determination of Structure and Reaction Kinetics of Epoxy/Amine Systems for the Naval Air Systems Command, Contract No. N00019-82-C-0244, from 9 July 1982 to 8 September 1983. The work was performed in the Chemical Physics Department, managed by Dr. D. P. Ames. The principal investigators were Dr. I. M. Brown and Dr. A. C. Lind; Dr. T. C. Sandreczki was a co-investigator. The project monitor was Mr. M. Stander, Naval Air Systems Command, Washington, DC.

CONTENTS

LIST OF ILLUSTRATIONS

LIST OF ILLUSTRATIONS (continued)

LIST OF ILLUSTRATIONS (continued)

LIST OF ILLUSTRATIONS (continued)

LIST OF TABLES

1. INTRODUCTION

The polymer material presently used for the structural components in fighter (F-18, AV8B) and transport aircraft (KC-10) is a carbon fiber-epoxy composite. The matrix material is an amine-cured epoxy polymer formed from the epoxy resin tetraglycidyl-4,4′-diaminodiphenylmethane (TGDDM). There is increasing evidence that the crosslinking reactions involved in this amine-cured epoxy matrix are incomplete; hence the polymer network formed after the cure is composed of regions of nonuniform crosslink density.[1-7] Details of these chemical crosslinking reactions and the kinetics of these reactions are important since they determine the crosslink network which determines mechanical properties and durability. Information about the molecular and morphological structures present in cured epoxy networks is of prime importance for predicting service lifetimes and improving the performance and reliability of these organic polymers in aerospace applications.

In this study we used the magnetic resonance spectrometric techniques, electron paramagnetic resonance (EPR) and nuclear magnetic resonance (NMR), to obtain information about the microstructures in amine-cured epoxy networks and the rates of some of the reactions relevant to the cure. In the EPR part of this work, nitroxide free radicals[8] were used to monitor their dynamic environments in the polymer. The nitroxide was employed either as a spin label where it was covalently bound at a known site on the epoxy or as a spin probe where it was randomly distributed throughout the polymer.[8-14]

The epoxy resins studied were tetraglycidyl-4,4′-diaminodiphenylmethane (TGDDM) either purified or in the form of the commercial resin MY720, obtained from Ciba Geigy Chemical Company, and diglycidyl bisphenol A (DGEBA) in the form of the commercial resin DER332, obtained from Dow Chemical Company. Curing agents used were difunctional aliphatic amine N,N′-dimethyl-1,6-diaminohexane (DDH), obtained from Aldrich Chemical Company, and tetrafunctional amine diaminodiphenylsulfone (DDS) in its commercial form Eporal, obtained from Ciba Geigy Chemical Company. The amines were used without further purification. Their molecular structures are shown in Figure 1.

Resins:

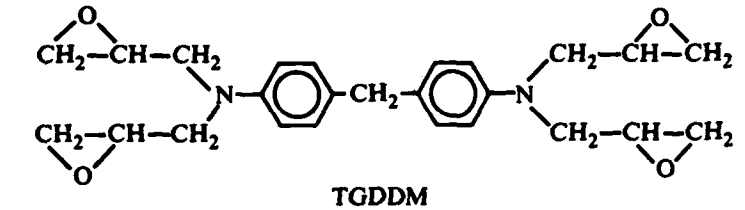

TGDDM

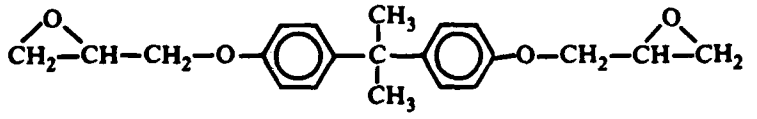

DGEBA

Curing agents:

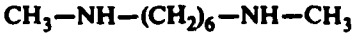

DDH

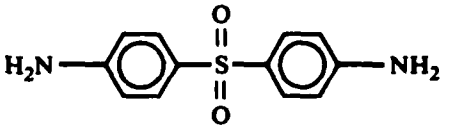

DDS

GP41-0053-8

Figure 1. Resins and curing agents studied.

The following specific EPR tasks were undertaken in this study:

1) Investigate and measure the kinetics of the reactions between nitroxide amines and TGDDM.
2) Qualitatively compare the reaction rates of nitroxide amines in TGDDM with those in MY720.
3) Investigate the dependence of molecular mobility on temperature and crosslink density for a series of chemically similar amine-cured epoxy resins.
4) Determine the amounts of unreacted epoxy and amine groups in amine-cured samples of TGDDM using amine nitroxides and glycidyl nitroxides, respectively.

The nitroxide amines used to label TGDDM in the kinetics experiments were 4-methylamino-2,2,6,6-tetramethylpiperidine-1-oxyl (METAMIN) and 4-dimethyl-

amino-2,2,6,6-tetramethylpiperidine-1-oxyl (DIMETAMIN).[11,12] The nitroxide 2,2,6,6-tetramethyl(1,2,3,6-tetrahydropyridine)-1-oxyl (TEMPENE) appeared as a by-product[11,12] in the labeling reactions and was also used as a spin probe in the molecular mobility investigations. The amine nitroxide 4-amino-2,2,6,6-tetramethylpiperdine-1-oxyl (TAMIN) and the glycidyl nitroxide 4-glycidoxy-2,2,6,6-tetramethylpiperidine-1-oxyl (glycidyl TANOL) were used to determine the number of unreacted functional groups in cured resin samples. The molecular structures for these nitroxides are shown in Figure 2.

The following three NMR tasks were undertaken in this study:

1) Use ^{1}H NMR to monitor the cure of MY720 and Eporal.
2) Use ^{13}C NMR with cross-polarization, high-power decoupling, and magic-angle spinning to quantitatively measure the composition of cured resins containing different amounts of TGDDM, DGEBA, and DDH.
3) Investigate two-dimensional ^{13}C NMR with cross-polarization, high-power decoupling, and magic-angle spinning for characterizing slow molecular motion in cured epoxy resins.

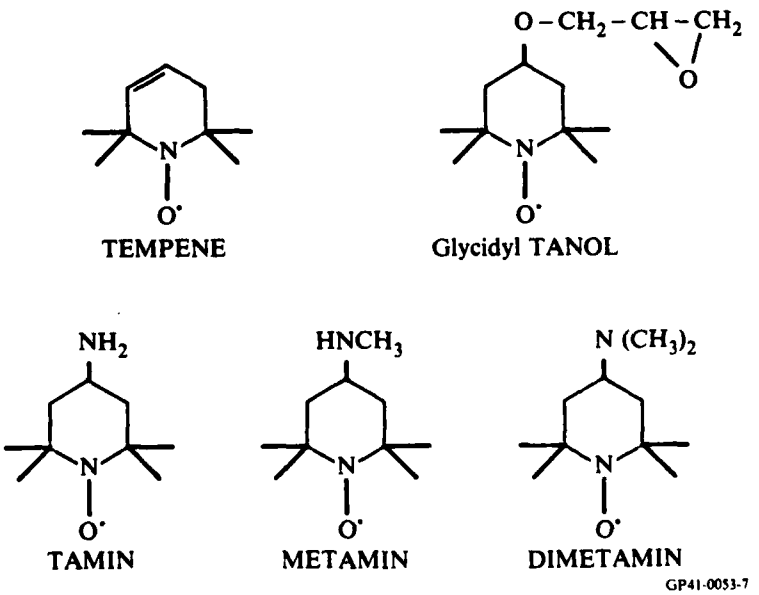

Figure 2. Spin probe and spin labels used.

2. EPR EXPERIMENTS ON EPOXY RESINS

2.1 Nitroxide-TGDDM Kinetics

EPR methods were used to measure the rates of reactions of two nitroxide amines with the epoxy resin TGDDM. In this technique, a paramagnetic molecule (the nitroxide) is bound to the epoxy at the oxirane ring following a ring opening by the amine functional group on the nitroxide.[11,12] Specific reactions studied were: 1) the binding of METAMIN to the TGDDM monomer to form the end label (Reaction 1 in Figure 3), and 2) the binding of the tertiary amine DIMETAMIN to the TGDDM monomer to form the spin-labeled quaternary base (Reaction 2 in Figure 3).

Reaction 1 can be viewed as a model for the initial step in the reactions involved in curing TGDDM with a conventional amine curing agent. Similarly, Reaction 2 can be considered as a model for the initial step in the reactions involved in the homopolymerization of TGDDM with a conventional tertiary amine as the initator.

Samples of purified TGDDM were prepared from the commercial resin MY720 by R. Levy of MDRL. Procedures of normal-phase, high-pressure liquid chromatography (HPLC) developed by Hagnauer[15] were used. This technique involved the elution of TGDDM from a preparative silica column with methylene chloride. The purified product was ~ 97% TGDDM compared to a TGDDM content of ~ 70% in MY720. Many of the impurities containing hydroxyl groups were trapped on the polar silica substrate and were eliminated from the resin. The viscosity of the purified TGDDM was less than that of MY720, as shown by the motional correlation times of the nitroxides in both uncured resin systems. This reduction in viscosity is intrinsic to the resins and is not the result of the presence of any eluting solvent, such as methylene chloride, in the TGDDM since the viscosity did not change following prolonged heating of the sample.

The samples were prepared in the following manner. TGDDM containing ~ 0.05 wt% nitroxide was pipetted into 4-mm-o.d. sample tubes which were then slipped into 5-mm-o.d. tubes.

The EPR spectra obtained at 313 K after certain times into Reaction 1 were stored on magnetic tape using a data acquisition system (Varian E-900).

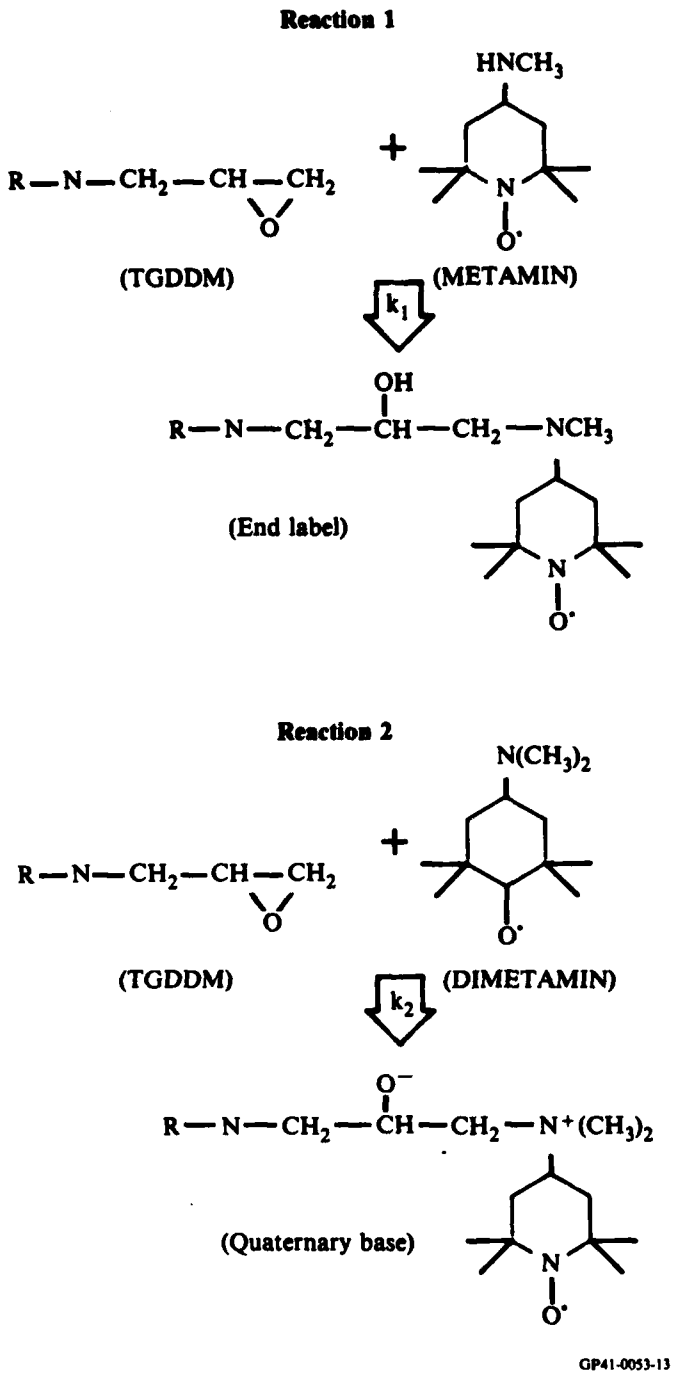

Figure 3. Reactions studied by EPR.

These spectra could then be field-shifted, scaled, subtracted, added, and integrated.

It can be seen from Figure 4, a typical sequence of spectra recorded at different times into Reaction 1, that as the METAMIN spin probe reacts with the epoxy to form the spin label, the initial spectrum is replaced by one having a longer motional correlation time; i.e., a slower tumbling nitroxide species is formed. It was assumed that the spectrum observed initially was that of the METAMIN spin probe and the spectrum obtained at the end of the reaction was that of the end label. The problem then was to measure accurately and reliably the areas under the spectra associated with the spin probe and end label in the composite spectrum as it developed in time.

The following method of analysis was used because it proved to be accurate and reliable. The height of each recorded spectrum was measured at two field values near the low-field derivative peak shown in Figure 5, viz., A and B for the spin label, A′ and B′ for the spin probe, and A′′ and B′′ for the composite spectrum. The following relations apply simultaneously:

$$xA + yA' = A'' \tag{1a}$$

$$xB + yB' = B'' \tag{1b}$$

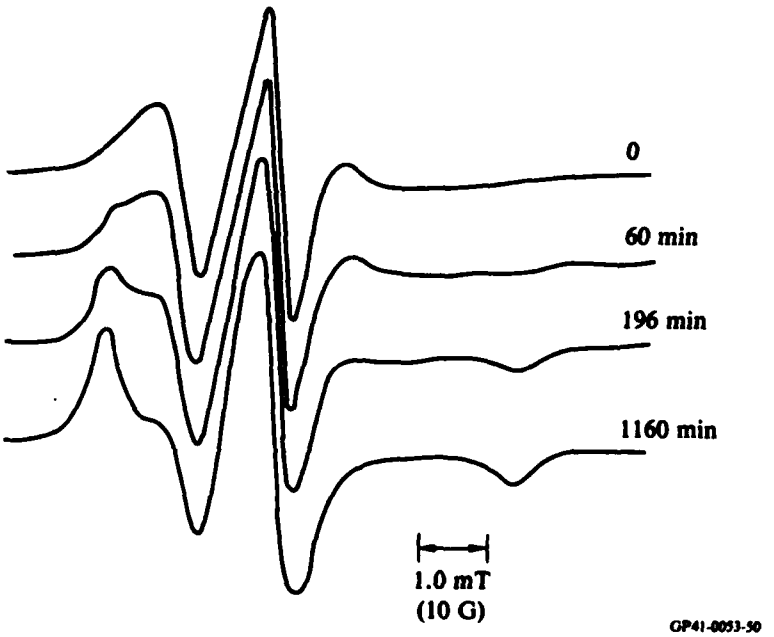

Figure 4. EPR spectra observed at 313 K for different times into Reaction 1, end-label formation. Reaction temperature = 353 K.

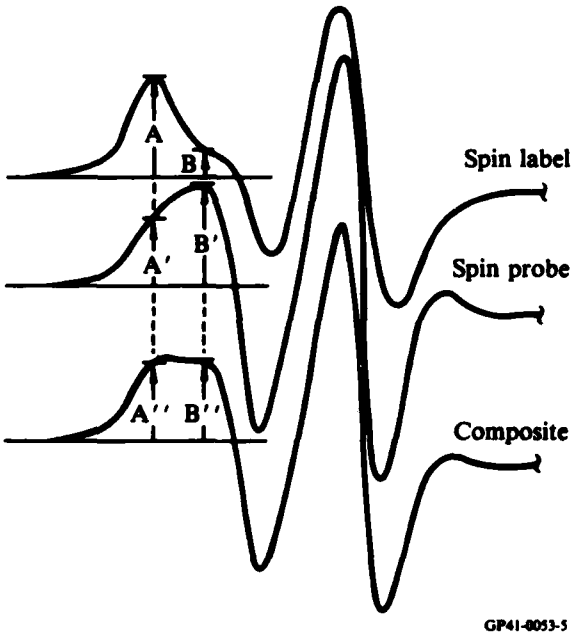

Figure 5. Definitions of spectral line amplitude parameters.

where x and y are the relative amounts of end label and spin probe present, respectively. The value of y (or x = 1 - y) was evaluated for each composite spectrum, and that value was used to scale the spin probe spectrum. This scaled spin probe spectrum was subtracted from each composite spectrum to obtain a difference spectrum which corresponds to the amount of spin label present. Figure 6 illustrates the typical results of such a procedure. The areas under the absorption line shapes (first integral of the experimentally determined derivative line shape) for the scaled spectrum and the difference spectrum were taken as the amount of spin probe and end label, respectively.

The actual data analysis was performed with a program written for the calculator (HP 9825) used in the data acquisition system. This program uses the horizontal and vertical cursors in the oscilloscope to measure the height of each specturm at the two designated field values. The scaling factor is calculated from the values of the parameters A'' and B'' in each spectrum. The area under each spectrum is normalized to the same value (that of the initial spectrum). The latter procedure was necessary because the total integrated intensities decreased with time as the nitroxide slowly decomposed when heated in the TGDDM resin to form diamagnetic products. The normalized

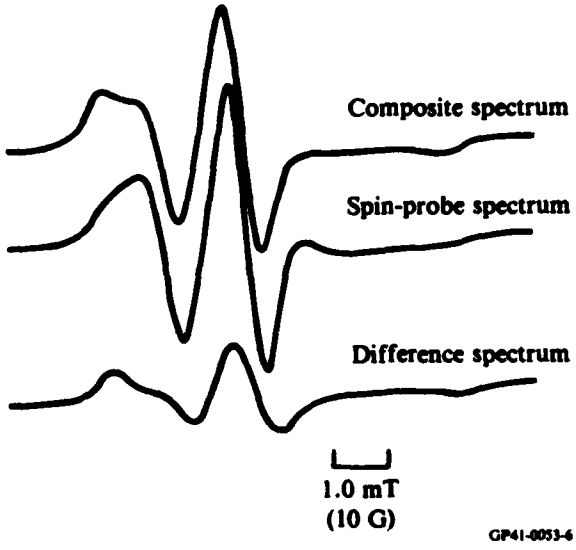

Figure 6. Typical line shapes observed from the composite spectrum, the spin-probe spectrum, and the difference spectrum (i.e., spin-label spectrum) in the EPR kinetics experiment.

amounts of spin probe (P/P_o) and spin label [$1 - (P/P_o)$] were printed by the calculator, where P_o and P are the concentrations of spin probe initially and at time t, respectively.

Reaction 1 was carried out at different temperatures from 333 to 383 K in a temperature-controlled convection oven (Imperial III, Lab-Line Instrument Company). The sample tube was removed from the oven at different times into the reaction, and all EPR spectra were measured at 313 K. The normalized amounts of spin probe, P/P_o, plotted as a function of time for Reaction 1 carried out at 333, 343, 353, 363, 373, and 383 K are shown in Figures 7, 8, 9, 10, 11, and 12, respectively.

The agreement with a single exponential time dependence in Figures 7-12 implies a pseudo-first-order reaction with the values of the rate constant k_1 at the different temperatures shown in Table 1. These values of the rate constant are plotted as a function of 1/temperature in Figure 13 where the data show an excellent fit to $k_1 = k_{01} \exp(-\Delta E/RT)$, where ΔE is the activation energy and k_{01} is the frequency factor. From the data in Figure 13, one obtains $\Delta E = 55 \pm 5$ kJ mol^{-1} and $k_{01} = 1.3 \times 10^4$ s^{-1}.

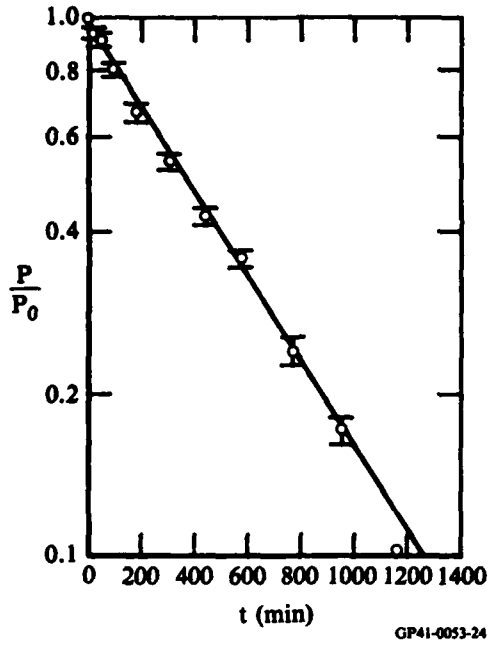

Figure 7. Time dependence of normalized spin-probe concentration, P/P_0, in TGDDM end-labeled with METAMIN (reaction temperature = 333 K).

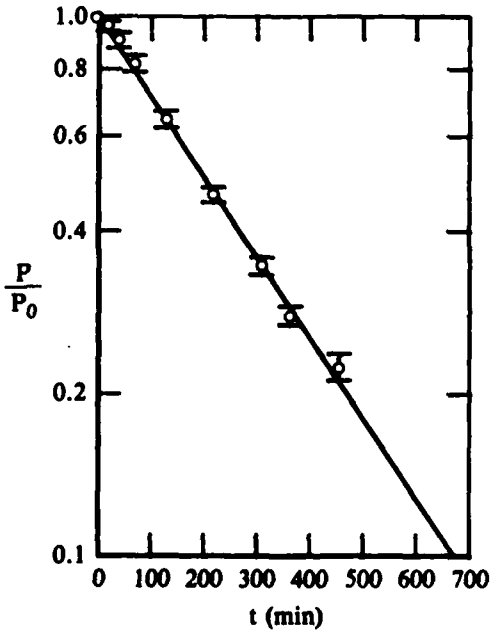

Figure 8. Time dependence of normalized spin-probe concentration, P/P_0, in TGDDM end-labeled with METAMIN (reaction temperature = 343 K).

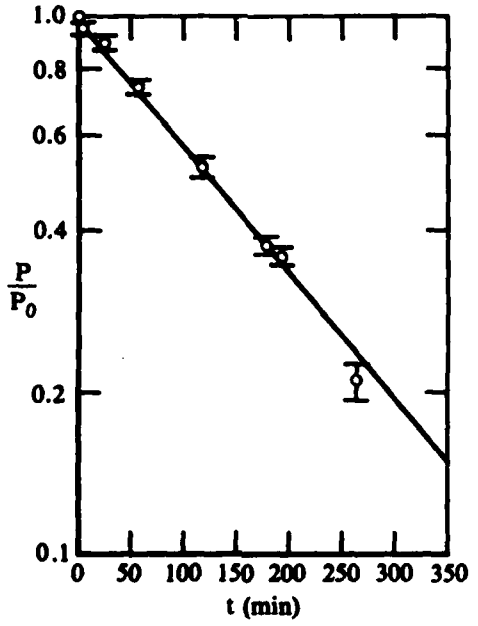

Figure 9. Time dependence of normalized spin-probe concentration, P/P_0, in TGDDM end-labeled with METAMIN (reaction temperature = 353 K).

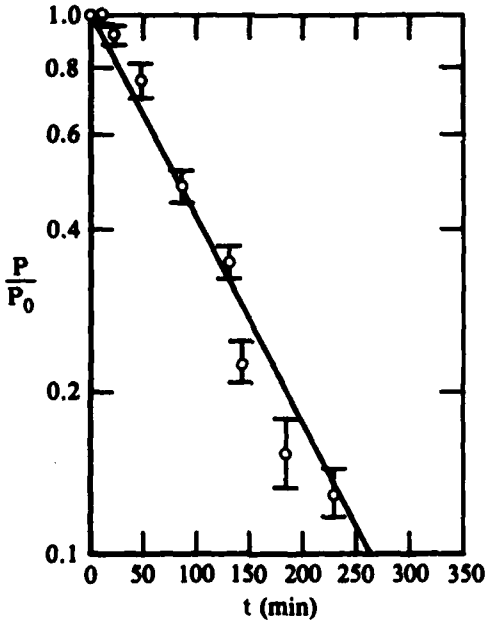

Figure 10. Time dependence of normalized spin-probe concentration, P/P_0, in TGDDM end-labeled with METAMIN (reaction temperature = 363 K).

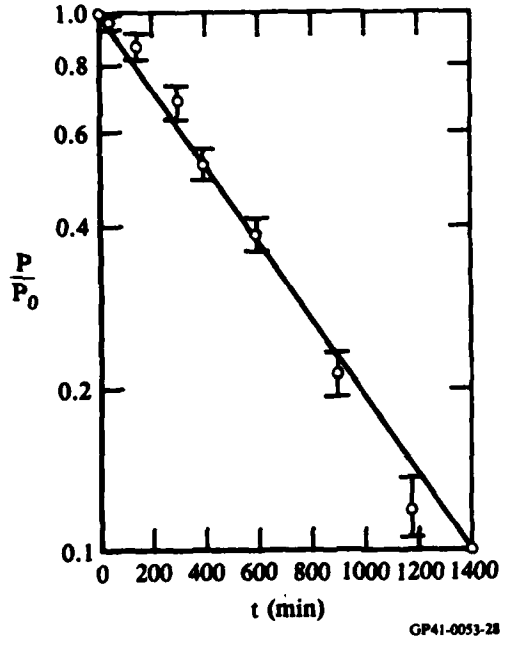

Figure 11. Time dependence of normalized spin-probe concentration, P/P_0, in TGDDM end-labeled with METAMIN (reaction temperature = 373 K).

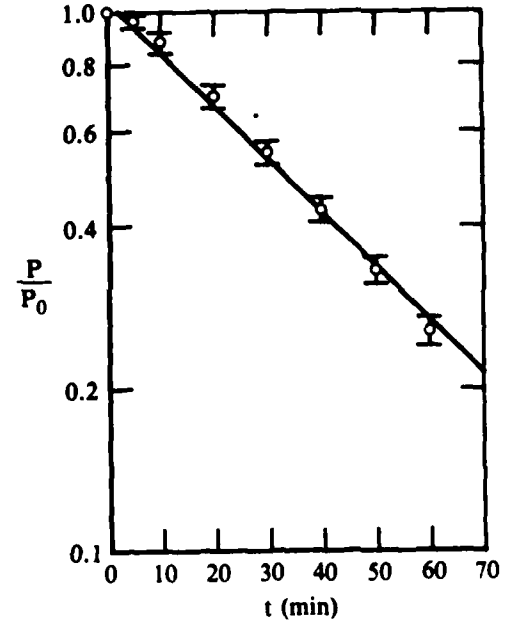

Figure 12. Time dependence of normalized spin-probe concentration, P/P_0, in TGDDM end-labeled with METAMIN (reaction temperature = 383 K).

TABLE 1. REACTION RATES OF NITROXIDE AMINES WITH TGDDM.

Nitroxide	Rate constant (k_1, k_2) (s^{-1})	Temperature (K)
METAMIN (k_1)	3.1×10^{-5}	333
	5.7×10^{-5}	343
	9.0×10^{-5}	353
	14.45×10^{-5}	363
	27.5×10^{-5}	373
	40.5×10^{-5}	383
DIMETAMIN (k_2)	8.75×10^{-6}	333
	1.95×10^{-5}	343
	3.1×10^{-5}	353
	3.85×10^{-5}	363
	4.7×10^{-5}	373
	5.45×10^{-5}	383
	6.0×10^{-5}	393

GP41-0053-2

The rates of the reaction of the tertiary amine DIMETAMIN with the epoxy resin TGDDM to form the spin-labeled quaternary base (Reaction 2 in Figure 3) were also measured at several temperatures between 333 and 383 K. All spectra were recorded at 313 K. Figure 14 shows a typical sequence of spectra observed at the times shown. The spectra were analyzed in the same manner as described above for the end label. The time dependence for the normalized spin probe concentration, P/P_o, at the reaction temperatures 333, 343, and 353 K are shown in Figures 15, 16, and 17. All the decays of P/P_o show good fits to a single exponential time dependence over the measured time range. This result implies that Reaction 2 also obeys pseudo-first-order kinetics between 333 and 353 K.

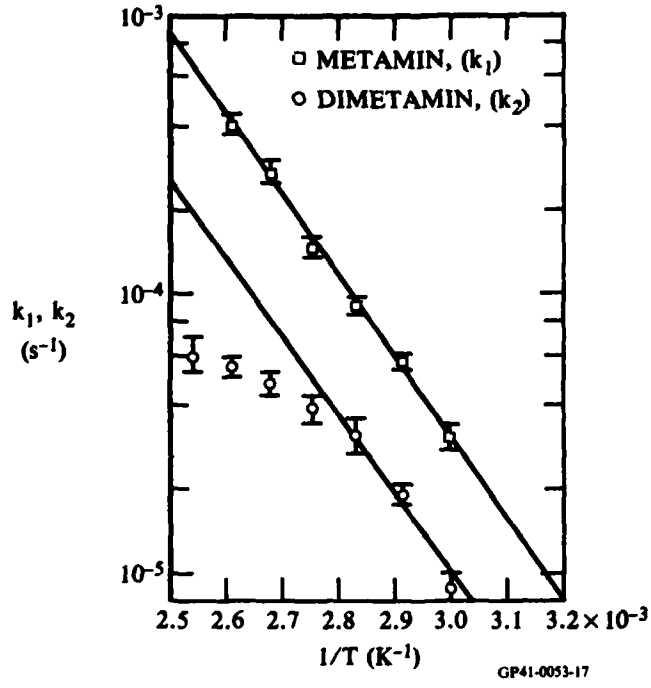

Figure 13. Temperature dependence of the rate constants k_1, k_2 for the METAMIN and DIMETAMIN reactions with TGDDM.

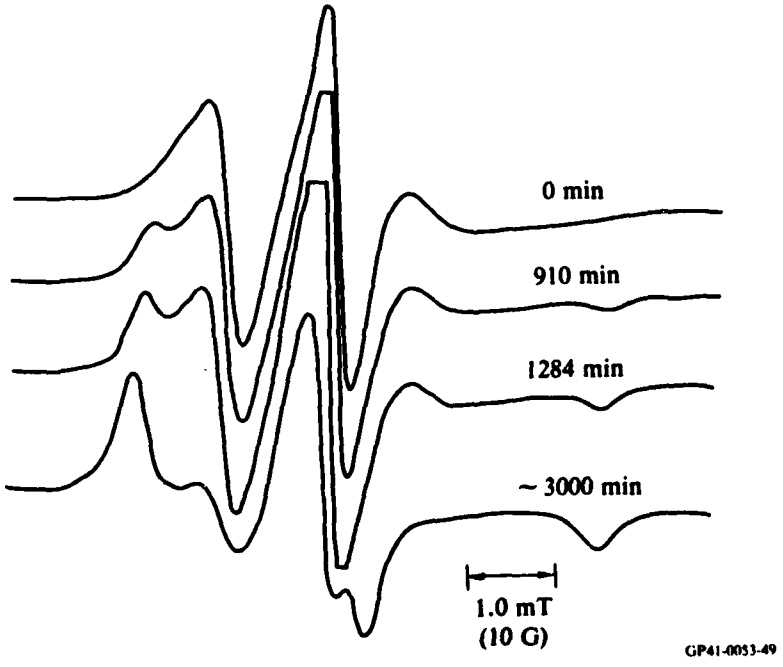

Figure 14. EPR spectra observed at 313 K for different times into Reaction 2, spin-labeled quaternary base formation. Reaction temperature = 333 K.

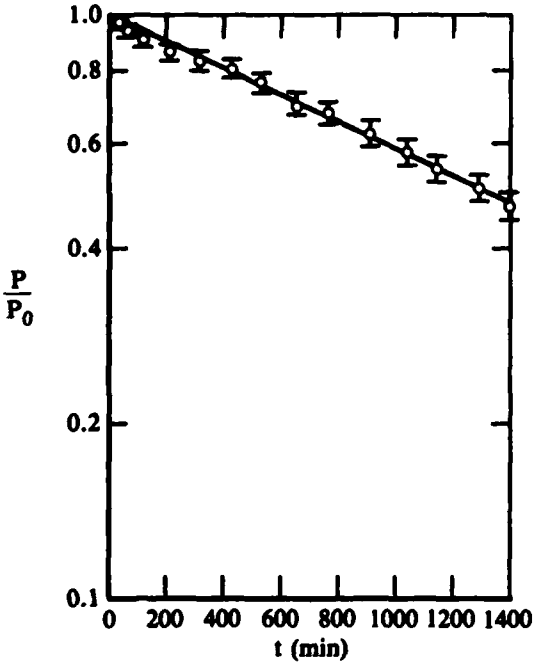

Figure 15. Time dependence of normalized spin-probe concentration, P/P_0, in reaction of TGDDM with DIMETAMIN to form spin-labeled quaternary base (reaction temperature = 333 K).

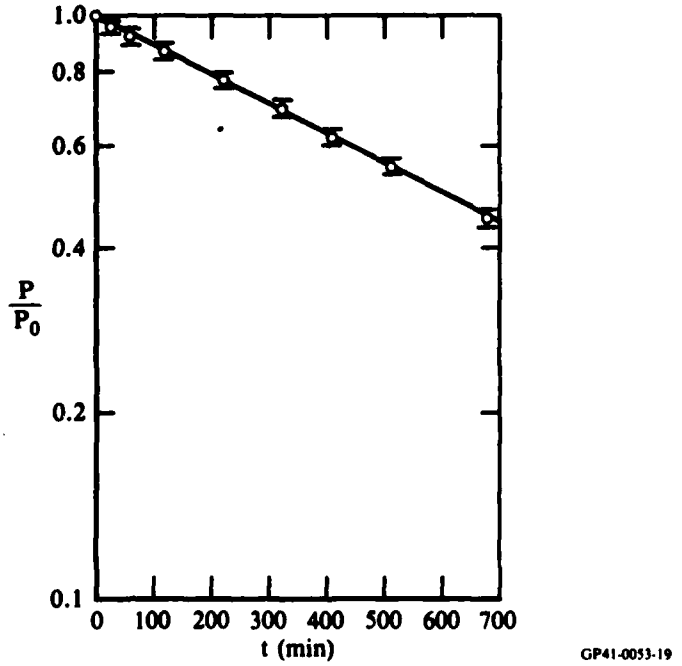

Figure 16. Time dependence of normalized spin-probe concentration, P/P_0, in reaction of TGDDM with DIMETAMIN to form spin-labeled quaternary base (reaction temperature = 343 K).

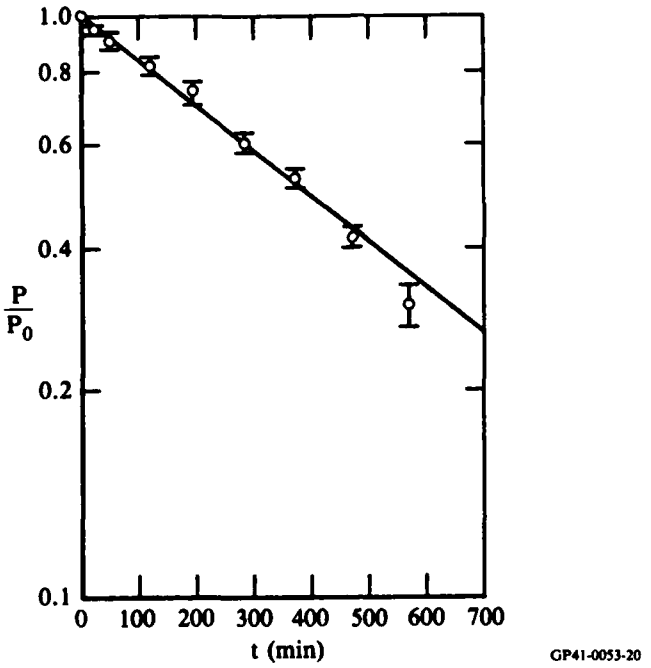

Figure 17. Time dependence of normalized spin-probe concentration, P/P_0, in reaction of TGDDM with DIMETAMIN to form spin-labeled quaternary base (reaction temperature = 353 K).

However, the data for the reaction temperatures 363, 373, and 383 K shown in Figures 18, 19, and 20 indicate distinct nonexponential behavior in plots of P/P_o as a function of time. The reason for the deviations from single exponential behavior is that the Hofmann elimination product, TEMPENE,[11,12] appeared before the complete disappearance of the DIMETAMIN spin-probe signal. Since the TEMPENE spectrum is similar to that of DIMETAMIN, the presence of TEMPENE made it appear, as shown in Figure 19, as though the spin-probe concentration were increasing again. In fact, as is shown in Figure 18, deviations from a single exponential behavior increase with increasing initial DIMETAMIN concentration. The reason for this behavior is that the rate of TEMPENE production at any fixed temperature increases with increasing initial nitroxide concentration. In Figures 18, 19, and 20 the initial slopes of the decays are assumed to give the reaction rate k_2.

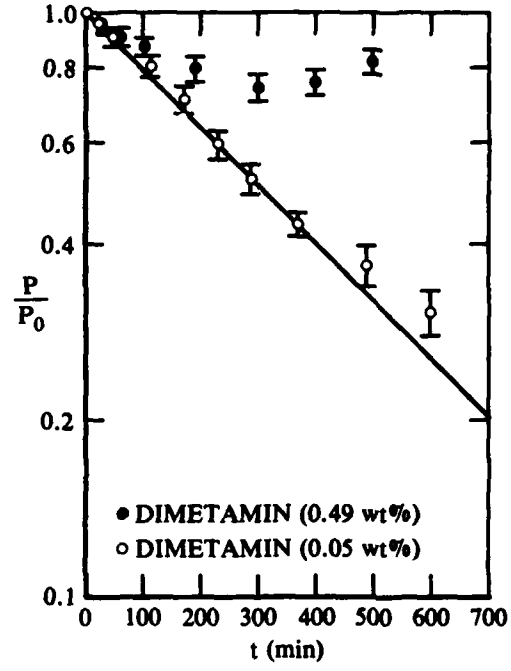

Figure 18. Time dependence of normalized spin-probe concentration, P/P_0, in reaction of TGDDM with DIMETAMIN to form spin-labeled quaternary base (reaction temperature = 363 K).

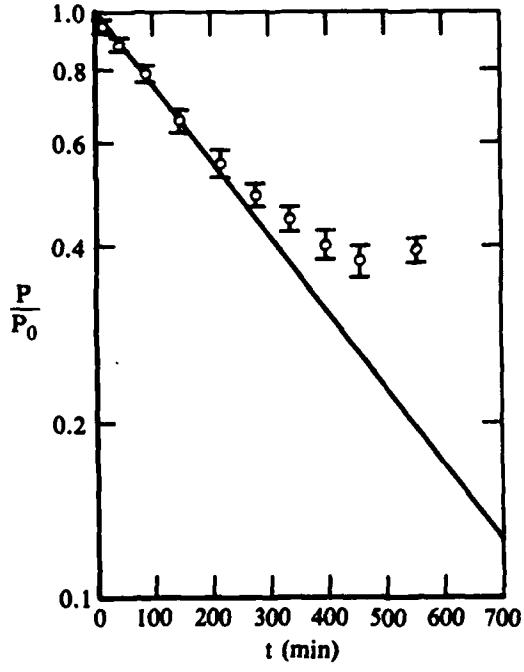

Figure 19. Time dependence of normalized spin-probe concentration, P/P_0, in reaction of TGDDM with DIMETAMIN to form spin-labeled quaternary base (reaction temperature = 373 K).

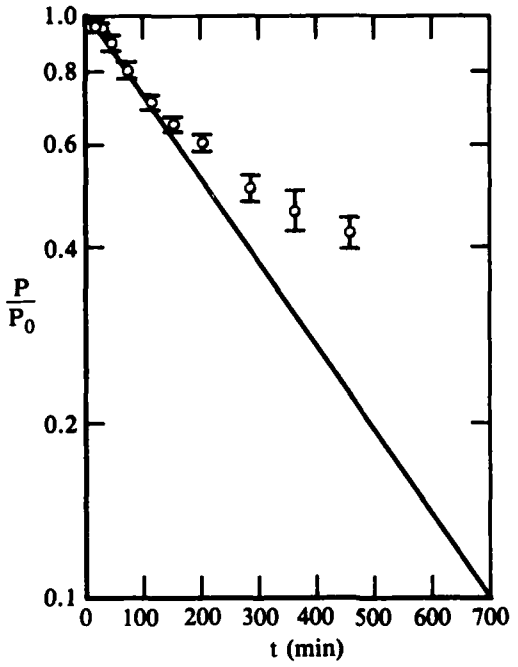

Figure 20. Time dependence of normalized spin-probe concentration, P/P_0, in reaction of TGDDM with DIMETAMIN to form spin-labeled quaternary base (reaction temperature = 383 K).

The values of k_2 obtained for the reaction performed at 333 to 393 K are listed in Table 1 and plotted in Figure 13. Although these values show a large deviation from Arrhenius behavior betwen 333 and 353 K, they show an approximate agreement with the form $k_2 = k_{02} \exp(-\Delta E/RT)$ with $\Delta E = 55 \pm 5$ kJ mol^{-1} and $k_{02} = 4 \times 10^3$ s^{-1}. In the high-temperature region, the data showed an approximate fit to $\Delta E = 18.5 \pm 3$ kJ mol^{-1} and $k_{02} = 1.7 \times 10^{-2}$ s^{-1}.

The rates of the Hofmann elimination reaction[11,12] were investigated, but it was impossible to measure them quantitatively with any reliability because of the presence of parallel reactions. These reaction are of the type described previously[12,13] involving charge separation caused by a stepwise addition of TGDDM following an oxirane ring opening by O^- groups. We concluded from the amounts of TEMPENE spectra observed in the total spectral line shapes that the rate of TEMPENE production increases with temperature and with initial nitroxide concentration. This observation provides conclusive proof that the Hofmann elimination can proceed through conformations that permit anti-orientations of the relevant β hydrogen with respect to the quaternary

nitrogen and that this anti-elimination involves an RO^- group that is located on an adjacent spin-labeled quaternary base.[12]

2.2 Nitroxide Decomposition Rates

In addition to the line shape changes associated with the different spin labeling reactions of TGDDM resin with the nitroxide amines, the total integrated EPR absorption decreased with increased heating time. This decrease in magnetic susceptibility indicates nitroxide decomposition and results from the nitroxide reacting with remnant impurities in the resin to form diamagnetic products. The paramagnetic susceptibility, evaluated from a double integration of the EPR derivative line shape, was measured for METAMIN and DIMETAMIN in TGDDM following different reaction times at temperatures from 333 to 383 K. The results for METAMIN in TGDDM are shown in Figure 21, where the susceptibilities have been normalized to the initial values. At all four temperatures the decays of the normalized susceptibilites show a single exponential time dependence up to several time constants beyond the time when the end label

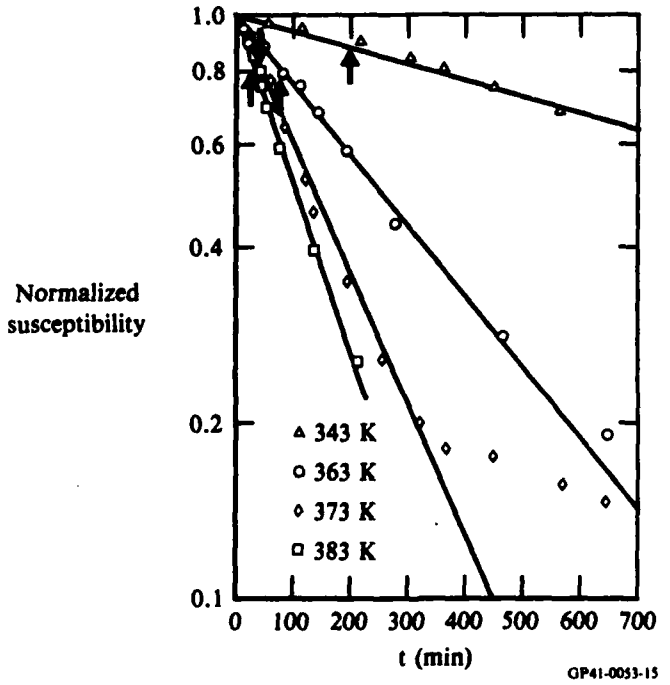

Figure 21. Integrated EPR signal intensity (normalized susceptibility) as a function of time for METAMIN in TGDDM at 343, 363, 373, and 383 K. Solid arrows indicate the time at which 50% of the METAMIN spin probe has been converted to spin label.

formation was 50% complete (this time is indicated by the solid arrows in Figure 21). This result suggests that the decomposition rates for the end label and the METAMIN spin probe are the same. Thus, the procedure of using the changes in the double integral of the EPR derivative spectrum of the end label (implicit in obtaining the rate data in Figure 13) should be a reliable measure of end-label production.

The measured data for the decomposition of DIMETAMIN in TGDDM are shown in Figure 22. In contrast with METAMIN, the decays of the normalized susceptibilties for DIMETAMIN usually showed a nonexponential time dependence. In fact, as can be seen from Figure 22, the decay shapes are concave up at temperatures above 353 K and concave down below 353 K. Results obtained at 363 K involving a determination of the normalized susceptibility decay at different initial DIMETAMIN concentrations (viz., 0.05 and 0.49 wt%) are shown in Figure 23. These results indicate that at high initial concentration (0.49 wt%) the decay has a single exponential time dependence, whereas at lower concentra-

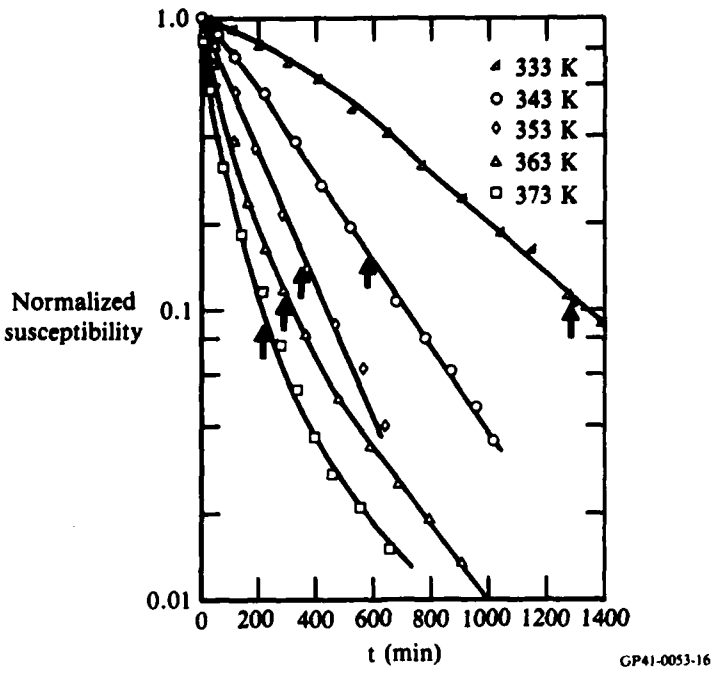

Figure 22. Integrated EPR signal intensity (normalized susceptibility) as a function of time for DIMETAMIN in TGDDM at 333, 343, 353, 363, and 373 K. Solid arrows indicate the time at which 50% of the DIMETAMIN spin probe has been converted to spin label.

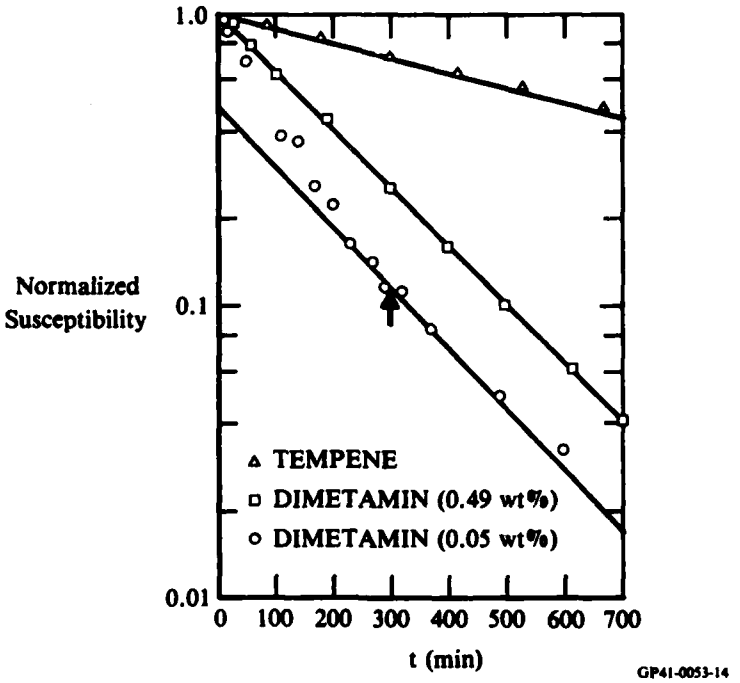

Figure 23. Integrated EPR signal intensity (normalized susceptibility) as a function of time for TEMPENE and DIMETAMIN in TGDDM at 363 K. The solid arrow indicates the time at which 50% of the DIMETAMIN spin probe has been converted to spin label.

tions the decay can be considered as the superposition of an initial faster decay and a slower decay which is the same as that at the high concentrations. A possible explanation for this behavior involves two remnant impurities in the TGDDM resin which give rise to two decay mechanisms for DIMETAMIN.

It is conceivable that different activation energies for these two mechanisms can lead to a situation where the initial decay is faster than ($T > 353$ K), equal to ($T = 353$ K) and slower than ($T < 353$ K) the final decay. Such activation energies would explain the shapes of the decays shown in Figure 22.

The decomposition rates for the nitroxides in TGDDM, shown in Figures 21, 22, and 23, could have important consequences for the conclusions drawn for the reaction rate data plotted in Figure 13. If the spin label in either Reaction 1 or 2 in Figure 3 has a decomposition rate slower (faster) than its spin probe precursor, then the rate constant for the reaction will appear to be faster (slower) than its true value. That this is not the case for the

METAMIN/TGDDM reaction is apparent from the data in Figure 21. Since the slopes of the decays to the right and left of the solid arrows are equal, the decomposition rates for the spin probe and spin label are the same.

In some of the data shown in Figure 21 for DIMETAMIN/TGDDM, the decomposition rates exhibit curvature close to the solid arrows. However, in view of the results in Figure 23, the argument given above involving two different impurities is more plausible than any difference in decomposition rates between the spin label and spin probe. Further evidence is shown in Figure 23 where the curvature in the decomposition rates that appears at low nitroxide concentrations disappears at high nitroxide concentrations. This change in the curvature suggests that one of the impurities is completely consumed by the nitroxide early in the decomposition process since the concentration of this impurity is much less than that of spin probe ($<<$ 0.5 wt%).

The decay of the normalized magnetic susceptibility for pure TEMPENE in TGDDM after heating at 363 K is also shown in Figure 23; it is significantly slower than that for DIMETAMIN in TGDDM. Consequently, TEMPENE formation as determined from its EPR spectra appears to be faster than it truly is. However, the area under the TEMPENE spectrum is never larger than 15% of the total spectrum. Moreover, the initial slopes used to evaluate k_2 should not be affected since there is little TEMPENE formed at the early stages of Reaction 2. All these results support our conclusion that the curvature in the temperature dependence in Figure 13 is a valid representation of the behavior of the rate constant k_2.

2.3 Qualitative Comparison of the Reaction Rates of Nitroxide Amines in TGDDM and MY720

In this task a qualitative comparison was made between the formation rates of spin labels formed in TGDDM and those formed in MY720.

The tertiary amine nitroxide DIMETAMIN was thoroughly mixed with TGDDM at 363 K by stirring for 15 min. The EPR line shapes were then obtained at 293, 308, 315, 322, and 331 K. Typical spectra are shown in Figure 24. At each temperature the observed spectrum can be characterized by one value of the motional correlation time. Thus, one nitroxide species was present, namely, the unreacted DIMETAMIN spin probe. The corresponding spectra obtained after 2 h heating at 363 K, i.e., 2 h into Reaction 1, are shown in

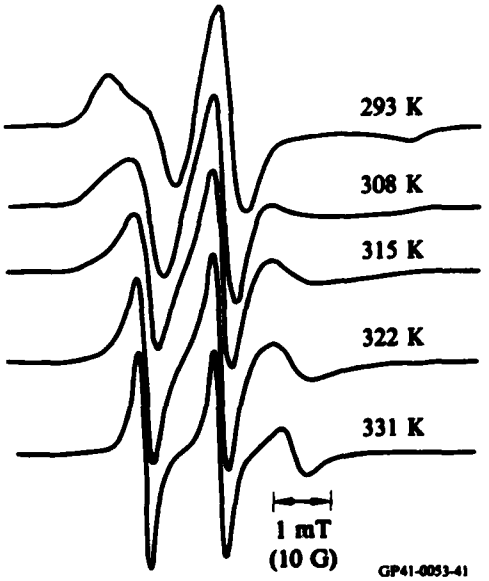

Figure 24. The EPR spectra observed at 293, 308, 315, 322, and 331 K from a sample of purified TGDDM containing DIMETAMIN after 15 min heating at 363 K. At each temperature, only derivative peaks associated with unreacted DIMETAMIN probe are observed.

Figure 25. These spectra should be compared with the line shapes shown in Figure 26, which were obtained from samples of DIMETAMIN in the unpurified commercial resin MY720. The spectra recorded at 315, 322, and 331 K, shown in Figure 25, have similar line shapes to the spectra recorded at 336, 345, and 356 K, respectively, and shown in Figure 26. The 20 K difference in the spectral correspondence is the result of the difference in viscosity of the two resins.

In both Figures 25 and 26, the observed spectra are superpositions of two component spectra, one arising from the unreacted DIMETAMIN spin probe (designated P) and the other from the spin-labeled quaternary base reaction product (designated Q). Comparison of Figures 25 and 26 reveals that the extent of Reaction 2, i.e., the amount of quaternary base formed in TGDDM after 2 h heating at 363 K, is approximately the same as the extent of the reaction in MY720 after only 15 min at 363 K. Thus, the reaction rate of DIMETAMIN in TGDDM is eight times slower than that of DIMETAMIN in MY720. Further confirmation of these reaction-rate differences is given in Figures 27 and 28. Figure 27 shows the spectra of a DIMETAMIN/TGDDM mixture recorded

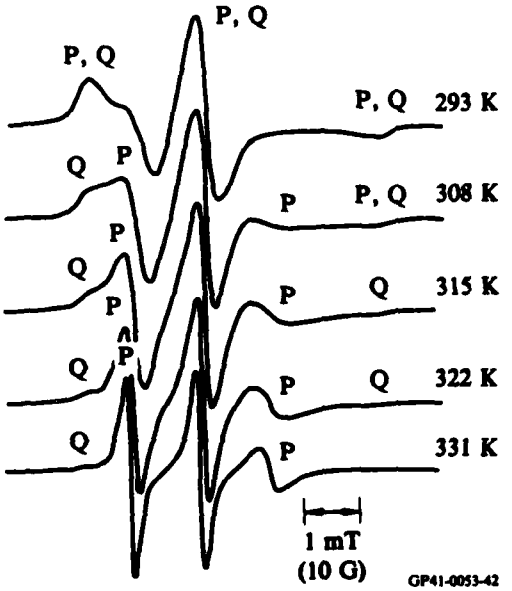

Figure 25. The EPR spectra observed at 293, 308, 315, 322, and 331 K from a sample of purified TGDDM containing DIMETAMIN after 2 h heating at 363 K. The derivative peaks associated with the probe and quaternary base are designated P and Q, respectively.

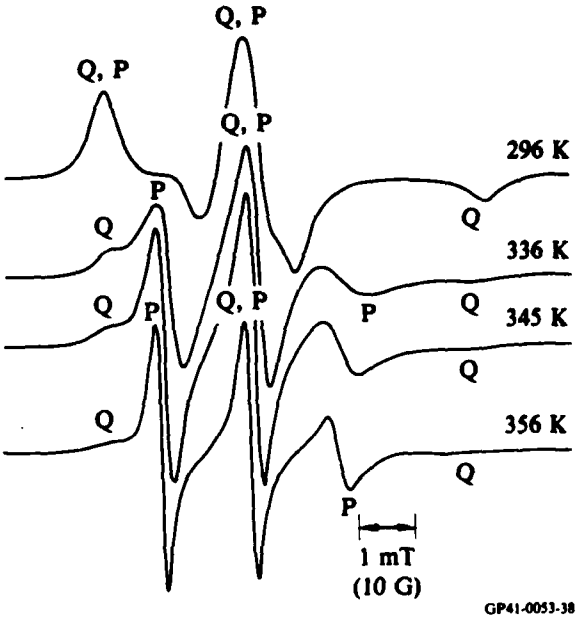

Figure 26. The EPR spectra observed at 296, 336, 345, and 356 K from a sample of MY720 containing DIMETAMIN after 15 min heating at 363 K. The derivative peaks associated with the probe and quaternary base are designated P and Q, respectively.

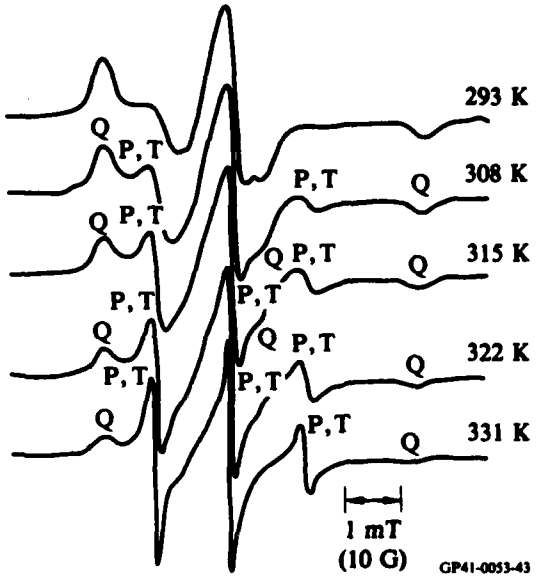

Figure 27. The EPR spectra observed at 293, 308, 315, 322, and 331 K from a sample of purified TGDDM containing DIMETAMIN after 14 h heating at 363 K. The derivative peaks associated with the spin probe, quaternary base, and TEMPENE are designated P, Q, and T, respectively.

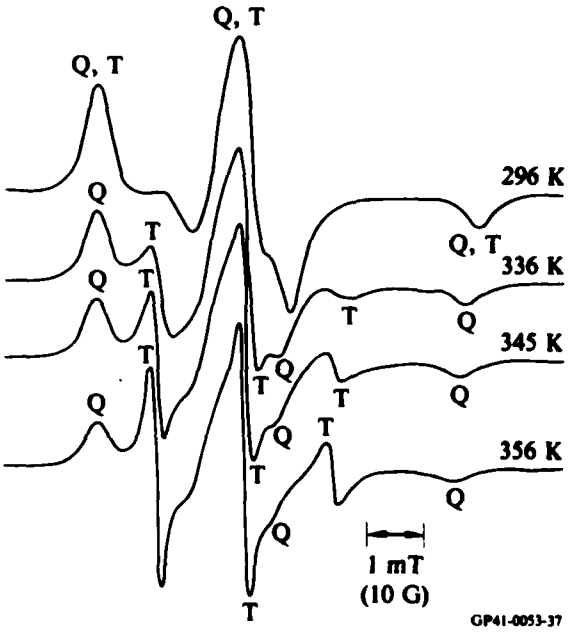

Figure 28. The EPR spectra observed at 296, 336, 345, and 356 K from a sample of MY720 containing DIMETAMIN after 90 min heating at 363 K. The derivative peaks associated with the quaternary base and TEMPENE are designated Q and T, respectively.

after 14 h heating at 363 K; Figure 28 shows the spectra of a DIMETAMIN/MY720 mixture recorded after 90 min heating at 363 K. The amount of spin-labeled quaternary base is approximately the same in both samples at the times shown.

After prolonged heating of the DIMETAMIN/TGDDM mixture at 363 K, the quaternary base can undergo a Hofmann elimination reaction[11,12] to produce the small spin probe TEMPENE. At some temperatures the spectrum of TEMPENE can be distinguished from that of the larger molecule DIMETAMIN by its narrower spectral lines, a result of its greater rotational mobility.

Examination of the spectrum recorded at 331 K, shown in Figure 27, reveals that after 14 h heating at 363 K TEMPENE is being produced. The spectrum of unreacted DIMETAMIN overlaps that of TEMPENE. However, the composite spectrum can be deconvoluted using spectral subtraction software which is part of the data acquisition system (Varian E-900) associated with the EPR spectrometer. Figure 29 shows the results of such a spectral subtraction. The unreacted DIMETAMIN spectrum at 331 K has been subtracted from the

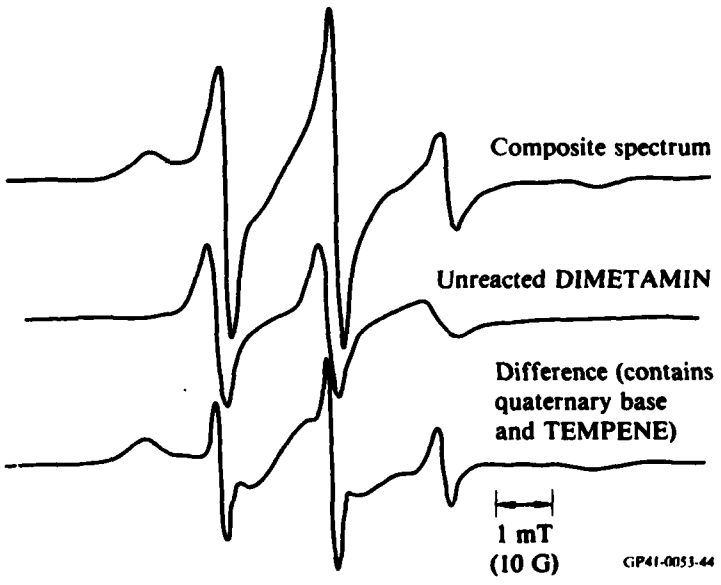

Figure 29. Spectral subtraction of unreacted DIMETAMIN spectrum from composite spectrum containing unreacted DIMETAMIN, quaternary base, and the Hofmann elimination product, TEMPENE in TGDDM. Difference spectrum contains only quaternary base and TEMPENE. Spectra recorded at 331 K; composite spectrum taken after 14 h heating at 363 K.

composite spectrum of a mixture of DIMETAMIN, quaternary base, and TEMPENE at 331 K. The difference spectrum does not contain the DIMETAMIN spectrum but clearly shows the presence of the TEMPENE spectrum. However, estimates of the relative rate constants for the production of TEMPENE from DIMETAMIN in TGDDM and MY720 could not be reliably determined.

In analogous experiments, METAMIN was dissolved in purified TGDDM and allowed to react at 363 K. At selected times during the reaction, EPR spectra were recorded at several temperatures. The spectra recorded immediately after mixing, shown in Figure 30, can be assigned to a single species, the unreacted METAMIN spin probe. After 90 min and 10.5 h at 363 K, the spectra shown in Figures 31 and 32, respectively, were recorded. In addition to the spin probe, a spectrum associated with the end label (structure shown in Figure 3) was observed. The two component-spectra are clearly detectable at 313 K, as shown in Figure 31. The spectra in Figure 31 resemble the spectra recorded for METAMIN in MY720 after 36 min at 363 K (Figure 33). For example, the 313 K spectrum in Figure 31 corresponds to the 336 K spectrum in Figure 33. It therefore appears that after 1.5 h at 363 K the METAMIN/TGDDM reaction produces less end label than the METAMIN/MY720 after 36 min at 363 K. These results are consistent with the difference in reaction rates found for DIMETAMIN in the two uncured resin systems. On the other hand, the results in Figures 32 and 34 are difficult to explain. These spectra indicate that the

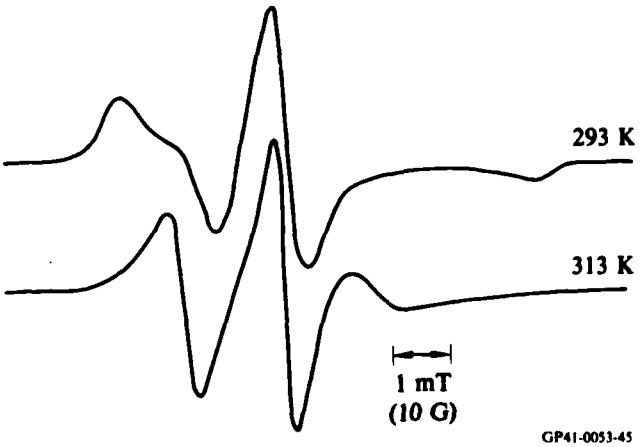

Figure 30. The EPR spectra observed at 293 K and 313 K from a sample of purified TGDDM containing METAMIN after 10 min heating at 363 K. At both temperatures only derivative peaks associated with unreacted METAMIN are observed.

amount of end label formed in TGDDM after 10.5 h at 363 K is comparable to that in MY720 after 15 h at 363 K, i.e., the rates of formation of end label are nearly the same in the two resin systems.

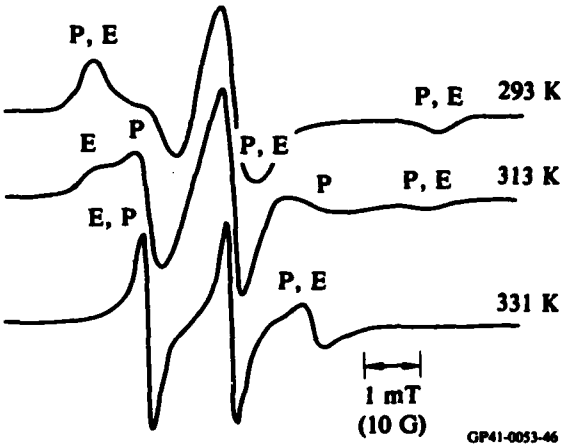

Figure 31. The EPR spectra observed at 293, 313, and 331 K from a sample of purified TGDDM containing METAMIN after 90 min heating at 363 K. The derivative peaks associated with the probe and end label are designated P and E, respectively.

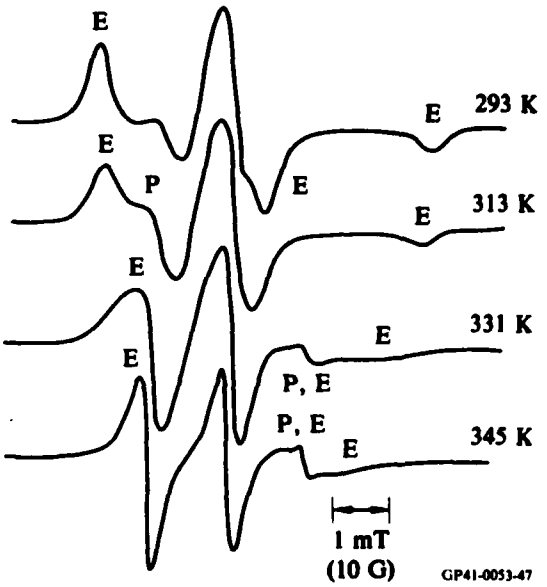

Figure 32. The EPR spectra observed at 293, 313, 331, and 345 K from a sample of purified TGDDM containing METAMIN after 10.5 h heating at 363 K. The derivative peaks are associated almost entirely with end label. Only a trace of probe-like component is observed, above 331 K.

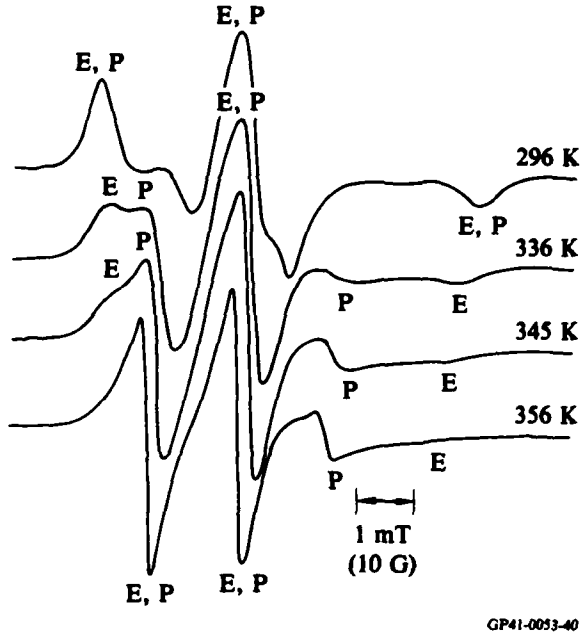

Figure 33. The EPR spectra observed at 296, 336, 345, and 356 K from a sample of MY720 containing METAMIN after 36 min heating at 363 K. The derivative peaks associated with the probe and end label are designated P and E, respectively.

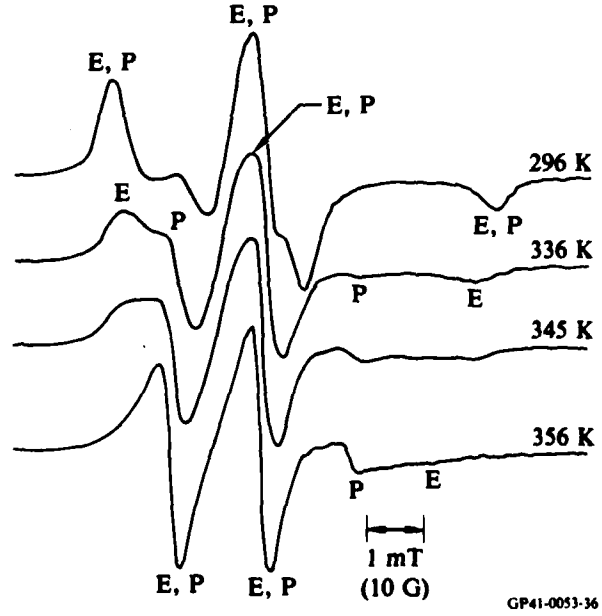

Figure 34. The EPR spectra observed at 296, 336, 345, and 356 K from a sample of MY720 containing METAMIN after 15 h heating at 363 K. The derivative peaks associated with the probe and end label are designated P and E, respectively.

The spectra obtained from METAMIN in TGDDM and in MY720 after 102 and 100 h heating at 363 K are shown in Figure 35 and 36, respectively. It is clear from the spectrum at 345 K in Figure 35 and at 356 K in Figure 36 that no quaternary base has formed in TGDDM whereas a large amount (~ 50% of the total spectrum) is present in MY720. This slow rate of quaternary base formation in TGDDM is consistent with the DIMETAMIN results.

2.4 Investigation of Crosslink Density in Amine-Cured Epoxies

In this task, the molecular mobility of a nitroxide spin probe was investigated in a series of amine-cured epoxy resins with different average crosslink densities. Information on molecular mobility is important since it affects sample toughness, impact strength, transport properties, and glass transition phenomena. In particular, the rotational mobility of the spin probe TEMPENE was studied in the cured epoxy host matrices as a function of temperature, free volume, and crosslink density.

The samples studied were prepared from the epoxy resins DGEBA and purified TGDDM. The curing agent used was DDH. Samples having different crosslink densities were prepared by mixing the difunctional DGEBA with the tetrafunctional TGDDM in different ratios, followed by the addition of the amount of DDH required to effect a complete stoichiometric reaction with the epoxy mixture. Samples were prepared in the following ratios, by equivalents, of

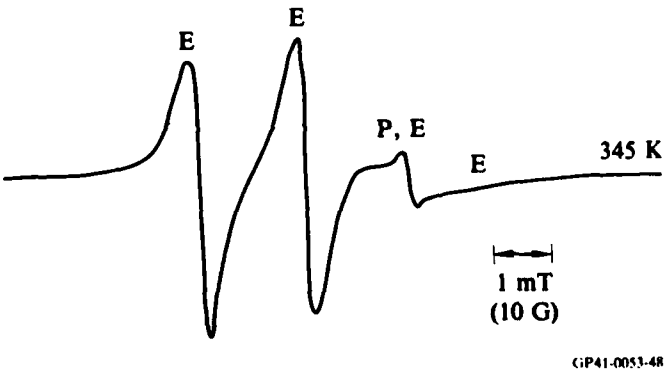

Figure 35. The EPR spectrum observed at 345 K from purified TGDDM containing METAMIN after 102 h heating at 363 K. The derivative peaks are associated almost entirely with end label (E), although a trace of probe-like component (P) is observed.

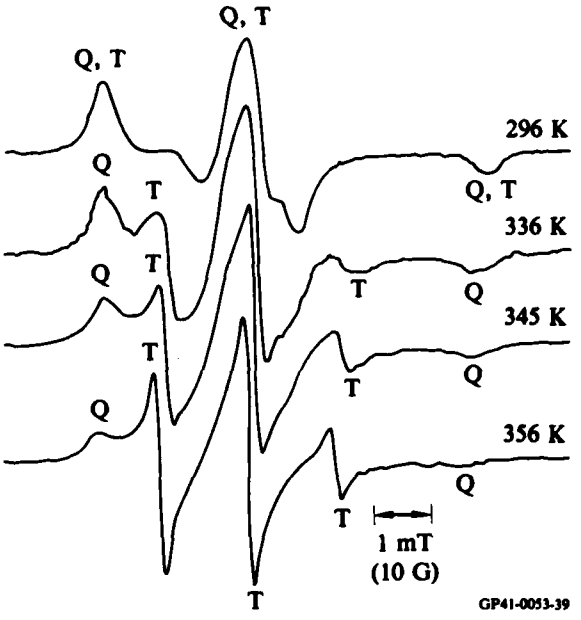

Figure 36. The EPR spectra observed at 296, 336, 345, and 356 K from a sample of MY720 containing METAMIN after 100 h heating at 363 K. The derivative peaks associated with the quaternary base and TEMPENE are designated Q and T, respectively.

TGDDM:DGEBA:DDH--0:5:5, 2:3:5, 3:2:5, and 0:5:5. Approximately 0.05 wt% TEMPENE was added to each resin mixture prior to the addition of DDH. The samples were cured overnight at 300 K, followed by postcuring at 363 K for 2 h and at 413 K for 15 min; i.e., all samples were postcured above their glass transition temperature T_g before any measurements were made.

Crosslink densities were calculated using the following equation:[16]

$$M = \left(\frac{2}{f}\right)\left(\frac{w}{m}\right) \qquad (2)$$

where M is the molecular weight between crosslinks, f is the functionality of the TGDDM (= 4), w is the sample weight, and m is the number of moles of TGDDM in the sample. In previous studies, it was established that Equation (2) yields reliable values of M that are in good agreement with those determined from dynamic mechanical analysis.[13] Values of M for the epoxy samples studied are listed in Table 2.

Glass transition temperatures were measured using a DuPont 990 differential scanning calorimeter (DSC). Typical DSC curves obtained are shown in

TABLE 2. MOLECULAR WEIGHT BETWEEN CROSSLINKS, GLASS TRANSITION TEMPERATURES, EXPANSION COEFFICIENTS, AND FREE-VOLUME CONTENTS FOR EPOXY SAMPLES.

Sample	M	T_g (K)	$\alpha \times 10^4$ (K^{-1})	$T - T_g$ ($\tau_c = 10^{-9}$s)	$T - T_g$ ($\tau_c = 10^{-10}$s)	f* ($\tau_c = 10^{-9}$s)	f* ($\tau_c = 10^{-10}$s)
0:5:5	∞	304	4.69	69	102	0.0574	0.0728
2:3:5	1080	307	4.02	76	116	0.0556	0.0716
3:2:5	680	319	3.82	78	122	0.0548	0.0716
5:0:5	355	340	3.40	81	128	0.0525	0.0685

*Assuming f (T_g) = 0.025

GP41-0053-3

Figure 37. The values of T_g listed in Table 2 and plotted in Figure 38 increase linearly with M^{-1}. These results are consistent with other reports.[17]

Molecular mobility in the samples was determined by using EPR to evaluate the rotational correlation time τ_c of TEMPENE dissolved in each epoxy matrix. The EPR line shapes for TEMPENE in these samples indicate that at each temperature the spectrum can be characterized by essentially one value of the rotational correlation time. Typical temperature dependence of the observed line shapes is shown in Figure 39.

Nitroxides exhibit slow-phase spectra when $\tau_c > 3 \times 10^{-9}$ s and fast-phase spectra when $\tau_c < 3 \times 10^{-9}$s. The onset of motional collapse occurs at $\tau_c \approx 10^{-7}$ s, whereas line narrowing occurs in the region $2 \times 10^{-11}\text{s} \lesssim \tau_c \lesssim 3 \times 10^{-9}$ s. Fast-phase spectra were observed for TEMPENE only when the host matrix was above its T_g value. In this region, $\tau_c < 3 \times 10^{-9}$ s, the rotational correlation time was evaluated from the EPR line shapes using the theory of Kivelson.[18] The equation used was:

$$\tau_c = 4 \left[\left(\frac{Y(0)}{Y(1)} \right)^{1/2} + \left(\frac{Y(0)}{Y(-1)} \right)^{1/2} - 2 \right] b^{-2} \, W(0)^{-1} \qquad (3a)$$

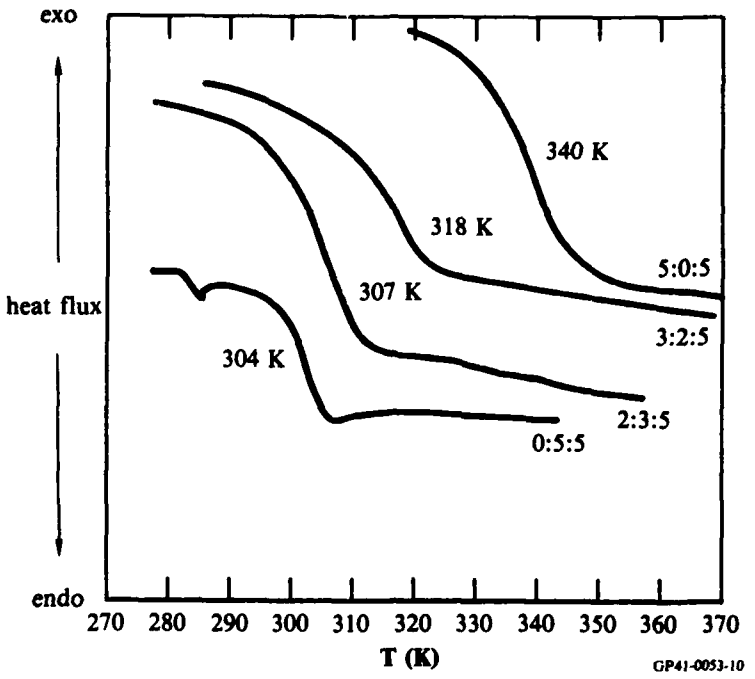

Figure 37. DSC curves showing glass transitions for epoxy samples having different crosslink densities.

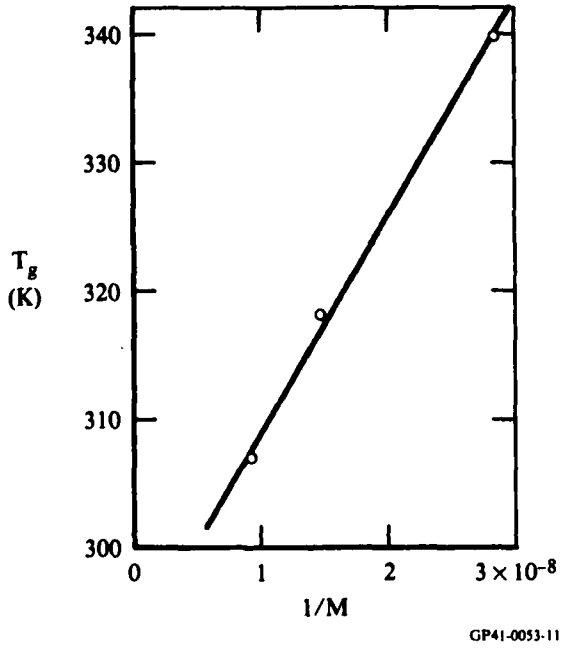

Figure 38. Glass transition temperatures of epoxy samples plotted as a function of the reciprocal of molecular weight between crosslinks.

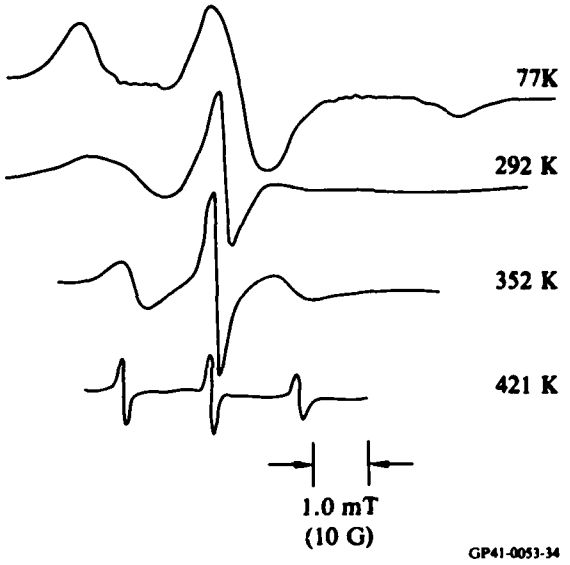

Figure 39. Spectra of TEMPENE in 3:2:5 TGDDM:DGEBA:DDH recorded at different temperatures.

with

$$b = \frac{4\pi}{3}\left[A_{zz} - \frac{1}{2}(A_{xx} + A_{yy})\right] \qquad (3b)$$

where Y(1), Y(0), Y(-1) are the intensities of the low, middle, and high field lines; A_{xx}, A_{yy}, and A_{zz} are the principal values of the nitrogen hyperfine interaction tensor; and W(0) is the width of the center line. The values A_{zz} = 3.51 mT and $A_{xx} = A_{yy}$ = 0.6 mT were used for TEMPENE.

The τ_c values were determined for TEMPENE in each of the TGDDM:DGEBA:DDH samples from T_g + 80 K to T_g + ~ 115 K. The calculated values are plotted on a logarithmic scale as a function of reciprocal temperature in Figure 40. The linearity of the plots over the range $\tau_c = 10^{-9}$s to $\tau_c = 10^{-10}$ s indicates that the data follow an Arrhenius behavior, viz.,

$$\tau_c = \tau_{co} \exp(\Delta E/RT) \qquad (4)$$

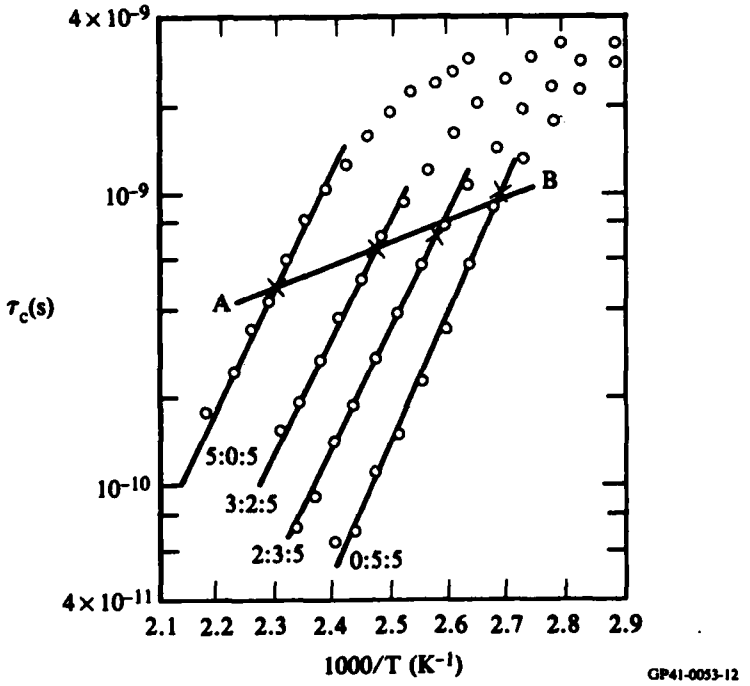

Figure 40. Correlation time of TEMPENE as a function of reciprocal temperature in samples having different crosslink densities. Along line AB, free volume is constant.

where τ_{co}^{-1} is the frequency factor and ΔE is an activation energy for the rotational motion of the spin probe. Typical values of $\tau_{co} = 10^{-20}$ s, $\Delta E = 50$ kJ mol^{-1} were obtained from the data. Since the former value has no physical meaning for times shorter than $\tau_{co} = 10^{-13}$ s, it seems unlikely that the observed temperature dependence of τ_c follows a true Arrhenius behavior, i.e., that the observed activation energy corresponds to a real physical barrier height.[19]

The temperature at which each sample has a given τ_c value (say, 10^{-9} s) depends on its crosslink density, as is evident from the line shapes shown in Figure 41 which were observed for TEMPENE in samples with different crosslink densities at approximately the same temperature. This dependence is a result of T_g increasing with crosslink density (see Figure 38). A related result, shown in Figure 42, is that $\log(\tau_c)$ increases linearly with crosslink density at constant temperature. This relation is a consequence of a) τ_c increasing with T_g and b) the slopes in Figure 40 being parallel.

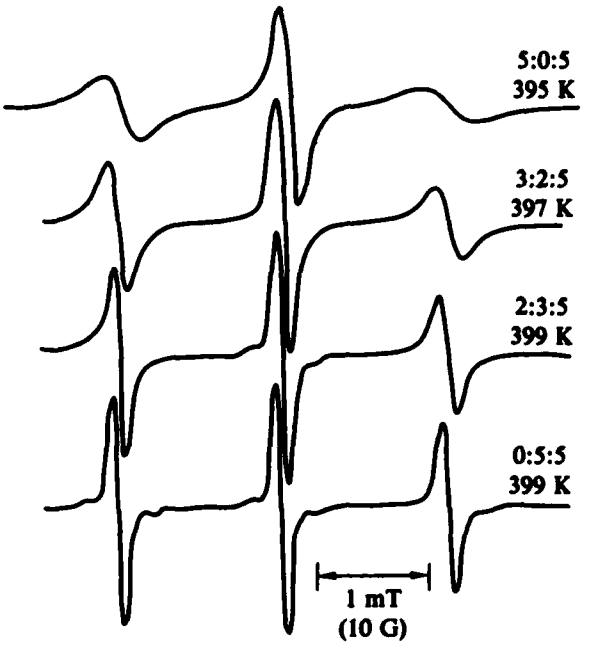

Figure 41. EPR spectra of TEMPENE in epoxy samples of different crosslink densities at nearly the same temperature. All samples are above their glass transitions.

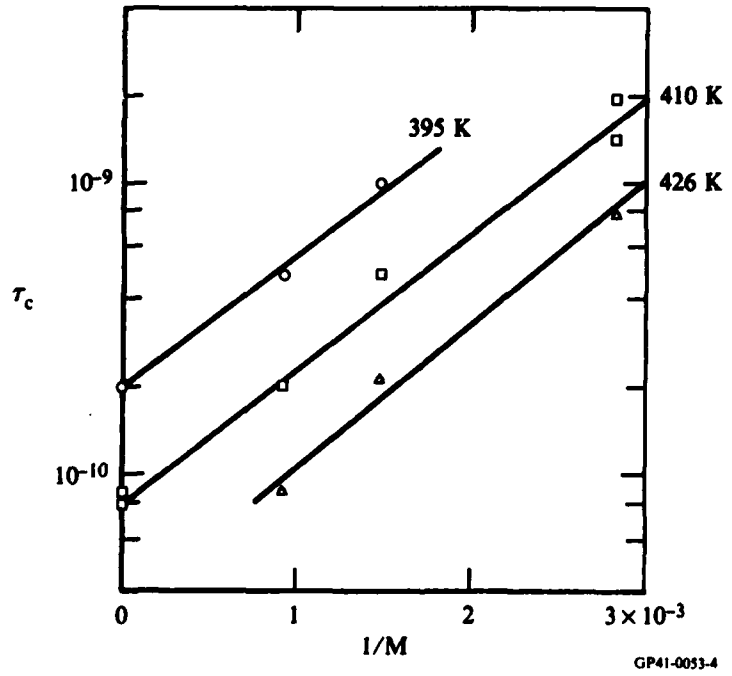

Figure 42. Correlation time for TEMPENE plotted as a function of crosslink density for epoxy samples at selected temperatures.

In addition, as shown in Figure 43, the correlation time data show excellent agreement with the following modified form of the WLF equation:[20]

$$-1/\ln(\tau_c/\tau_{cR}) = f_R^2/[B\alpha(T-T_R)] + f_R/B \qquad (5)$$

where τ_c and τ_{cR} are the rotational correlation times of the spin probe at temperature T and reference temperature T_R, respectively; f_R is the free volume fraction at T_R; B (≈ 0.4 to 0.6) is the coefficient that appears in the Doolittle equation;[20] and α is the difference in thermal expansion coefficients above and below T_g. Typical plots of $-1/\ln(\tau_c/\tau_{cR})$ as a function of $1/(T-T_R)$ for all samples are shown in Figure 43. The linearity indicates that TEMPENE follows Equation (5) in all cases. Agreement of the data with Equation (5), which is based on the concept of free volume, implies that above T_g the τ_c values for TEMPENE depend on the fractional free volume in the host polymer.

It is clear, however, that τ_c does not depend exclusively on sample free volume since the spectral line shapes (and therefore the τ_c values) change

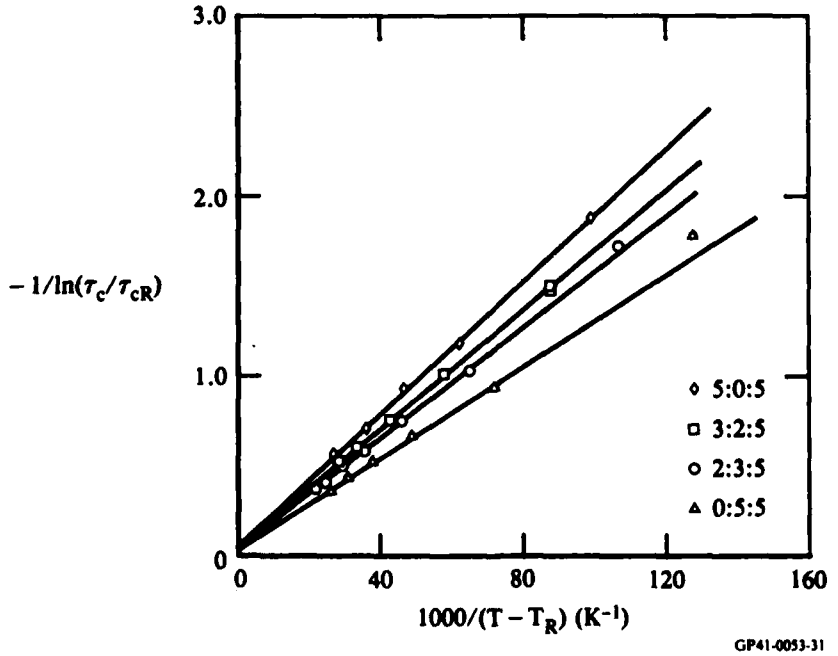

Figure 43. WLF plots for TEMPENE in samples of different crosslink density. Explicit temperature dependence has not been subtracted.

with temperature even below T_g where the free volume is considered to be constant (ignoring physical aging effects). We can therefore reasonably assume that above T_g, there is an explicit dependence of the TEMPENE motional correlation times on absolute temperature in addition to the temperature dependence in the modified WLF equation. The following evidence supports this contention.

The free volumes were calculated from the thermal expansion coefficients which were, in turn, determined from linear expansion data obtained with a thermomechanical analyzer (DuPont 942) interfaced with a console (DuPont 1090). Typical thermal expansion data as a function of temperature for several epoxy samples are shown in Figure 44. Linear expansion coefficients were measured over a range from T_g - 70 K to T_g + 80 K and the free volume contents were calculated using the following equation:

$$f(T) = f(T_g) + \alpha\ (T-T_g) \qquad (6)$$

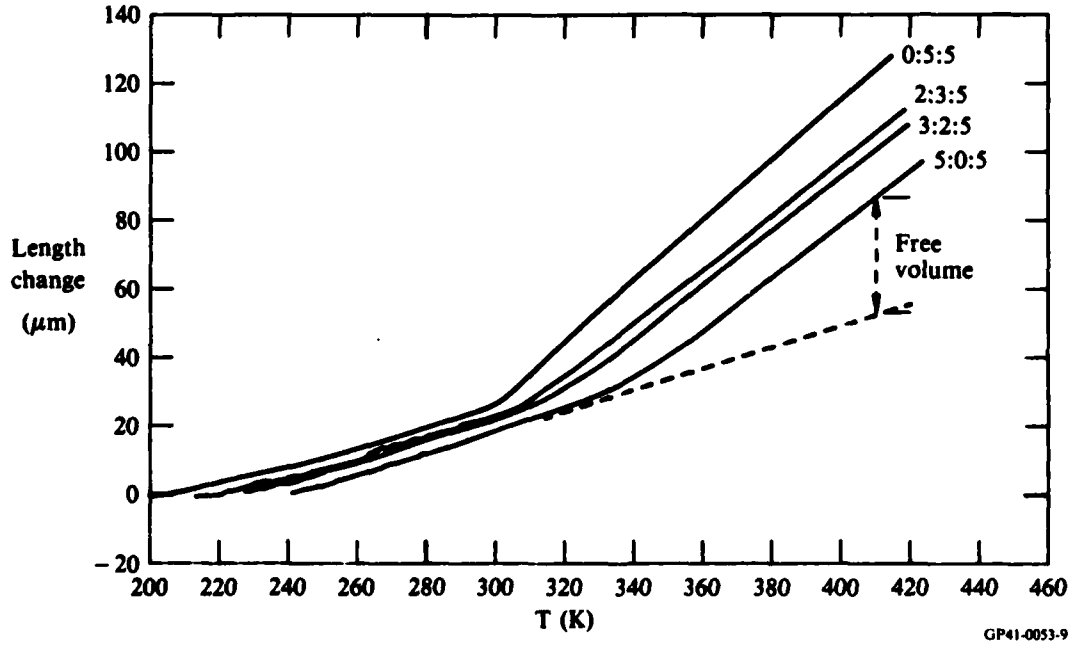

Figure 44. Thermal expansion of epoxy samples having different crosslink densities. Sample lengths are normalized to an initial value of 4.0 mm.

where f(T) and $f(T_g)$ are the fractional free volumes at T and T_g, respectively, and α is the difference in volume expansion coefficients above and below T_g. The value 0.025 was used for $f(T_g)$ for all samples. It is implicit in the free volume calculations that each sample has the same free volume fraction at T_g (whether the exact value is 0.025 is unimportant). The spectral evidence to support this assumption is shown in Figure 45. Thus, at the same absolute temperature, the line shapes (and hence the τ_c value) for TEMPENE in all epoxy samples below T_g are almost the same.

Expansion coefficients are listed in Table 2 along with fractional free volume values of the samples at $\tau_c = 10^{-9}$ s and $\tau_c = 10^{-10}$ s. From this table, the fractional free volume corresponding to $\tau_c = 10^{-9}$ s for the 0:5:5 sample is 0.057. Using Equation (6) and the measured T_g and α values shown in Table 2, this same free volume content corresponds to the temperature 388, 404, and 435 K in the 2:3:5, 3:2:5, and 5:0:5 samples respectively. These temperatures are denoted by "X" in Figure 40. Line AB drawn through these points is a calculated "iso-free volume" line and can be considered the temperature dependence of τ_c in a sample maintained, by an appropriate adjustment

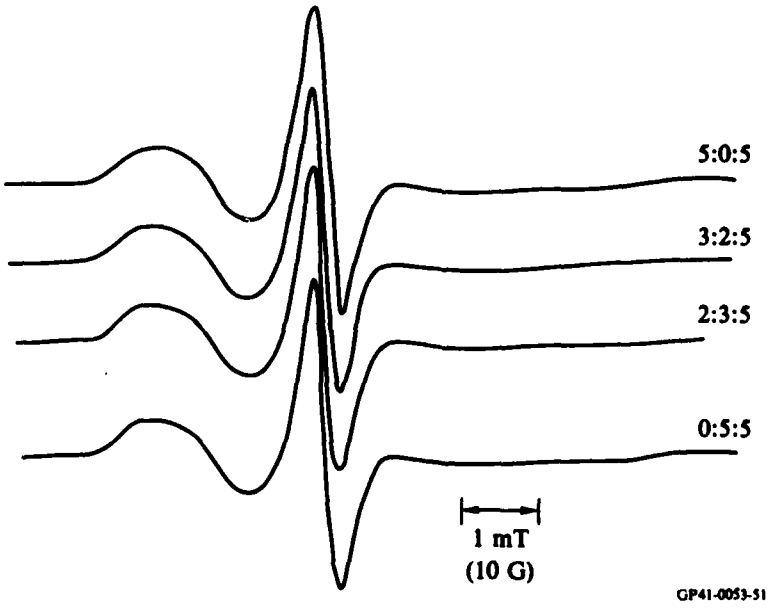

Figure 45. EPR spectra of TEMPENE in epoxy samples of different crosslink densities at the same temperature. All samples are below their glass transitions.

of the crosslink density, at a constant free volume value of 0.057. Analysis of line AB yields an activation energy $\Delta E = 14$ kJ mol^{-1} from the slope and a frequency factor $\tau_{co}^{-1} = 10^{-11}$ s^{-1}. Since line AB describes an Arrhenius contribution to the temperature dependence of τ_c, the quantity $\Delta E = 14$ kJ mol^{-1} can be considered a barrier height for the TEMPENE rotational motions.

To describe quantitatively the above results for the rotational correlation time for TEMPENE, we use an expression that explicitly includes both free volume and temperature as the independent variables determining τ_c. This expression is analogous to one describing the temperature dependence of translational diffusion[20] and can be written in the following form

$$\ln \frac{\tau_c}{\tau_{cR}} = \ln \frac{\tau_c}{\tau_{cR'}} + \ln \frac{\tau_{cR'}}{\tau_{cR}} \tag{7a}$$

with

$$\ln \frac{\tau_c}{\tau_{cR'}} = B\left(\frac{1}{f} - \frac{1}{f_R}\right) \tag{7b}$$

and

$$\ln \frac{\tau_{cR'}}{\tau_{cR}} = \frac{\Delta E}{R}\left(\frac{1}{T} - \frac{1}{T_R}\right) \tag{7c}$$

where τ_c is the rotational correlation time for TEMPENE at temperature T and free volume fraction f calculated from Equation (6) assuming $f(T_g) = 0.025$; τ_{cR} is the corresponding value of τ_c at T_R and f_R, the reference temperature and free volume fraction, respectively; $\tau_{cR'}$ is the value of τ_c at T and f_R (e.g., for the 0:5:5 sample, $\tau_{cR'}$ lies on line AB); and B is the Doolittle parameter. The free volume dependence of τ_c in Equation (7b) is in the form of the Doolittle equation,[20] whereas the explicit temperature dependence of τ_c in Equation (7c) is written in the form of an Arrhenius equation.

The relative contributions to τ_c from Equations (7b) and (7c) can be seen from the plot for the 0:5:5 sample in Figure 40. The isothermal change in τ_c from $\tau_{cR'}$ to τ_c is given by Equation (7b); the change in τ_c from its reference value 10^{-9} s to the value on line AB is given by Equation (7c), for example, at 406 K, $\tau_{cR} = 10^{-9}$ s, $\tau_{cR'} = 6.3 \times 10^{-10}$ s, and $\tau_c = 10^{-10}$ s. Thus, as the sample is heated so that τ_c goes from 10^{-9} s to 10^{-10} s, approximately 20% of the change in τ_c arises from the explicit temperature dependence, whereas 80% of the change is due to a change in the fractional free volume.

Plots of $\ln(\tau_c/\tau_{cR'})$ as a function of 1/f are shown in Figure 46. It is clear from the linearity of the plots that the motional correlation times after removing the Arrhenius contribution follows Equation (7b). The same data are shown in Figure 47 in the form of WLF plots. The linearity in these plots indicates that the τ_c values obey the WLF equation, Equation (5), even after correcting for the explicit temperature dependence. The slopes of the lines in Figure 46 are equal to -B, the Doolittle parameter, and are in the range 0.3 to 0.5. Rotational diffusion of TEMPENE is therefore less sensitive to free volume changes than is translational diffusion where B ≈ 1. This result is not surprising since translational diffusion requires free volume

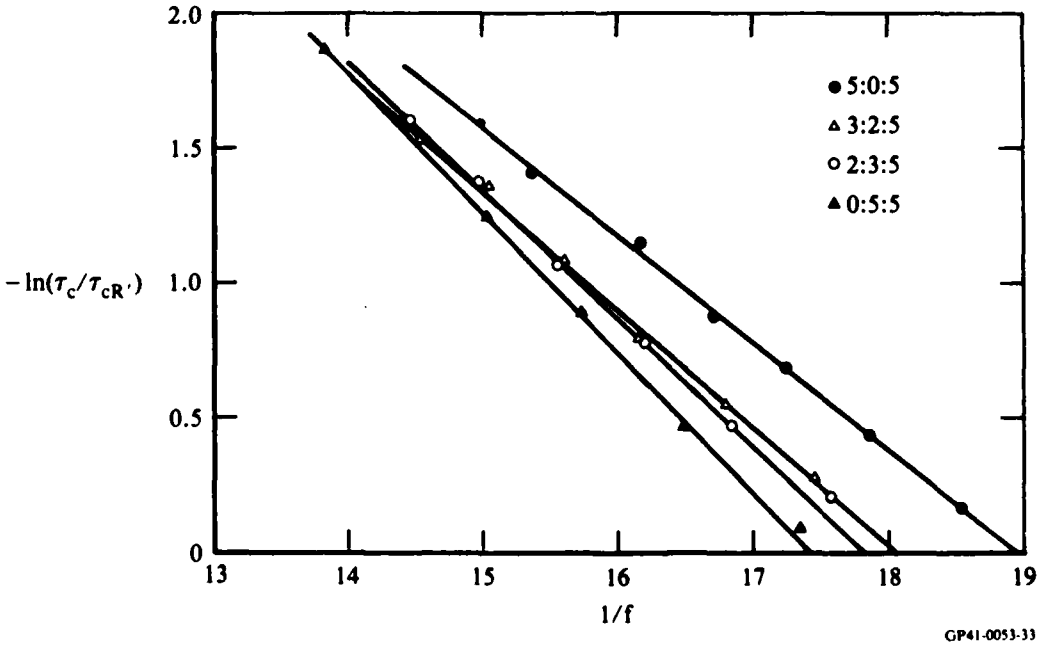

Figure 46. Plots of $-\ln(\tau_c/\tau_{cR'})$ as a function of 1/f for TEMPENE in samples having different crosslink densities.

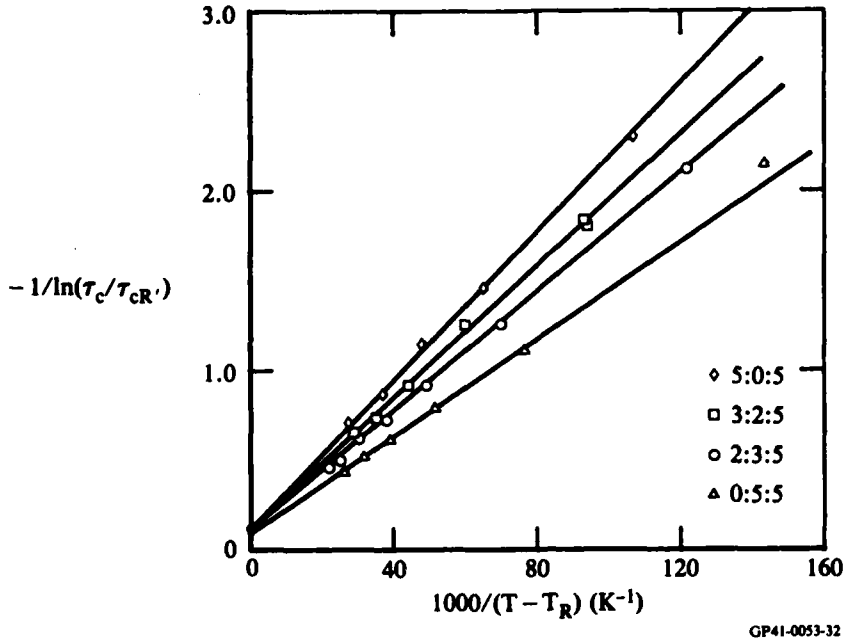

Figure 47. WLF plots for TEMPENE in samples of different crosslink density. Data corrected for explicit temperature dependence (Arrhenius contribution to τ_c).

holes, approximately the diameter of the diffusing molecule, whereas rotational diffusion requires much smaller free volume holes.[21]

2.5 Determination of the Number of Unreacted Functional Groups

In this task, we further investigated our previously devised methodology[13] of using the spin-label/spin-probe EPR technique to determine the number of unreacted functional groups in an amine-cured epoxy sample. The procedure consists of introducing amine nitroxide (glycidyl nitroxide) spin probes into a plasticized sample of the cured epoxy polymer for a long enough time to allow them to react with the unreacted epoxy groups (amine groups) and bind into the polymer network. Any unreacted nitroxide spin probe is removed by successive washes of the sample. The spin count determined from the area under the EPR absorption line shape of the dry sample then gives the number of unreacted functional groups.

The epoxy systems investigated were TGDDM and DGEBA, each cured with a stoichiometric amount of DDH. The TGDDM samples were postcured at 365 K for 2 h. These samples were sliced into ~ 0.1-mm shavings and immersed for ~ 1

month in benzene solution containing either 25 wt% TAMIN or ~ 15 wt% glycidyl TANOL. DGEBA samples (shavings) which were not postcured were immersed for ~ 10 months in benzene solution containing either ~ 15 wt% METAMIN or ~ 15 wt% DIMETAMIN. In addition, benzene-swelled DGEBA/DDH samples (solid 5-mm-diameter cylinders), both postcured and nonpostcured, containing a few percent TAMIN were allowed to react for ~ 10 months. All samples were continuously washed with methylene chloride for > 2 days using a Soxhlet extractor and dried at room temperature in a vacuum oven before the EPR measurements were made. The number of unreacted epoxy and amine groups found in the amine-cured epoxy samples with this technique are shown in Table 3.

Both unreacted epoxy and unreacted amine groups were found in the TGDDM samples. The amount of glycidyl TANOL that reacted to form a spin label was approximately three times greater than the amount of TAMIN that reacted. Thus, there are three times as many unreacted amine groups as there are unreacted epoxy groups. This result can be attributed to a) the inadvertent use of a slight excess (~ 2.0 wt%) of DDH, and/or b) some of the amine groups

TABLE 3. UNREACTED FUNCTIONAL GROUP CONTENT IN CURED DDH/TGDDM AND CURED DDH/DGEBA SAMPLES.

Sample	Percent unreacted amine or epoxy
Glycidyl TANOL in DDH/TGDDM(1)	3.0 (Amine)
TAMIN in DDH/TGDDM(1)	0.95 (Epoxy)
TAMIN in DDH/DGEBA(1)	1.5 (Epoxy)
TAMIN in DDH/DGEBA(2)	0.4 (Epoxy)
METAMIN in DDH/DGEBA(2)	0.7 (Epoxy)
DIMETAMIN in DDH/DGEBA(2)	1.5 (Epoxy)

GP41-0051-1

1) Postcured
2) Nonpostcured

exhibiting higher than expected functionalities through formation of quaternary nitrogen groups, and/or c) the glycidyl TANOL binding to a tertiary amine to form a spin-labeled quaternary base.

It is, at first sight, surprising that 0.95 wt% unreacted epoxy groups were detected in the presence of ~ 3.0 wt% unreacted amine groups. This result implies that steric constraints imposed on both unreacted groups by the network rigidity prevent them from reacting with one another.

Only the number of unreacted epoxy groups were measured in the DGEBA samples. The values reported in Table 3 are much greater than the values determined in our previous study.[9] The experimental difference is that in this study the samples were exposed to the nitroxide for ~ 10 months, whereas previously they were exposed for only ~ 10 days. Thus, the reaction rates of the nitroxides in the plasticized epoxy are very slow, occurring over a time scale greater than one month. For this reason, even the values listed in Table 3 probably underestimate the actual amount of unreacted groups present and should be considered only as lower limit values.

The attractive feature of this method of using amine nitroxides and glycidyl nitroxides to determine the number of unreacted epoxy and amine groups, respectively, in a cured epoxy sample is the inherent sensitivity. Our estimate of the minimum detectable amount of unreacted epoxy groups is 10^{-3} wt%. The disadvantage of this method is the slow rate of reaction of the nitroxides with the functional groups trapped in the polymer network.

2.6 Discussion of EPR Results

The results of several previous studies[22-26] of amine-cured epoxy reactions indicated that an S_N2 mechanism was followed. These studies included a measurement of the kinetics which were usually second order and a delineation of the stereochemistry involved in the ring opening reactions.

In our studies of the reactions between the nitroxide amines and TGDDM, pseudo-first-order reaction kinetics are obeyed because the amine concentrations are so low, < 0.08 wt%, that the TGDDM concentration effectively remains constant throughout the reaction. One would expect the rates for METAMIN and DIMETAMIN to differ if the difference between the nucleophilic character of the amines is large enough. Since basicity is a measure of nucleophilic

character, the basicities of METAMIN and DIMETAMIN were measured from the pH values of their aqueous solutions. The results show that $K_b = 10^{-6}$ mol L^{-1} for DIMETAMIN and $k_b = 3 \times 10^{-7}$ mol L^{-1} for METAMIN (assuming no carbonate is present). Hence, if the nucleophilic character of the amine is important, then k_2 should be greater than k_1. However, the results in Figure 13 show that k_2 is always less than k_1.

There is considerable evidence to indicate that amine-epoxy reaction rates can be accelerated in solvents that can hydrogen bond with either the epoxy or the amine,[24-26] e.g., water, alcohols, or acids. The rate-determining step in such reactions involves transition states of the form shown in Figure 48. In the nitroxide amine reactions with TGDDM, remnant impurities in the TGDDM may play the role of hydrogen-bond donors. Both nitroxides can form transition states of the type in the Smith model (Figure 48a) but only METAMIN can form the Mika and Tanaka type (Figure 48b) since DIMETAMIN is a tertiary amine and it possesses no hydrogen-bond donors.

The Arrhenius dependence of k_1 (see Figure 13) indicates one value of the activation energy, 55 kJ mol^{-1}, which in turn implies that one transition-state complex is associated with the formation of TGDDM end-labeled with METAMIN. On the other hand, the curvature of the data in Figure 13 for DIMETAMIN could be interpreted as indicating the importance of two values of activation energy: 55 kJ mol^{-1} at 333 K and 18.5 kJ mol^{-1} at 383 K, evaluated from the straight lines shown. We can only speculate as to the nature of the two transition-state complexes associated with these values, but they probably involve two different hydroxyl-containing impurities. The difficulty comes in

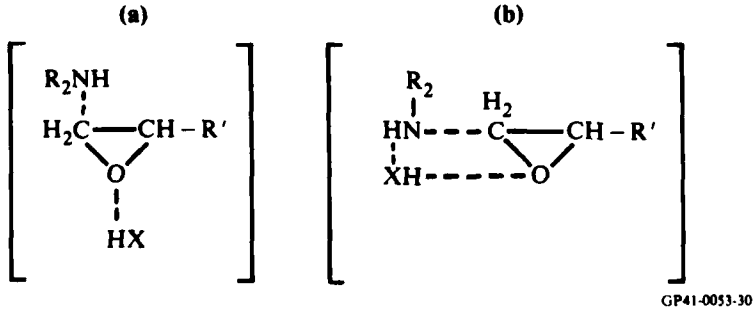

Figure 48. Proposed transition states involved in amine-epoxy curing reactions for (a) the Smith model and (b) the Mika and Tanaka model.

explaining the lower value of the activation energy at the higher temperatures. One possible explanation involves a temperature dependence of concentrations of species which are precursors to the formation of the transition-state complexes. Such a scheme is depicted in Figure 49. At low temperatures, 333 K, the concentration of AB_1 is large compared with the concentration of AB_2, and mechanism 1 with activation energy ΔE_1 dominates. At higher temperatures, ~ 383 K, the AB_1 concentration is reduced, and mechanism 1 is effectively "turned off." Mechanism 2 with activation energy ΔE_2 then dominates. As described above, the data shown in Figure 22 also suggest that more than one impurity is present in TGDDM.

It is interesting to compare the values of k_1, k_2 in TGDDM and the corresponding values for DGEBA.[13] These values are summarized in Table 4 where the values have been normalized to the slowest value measured, i.e., k_2 in TGDDM at 333 K. The value of k_1 in DGEBA at 333 K is 33 times faster than the corresponding value in TGDDM. The reason for this may not be in the inherent rates for epoxy-amine reactions but in the fact that purified TGDDM contains less hydroxyl-containing impurities than DGEBA. Furthermore, in DGEBA $k_1 = k_2$ whereas in TGDDM $k_1 > k_2$ at all temperatures studied. Thus, only in the highly purified TGDDM does the nature of the amine produce significant differences in the rate constant although, as stated earlier, this does not involve the nucleophilic character of the amine.

As shown in Table 4, at 333 K the value of k_1 in TGDDM is 3.5 times faster than k_2 in TGDDM. Using transition state theory, one can explain this rate differences in terms of an activation entropy difference. Since the activation energies for the two resins are the same at 333 K, one can write

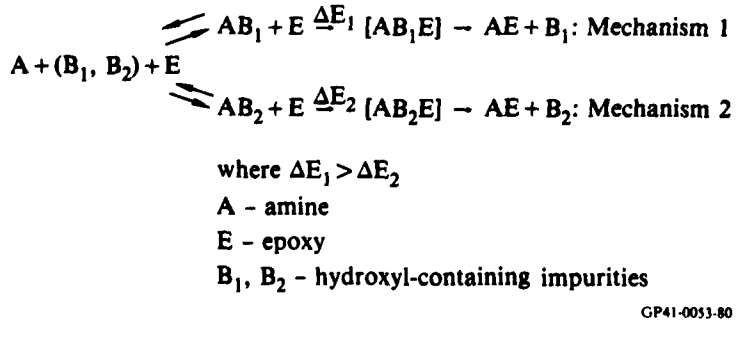

Figure 49. Two possible reaction mechanisms.

TABLE 4. RELATIVE* RATE CONSTANTS FOR METAMIN (k_1) AND DIMETAMIN (k_2) IN TGDDM.

Rate constant	Resin	T = 333 K	T = 373 K
k_1	DGEBA	115	26
k_1	TGDDM	3.5	31
k_2	DGEBA	115	26
k_2	TGDDM	1	31

*Rate constants are normalized to the value of k_2 in TGDDM at 333 K.

GP41-0053-82

$$\Delta S_1^{\ddagger} - \Delta S_2^{\ddagger} = R \ln \frac{k_1}{k_2} \qquad (8)$$

where $\Delta S_1^{\ddagger}$ and $\Delta S_2^{\ddagger}$ are the activation entropies associated with reaction rates for METAMIN in TGDDM and DIMETAMIN in TGDDM, respectively. Since $k_1/k_2 = 3.5$, $\Delta S_1^{\ddagger} - \Delta S_2^{\ddagger} = 10.4$ J mol^{-1} K^{-1}, the difference in activation entropy may be attributed to the larger steric hindrance around the quaternary nitrogen.

The work on molecular mobility described in Section 2.4 shows that the nitroxide TEMPENE functions as a probe of its environment in the amine-cured epoxies. Above T_g its rotational correlation time is sensitive to the following sample parameters:

(a) free volume,
(b) absolute temperature,
(c) temperature above T_g, and
(d) average crosslink density.

The results in Section 2.5 demonstrate that both unreacted amines and unreacted epoxy groups can be detected in the same sample, with glycidyl nitroxides and amine nitroxides, respectively. Further work is necessary to ascertain how important spin-labeled quaternary base formation is to the values obtained for the amounts of unreacted amine present. Yet, it seems likely that from the numbers obtained in any particular sample, it should be possible to identify the exact reason for the unreacted groups; i.e., whether they arise from the use of nonstoichiometric amounts of resin and curing agent, inadequate mixing, or steric constraints imposed by the polymer network that prevent reaction of all the functional groups.

3. NMR EXPERIMENTS ON EPOXY RESINS

3.1 ^{1}H NMR Monitor of MY720 Cure with Eporal

Pulsed hydrogen NMR measurements were performed on a single-coil spectrometer operating at 100 MHz. An external fluorine lock sample at 94 MHz was used to control a magnet (Varian V-4014) so that small signals could be signal averaged for a long time without attendant drift. The 100- and 94-MHz rf signals were derived from a frequency synthesizer (Hewlett Packard HP5100), and the 8-mT pulsed rf magnetic field was generated using a programmable digital pulser and a 100-W linear amplifier (Electronic Navagation Industries 3100L). The dead time of the receiver was < 6 μs. A digital oscilliscope (Nicolet 4094) was used to acquire and store the signals, and a computer (Digital Equipment Corp. MINC) was used to analyze the signals.

Three different pulsed ^{1}H NMR experiments were performed:

1) a (single 90°_x, collect signal) pulse experiment for measuring the relative amounts of rigid and mobile phases and their spin-spin relaxation times T_2, provided the T_2's were less than 1 ms.
2) a [90°_x, (sample signal, τ, 180°_y, τ)$_n$] pulse experiment for measuring the relative amounts of rigid and mobile phases and their spin-spin relaxation times T_2,[27] for T_2's greater than 1 ms, and
3) a (180°_x, τ, 90°_x, collect signal) pulse experiment to determine the spin-lattice relaxation times T_1.[28]

The epoxy resins were prepared from MY720 (a Ciba-Geigy product which is approximately 70% TGDDM) and Eporal (a Ciba-Geigy product which is more than 90% diaminodiphenylsulfone, DDS). MY720 was heated briefly to about 340 K and mixed with 27 parts Eporal per hundred parts MY720. The mixture was continuously stirred while the temperature was increased to 423 K. Long pipettes were used to transfer approximately 100-mg quantities of the mixture to several 5-mm NMR tubes. These tubes were sealed with plastic caps and stored at 250 K until they were used in the NMR experiments. While this mixing procedure caused some preliminary curing, it was a compromise chosen to eliminate errors caused by poor mixing.

The MY720/Eporal curing studies were performed in situ in a ^1H NMR probe heated with forced air. Four different isothermal curing temperatures were employed; 272, 388, 418, and 437 K. Prior to each experiment, an NMR tube containing a thermocouple immersed in 100-mg oil was inserted into the NMR probe. This thermocouple and thermocouples at the air inlet and outlet of the probe were monitored while the air flow and heater current were adjusted to achieve the desired sample temperature. During an experiment both the inlet and outlet temperatures were monitored and controlled, maintaining the sample temperature within 2 K of the desired temperature. When the duration of a curing study exceeded 8 h, the sample was removed from the probe and stored at 250 K until the next day. The samples were always placed in a preheated probe so that the sample temperature reached equilibrium in less than 5 min.

The NMR signals resulting from Experiments 1 and 2 generally contained two components, as shown in Figure 50. The computer performed a least-squares fit to the signals to determine the five parameters A_L, T_{2L}, A_G, T_{2G}, and n.

In the early stages of curing, only a single Lorentzian component was present ($A_L \neq 0$ and $A_G = 0$), as a result of the homogeneous, low-viscosity mixture in which the molecules were all free to undergo rapid, isotropic, liquid-like motion. As curing took place, a second Lorentzian component appeared; it had a small amplitude ($A_G < A_L$) and a shorter spin-spin relaxation time ($T_{2G} < T_{2L}$). The two Lorentzian components resulted from the formation of an inhomogeneous mixture in which some molecules were more free

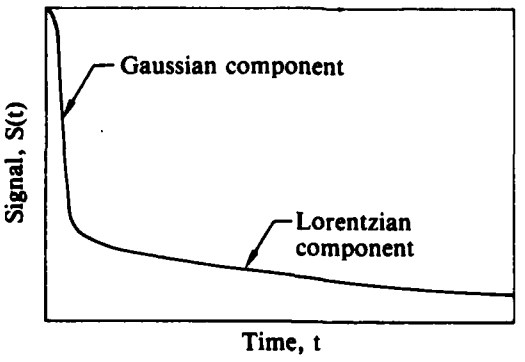

Signal = Gaussian component (rigid) + Lorentzian component (mobile)

$$S(t) = A_G \exp\left\{-(t/T_{2G})^n\right\} + A_L \exp\left\{-t/T_{2L}\right\}$$

GP41-0053-81

Figure 50. Hydrogen NMR decay signal.

to move, producing the L component, than others that were more restricted, producing the G component. A similar NMR effect has been reported for a different epoxy system[29] and supports the hypothesis of the formation of a nodular structure in epoxies.[2-7,9,10,13] As the curing proceeded, both T_{2L} and T_{2G} decreased and A_G increased at the expense of A_L, as a result of the decreased molecular motion caused by curing. In the last stages of curing, the parameter n increased from n = 1, characteristic of a liquid-like Lorentzian component, to n = 2, characteristic of a rigid Gaussian component.

The spin-spin relaxation times during the isothermal cures at the four temperatures are shown in Figures 51-54. At the lowest curing temperature, 372 K, only a single Lorentzian component was observed during the first 200 min of cure, whereas two components were observed almost from the start in the other, higher-temperature cures. The relative amounts of the two components will be discussed later. At zero cure time the spin-spin relaxation time increased from 0.08 to 0.55 s with increasing cure temperature, from 372 to 437 K, as a result of the reduced viscosity at the higher temperatures. However, in the last stages of curing, it appears that the two components approach similar limiting values for the four different cure temperatures,

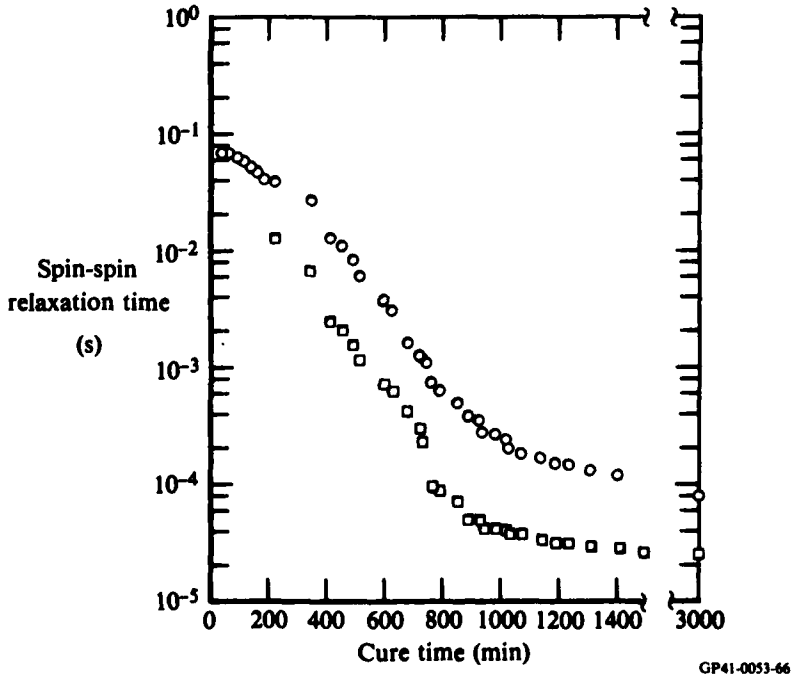

Figure 51. Spin-spin relaxation times of the mobile (○) and rigid (□) components during isothermal cure at 372 K.

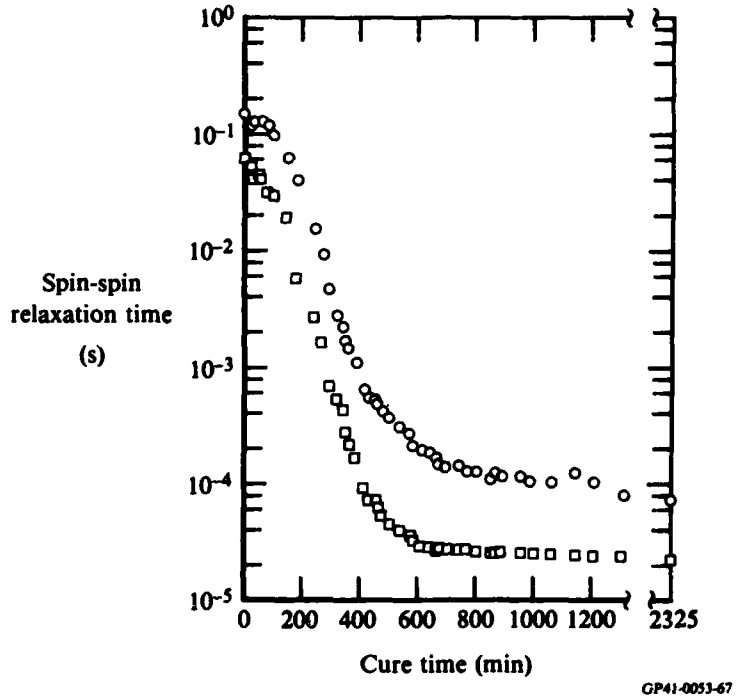

Figure 52. Spin-spin relaxation times of the mobile (○) and rigid (□) components during isothermal cure at 388 K.

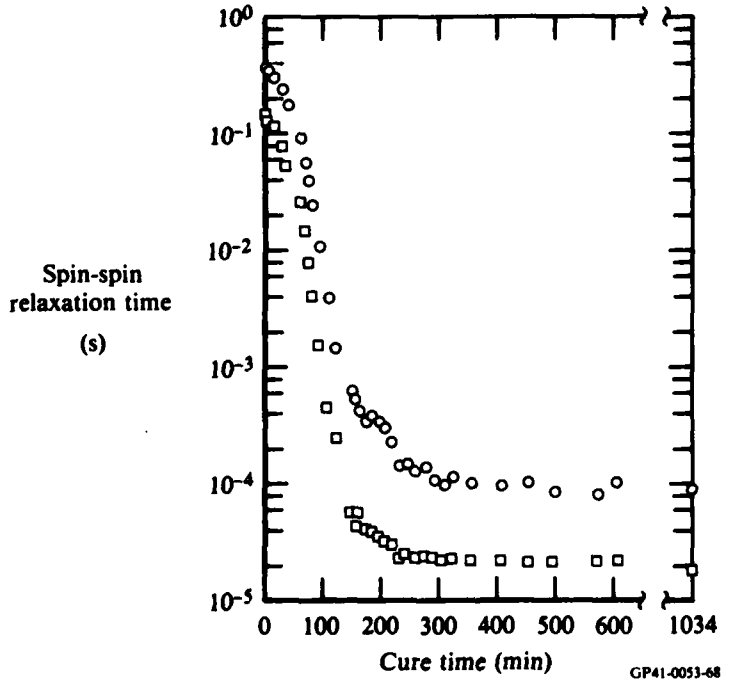

Figure 53. Spin-spin relaxation times of the mobile (○) and rigid (□) components during isothermal cure at 418 K.

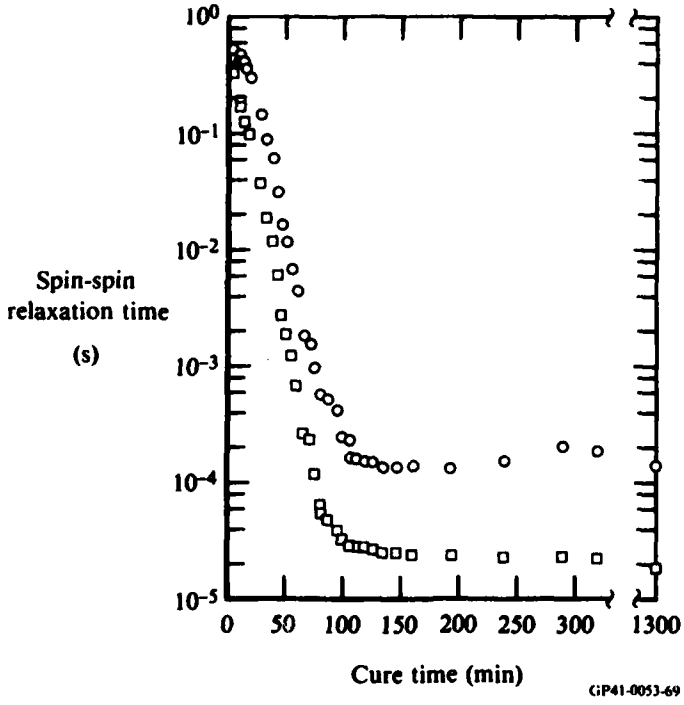

Figure 54. Spin-spin relaxation times of the mobile (○) and rigid (□) components during isothermal cure at 437 K.

$T_{2L} \sim 8 \times 10^{-5}$ s and $T_{2G} \sim 2 \times 10^{-5}$ s. In these measurements as well as others discussed in this report, the limiting values were obtained in the last stages of curing, which are identified in the figures.

Since the four samples have the same composition, it appears unusual that they should have almost identical spin-spin relaxation times after long cures at widely differing temperatures. One might expect that the sample at the highest temperature would have a largest spin-spin relaxation time because of the increased molecular motion at the highest temperature. The equality of the spin-spin relaxation times can be explained in terms of the Enns and Gillham model for curing of thermosetting polymers,[30] which states that a sample cured for a sufficiently long time at a temperature T_c which is below its ultimate glass transition temperature $T_{g\infty}$ will have a glass transition temperature $T_g = T_c$. Hence, all four samples at their respective cure temperatures are at their glass transition temperatures and therefore have similar spin-spin relaxation times. While it was not done, if the sample that was cured at the lowest temperature had been heated to the highest cure tempera-

ture, its spin-spin relaxation times, T_{2L} and T_{2G}, would have been much greater because the sample would have been at a temperature above its glass transition temperature (until it experienced additional curing).

The relative amounts of the two components are shown in Figures 55-58 where the fraction of the more mobile component, $A_L/(A_L + A_G)$, is plotted as a function of the cure time for the four cure temperatures. Because the mobile fraction is equal to 1 at the start of the low-temperature cure, we assume that it is equal to 1 at the start of all the cures. Extrapolating the data back to zero cure time for the higher temperature cures shows the data in agreement with this assumption. It is interesting that the cure at 372 K has a 200-min delay before the mobile fraction decreases, the cure at 388 K shows an almost linear decrease in the logarithm of the mobile fraction from zero cure time to the end of the cure, and the higher temperature cures show a rapid decrease in the mobile fraction at zero cure time, followed by a slower decrease at later cure times. Presently we have no explanation for these behaviors, although they are probably related to the nature of the crosslink structures forming during the cures at the different temperatures.

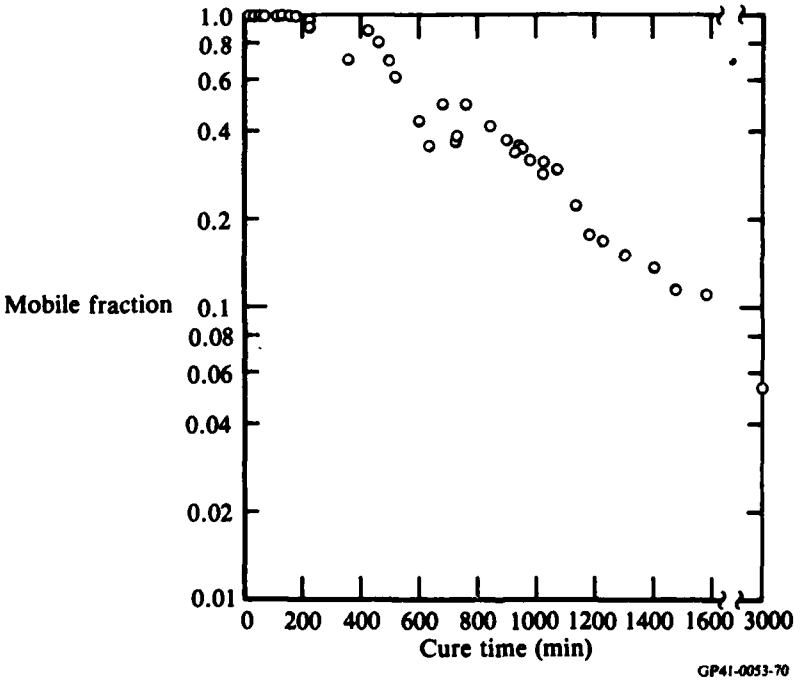

Figure 55. Mobile fraction during isothermal cure at 372 K. The limiting value was obtained after 3000 min cure.

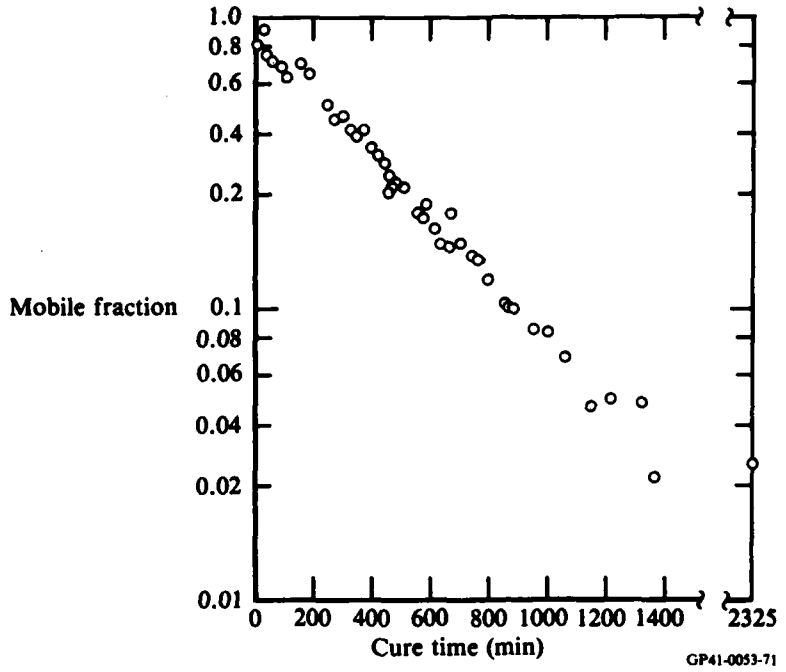

Figure 56. Mobile fraction during isothermal cure at 388 K.

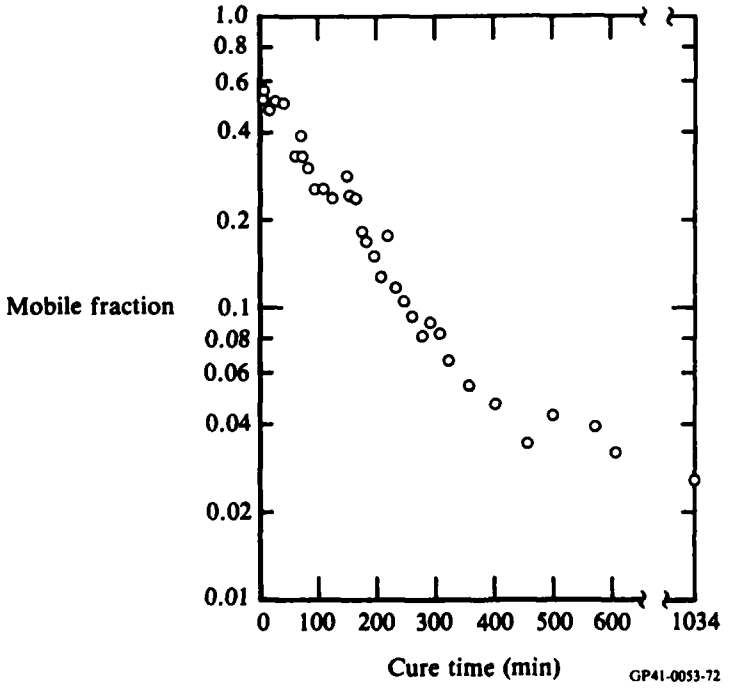

Figure 57. Mobile fraction during isothermal cure at 418 K.

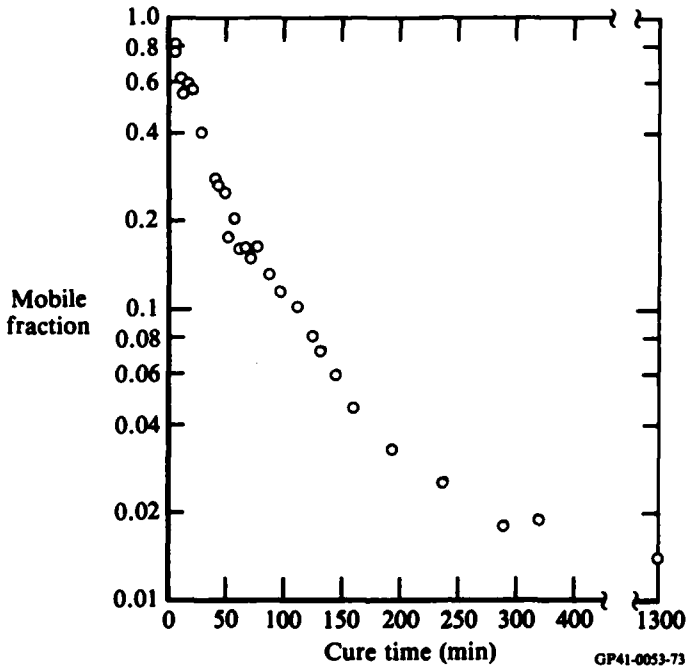

Figure 58. Mobile fraction during isothermal cure at 437 K.

The mobile fractions remaining in the last stages of curing are different for the different cure temperatures. This difference could result from not waiting long enough to correctly determine the limiting value. At the time the measurements were taken, it was thought that sufficient time had elapsed to reach equilibrium. However, calculated reaction rates based on measured activation energies (presented below) suggest that equilibrium may not have been reached. A positive result of these measurements is that they show that the mobile fraction is a sensitive indicator of the last stages of curing.

The third experiment listed above yielded spin-lattice relaxation times T_1's of the epoxies during their cures at the four different temperatures. As with the previous measurements, these were also made at the curing temperature. Generally, spin-lattice relaxation is fastest when the motion of some molecular group has a strong frequency component equal to that of the NMR frequency, 100 MHz in this case. This corresponds to a correlation time for molecular motion about 10^{-9} s. Since curing is expected to increase the correlation time for molecular motion, if the correlation time of a molecular group passes through 10^{-9} s during curing, the spin-lattice relaxation time should go through a minimum at the time when the correlation time is 10^{-9} s.

The spin-lattice relaxation times T_1 during the four different isothermal cures are shown in Figures 59-62. It is convenient to explain the data for the highest temperature cure at 437 K first (Figure 62), and then relate the data from the other cures to this one. As the curing proceeds, the spin-lattice relaxation time decreases from about 0.5 s in the uncured resin to a minimum of 0.27 s after 35 min of curing. The minimum is caused by molecular motion having a correlation time of 10^{-9} s. The spin-lattice relaxation time then increases to a limiting value of about 0.9 s. While it was not done, if the curing had been performed in a nitrogen atmosphere (in the absence of oxygen), the spin-lattice relaxation time would have undoubtedly increased to a larger value. Oxygen is paramagnetic and causes spin-lattice relaxation.

The spin-lattice relaxation time of the uncured resin before the cure at 418 K (Figure 61) is 0.36 s, smaller than that for the cure at 437 K (0.50 s). At the lower cure temperature, molecular motion is decreased, similar to the decrease in molecular motion caused by a 15-min cure at 437 K (Figure 62). However, the decrease in molecular motion caused by decreasing the temperature (increasing viscosity) is not the same as the decrease in

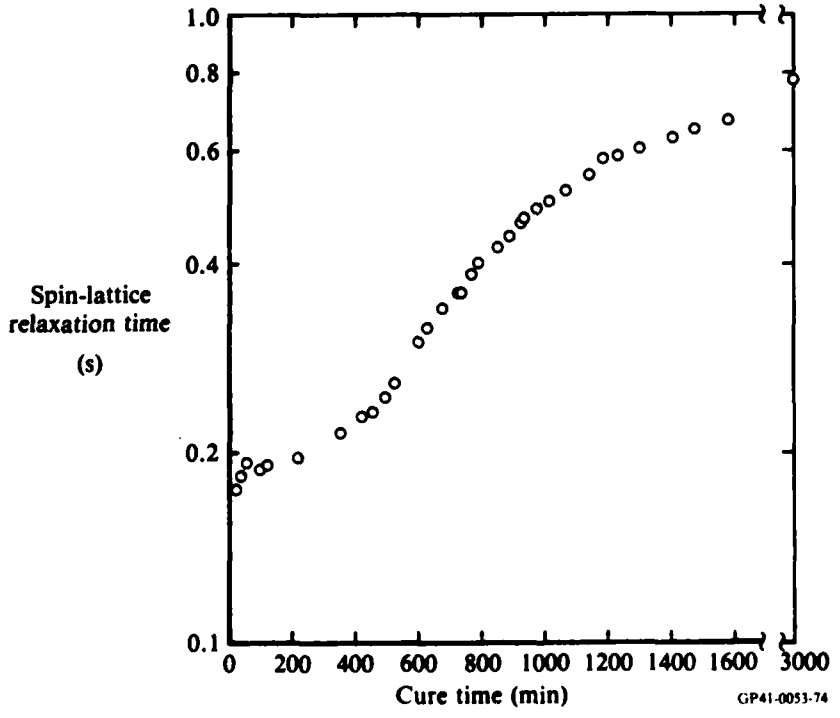

Figure 59. Spin-lattice relaxation time during isothermal cure at 372 K.

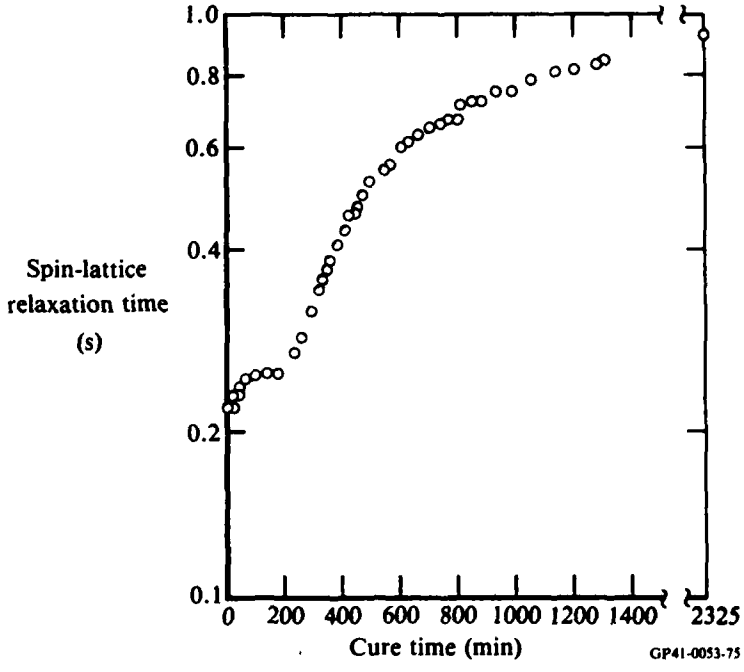

Figure 60. Spin-lattice relaxation time during isothermal cure at 388 K.

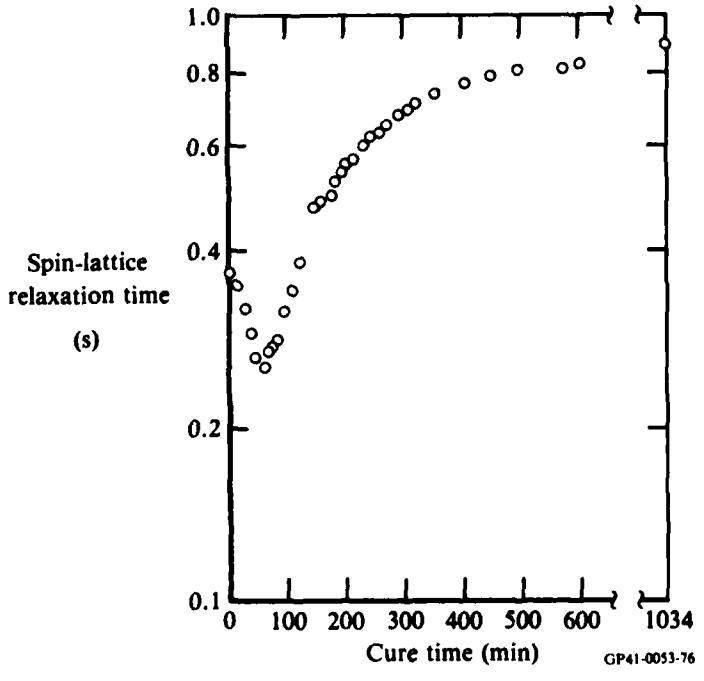

Figure 61. Spin-lattice relaxation time during isothermal cure at 418 K.

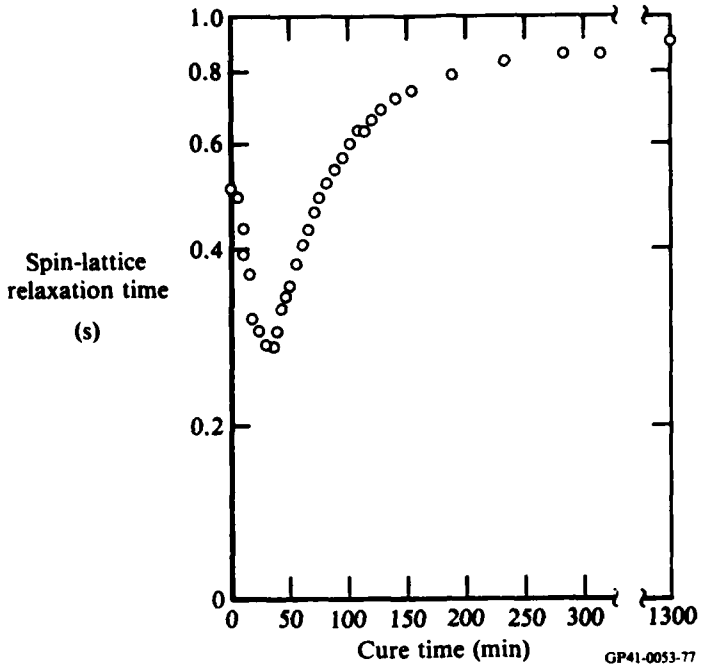

Figure 62. Spin-lattice relaxation time during isothermal cure at 437 K.

molecular motion caused by curing because different molecules are formed during curing. Thus, decreasing the cure temperature to 388 K (Figure 60) decreases the value of T_1 of the uncured resin to 0.215 s, and decreasing the cure temperature to 372 K (Figure 59) decreases the value of T_1 of the uncured resin to 0.17 s. However, a trace of a minimum in T_1 persists at all cure temperatures relatively early in the cure, and we conclude that this minimum results from the motion of a molecular group that is the product of the curing reaction which has a correlation time of 10^{-9} s. The identity of this molecular group has not yet been determined, nor has the group responsible for the minimum that appears to be at a temperature lower than 372 K in the uncured resin.

Five different methods were used to define a characteristic cure time for the cure at any temperature. The most obvious time is that required for the Gaussian or Lorentzian spin-spin relaxation times, T_{2G} or T_{2L}, to come to their limiting values. Because they approach their limiting values asymptotically, the time at which the extrapolated straight line section intersects the limiting value was taken to be the characteristic cure time.

A similar method was planned for the mobile fraction data, but the limiting values may be in error because the mobile fraction may continue to decrease for a longer time than expected. As a result, we arbitrarily chose the time at which the mobile fraction had decreased to 0.10. The fourth method was to plot the value of the parameter n as a function of cure time, as shown in Figure 63, and define the characteristic cure time as the time at which n = 1.5 (half-way between Lorentzian and Gaussian). The fifth method was to define the characteristic cure time as the time of the occurrence of the minimum in T_1.

The results of these five methods for defining a characteristic cure time are shown in Figure 64. The characteristic cure times defined by the T_{2G}, T_{2L}, and n data are in good agreement, and they fall nearly on the same straight line when the logarithm of their values are plotted as a function of 1/T. The slopes of these lines yield activation energies of 49.6 kJ/mol for the T_{2G} data, 52.2 kJ/mol for the T_{2L} data, and 47.3 kJ/mol for the n data. Characteristic cure times defined by the mobile fraction data are somewhat larger than those defined by the other methods. Nevertheless, they also fall on a straight line whose slope yields an activation energy of 54.7 kJ/mol. The data for the time of occurrence of the minimum in T_1 (no minimum in T_1 was observed for the cure at 372 K) yielded an activation energy of 45.4 kJ/mol. The average of these five results is 49.8 kJ/mol, and their standard deviation is 3.7 kJ/mol.

These results agree with activation energies determined from dielectric measurements and dynamic mechanical measurements on Narmco 5208, which is primarily MY720 and Eporal.[31] In the dielectric measurements two relaxation peaks were observed, one early in the reaction and one later. The time of the occurrence of the first peak yielded an activation energy of 46.0 kJ/mol, while that of the second yielded 55.7 kJ/mol. These agree very well with those determined with NMR, and both techniques showed an increase in activation energy as the curing proceeded. The dynamic mechanical measurements also showed two relaxation peaks which yielded activation energies of 67.6 and 50.7 kJ/mol, which do not agree as well.

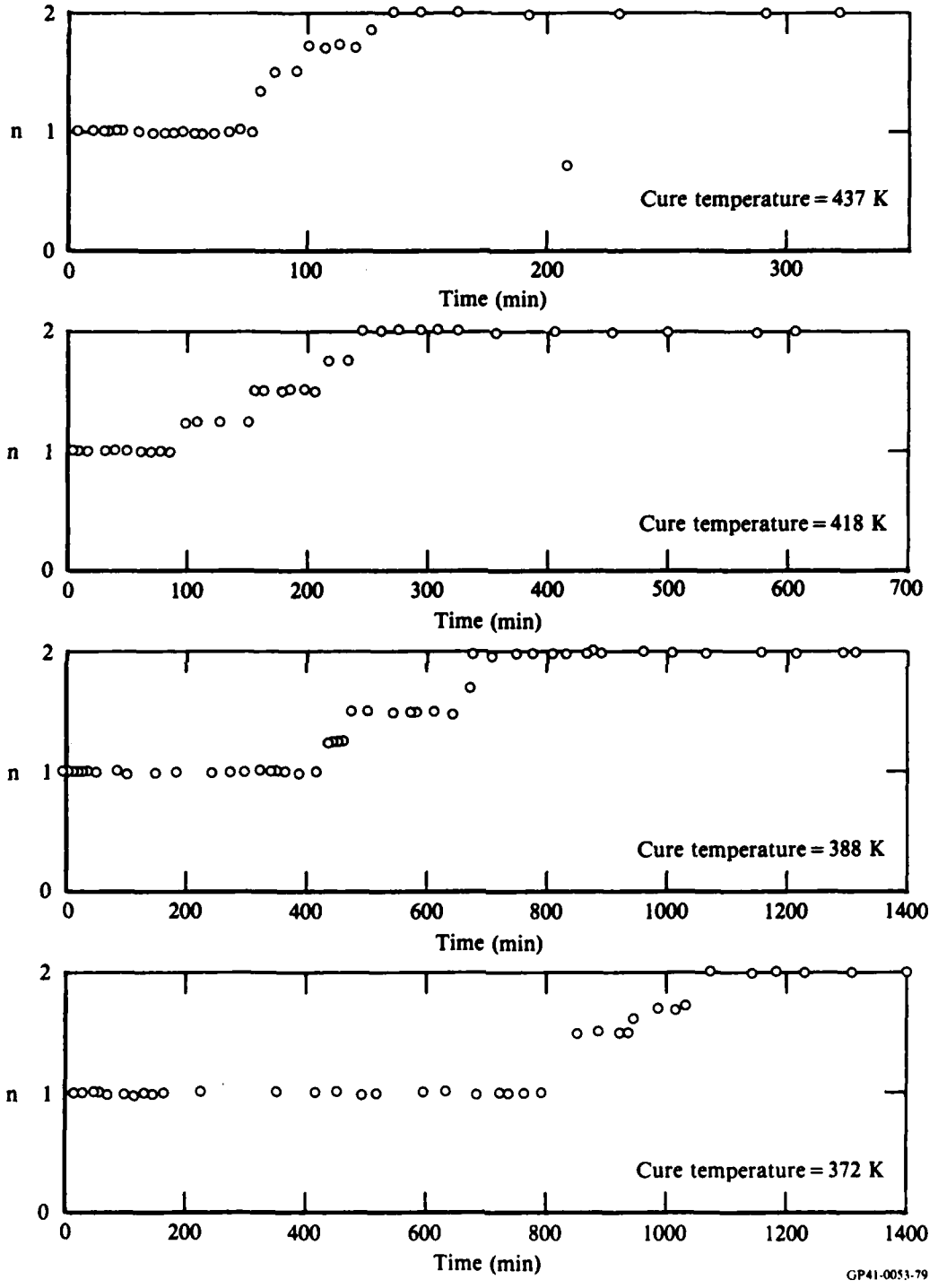

Figure 63. Value of parameter n during isothermal cures.

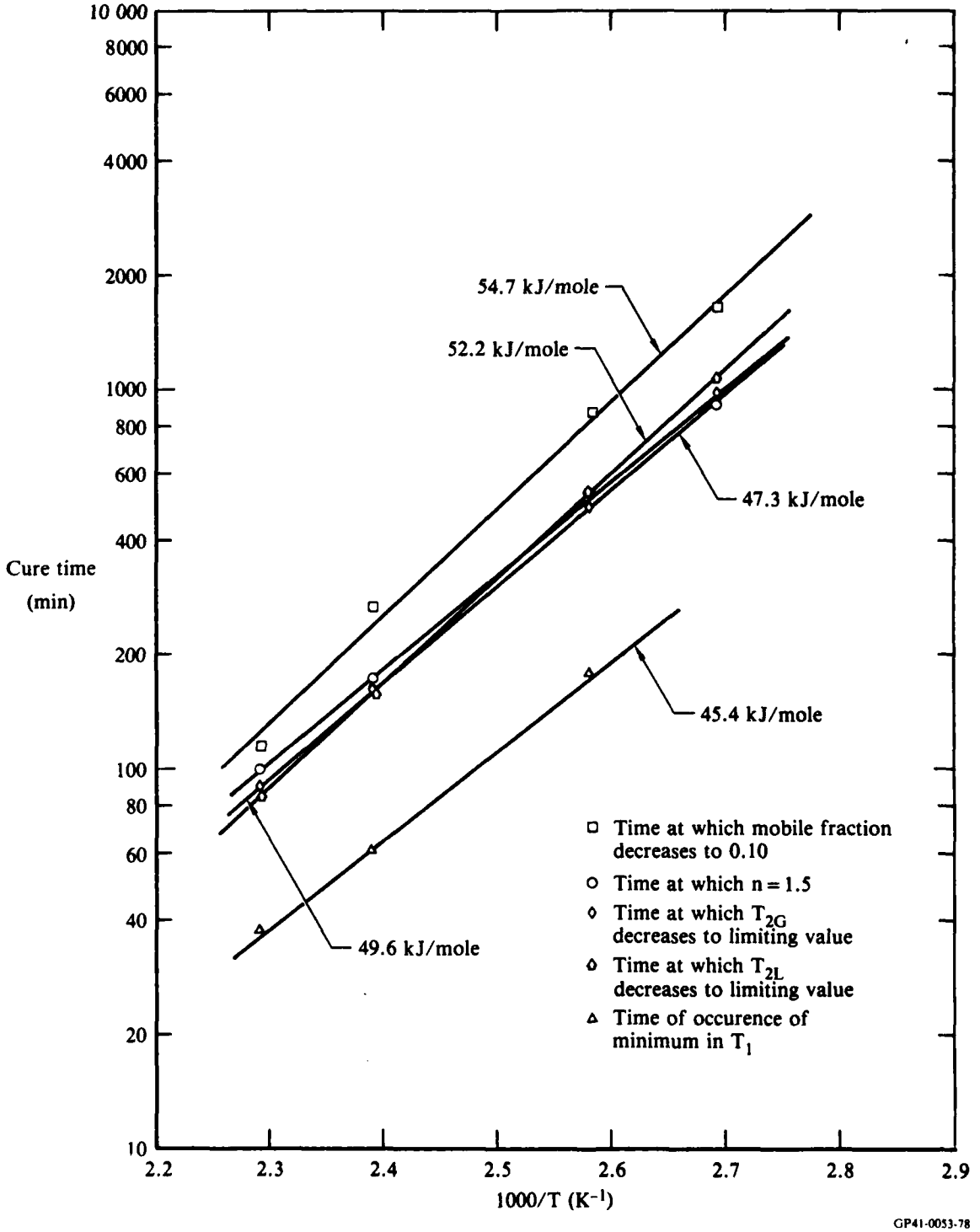

Figure 64. Cure times determined by five different methods plotted as a function of the reciprocal of the isothermal cure temperature. The slopes of the linear least-square-fit lines yield activation energies shown.

3.2 ^{13}C NMR Determination of the Composition of Cured Epoxies

In an effort to study the curing of epoxy resins through gelation into the solid state, ^{13}C NMR experiments were conducted to provide baseline spectra for the quantitative determination of compositions of cured epoxy resins.

The ^{13}C NMR experiments were performed at 15 MHz on a JEOL FX-60QS spectrometer equipped with a magic-angle spinner probe. The pulse sequence shown in Figure 65 was used for cross-polarization and high-power decoupling.[32,33] The magic-angle spinner bodies were fabricated from Kel-F; as a result they produced no ^{13}C spectral lines that could interfere with those of the samples. The spinner was usually operated at 2.4 kHz, which was sufficient to reduce the area beneath the sideband peaks to less than 5%. Cross polarization was accomplished using a Hartmann-Hahn[34] double resonance at approximately 50 kHz. Cross-polarization contact times between 0.5 and 5 ms were used; 1 ms was found to be optimum. The high-power decoupling field was 1.2 mT. The measurements were performed at 303 K. Spectra with good signal-to-noise ratios were obtained only after 10,000 or more accumulations.

Preparation of the four cured epoxy resin samples whose compositions were measured with solid-state ^{13}C NMR was as described in Section 2.4. Samples were prepared containing TGDDM:DGEBA:DDH ratios (by equivalents) of 5:0:5, 3:2:5, 2:3:5, and 0:5:5. In Figure 66 the carbon atoms in the epoxy and amines used in these samples are labeled by letters to aid in the discussion of the ^{13}C NMR spectra.

Figures 67-70 show the ^{13}C NMR spectra of the four cured epoxy resin samples that were obtained after 10,000 accumulations. The chemical shifts of the prominant resonances are shown below the spectra. A cross-polarization time of 1 ms was used because it produced spectra in which the areas beneath the resonance peaks were nearly proportional to the number of carbons causing the resonances. This proportionality is illustrated in Figure 71 which shows stick spectra. The heights of the solid sticks are equal to the measured fractional areas beneath the resonance peaks in the spectra shown in Figures 67-70, and the heights of the dotted sticks are equal to the calculated fractions of carbon nuclei producing the resonance peaks. The letters above the sticks, which identify the carbon nuclei producing the resonances (see Figure 66), were assigned using the results of liquid NMR studies.[13,35] The agree-

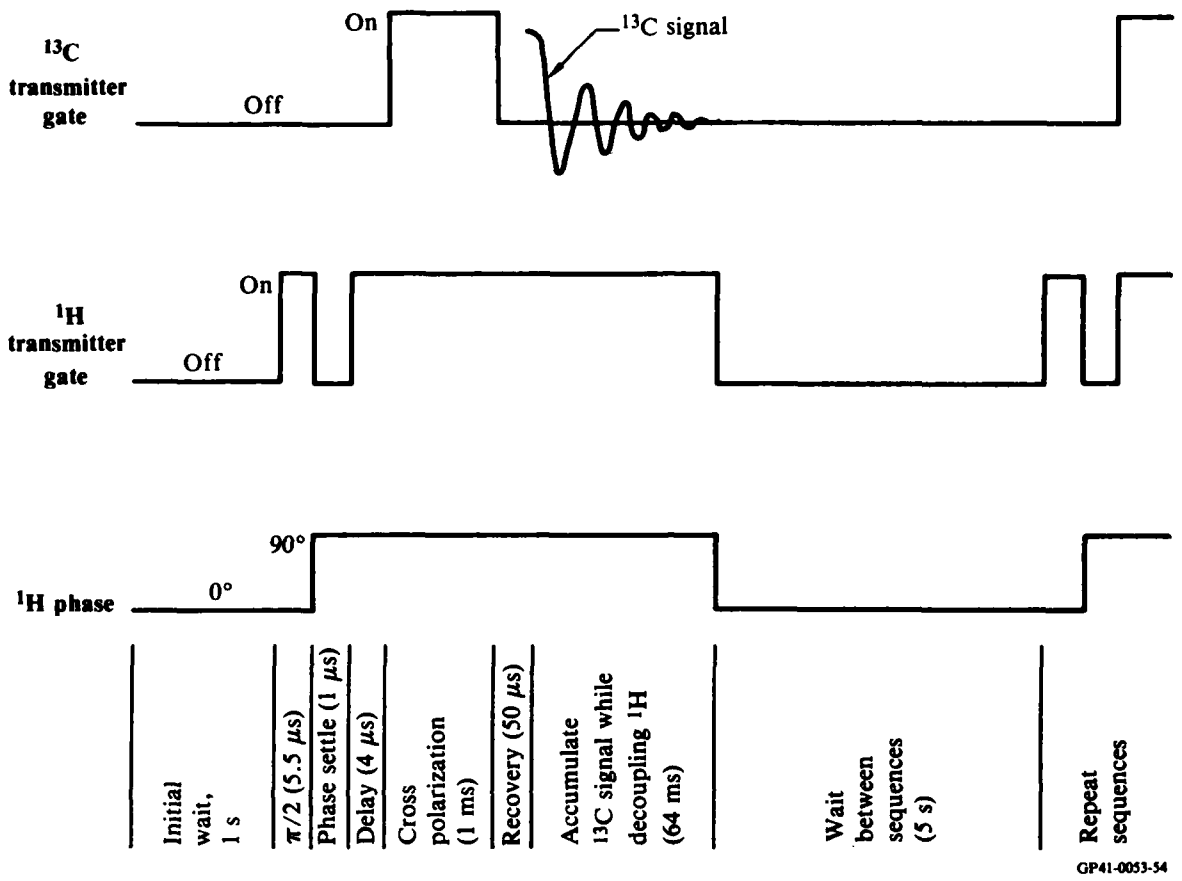

Figure 65. Pulse sequence for cross-polarization and high-power decoupling.

ment between the measured and calculated areas is not perfect because a variety of relaxation processes act to increase and decrease the polarization of nonequivalent carbon nuclei differently. The 1 ms cross-polarization time is a compromise which produces optimum, but not perfect, results.

The spectral lines labeled i in Figure 71 are produced by the aromatic carbon adjacent to the oxygen in DGEBA which is not present in TGDDM. As a result, these lines are particularly sensitive to the composition of the resin. Using only the area beneath the i resonance, it is possible to correctly identify the composition of the four different cure epoxies.

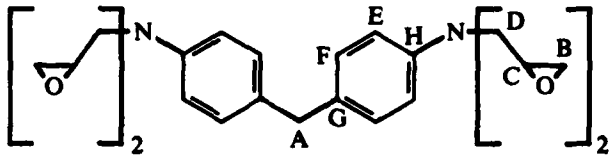

TGDDM

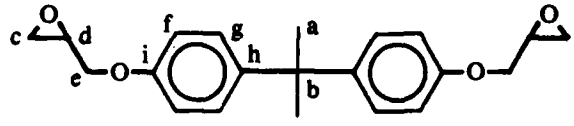

DGEBA

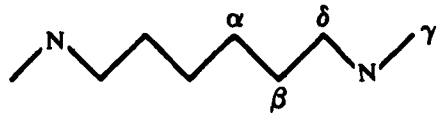

DDH

GP41-0053-60

Figure 66. Epoxies and amines used in this study with carbon atoms labeled to aid in discussion of ^{13}C NMR spectra.

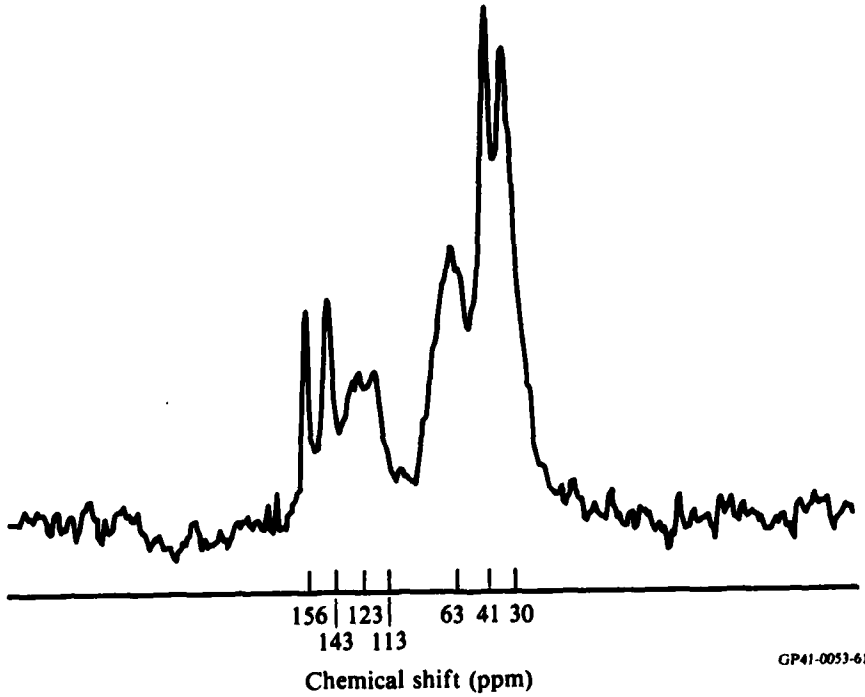

Figure 67. ^{13}C NMR spectrum of 0:5:5 sample.

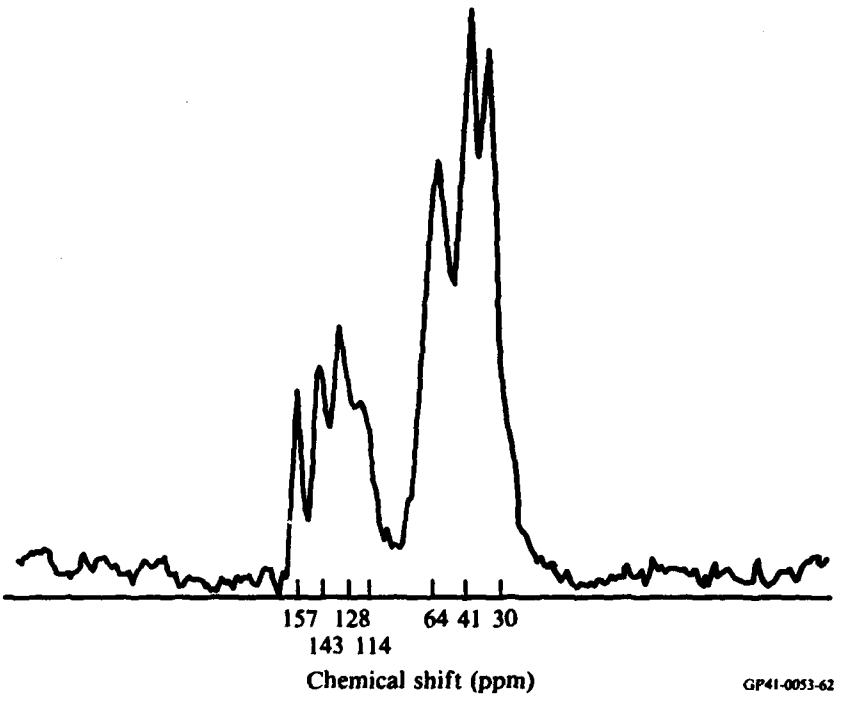

Figure 68. ^{13}C NMR spectrum of 2:3:5 sample.

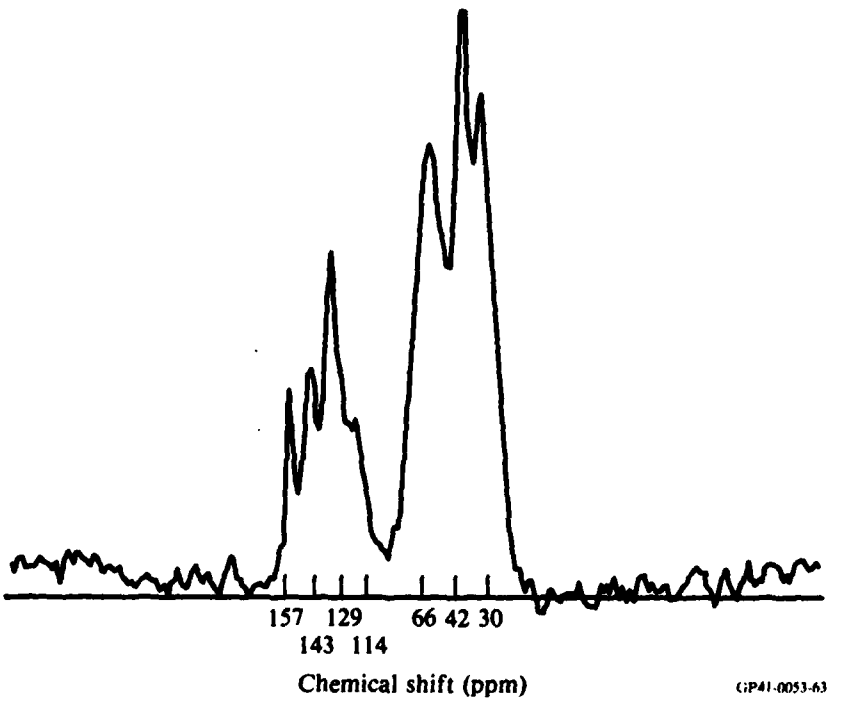

Figure 69. ^{13}C NMR spectrum of 3:2:5 sample.

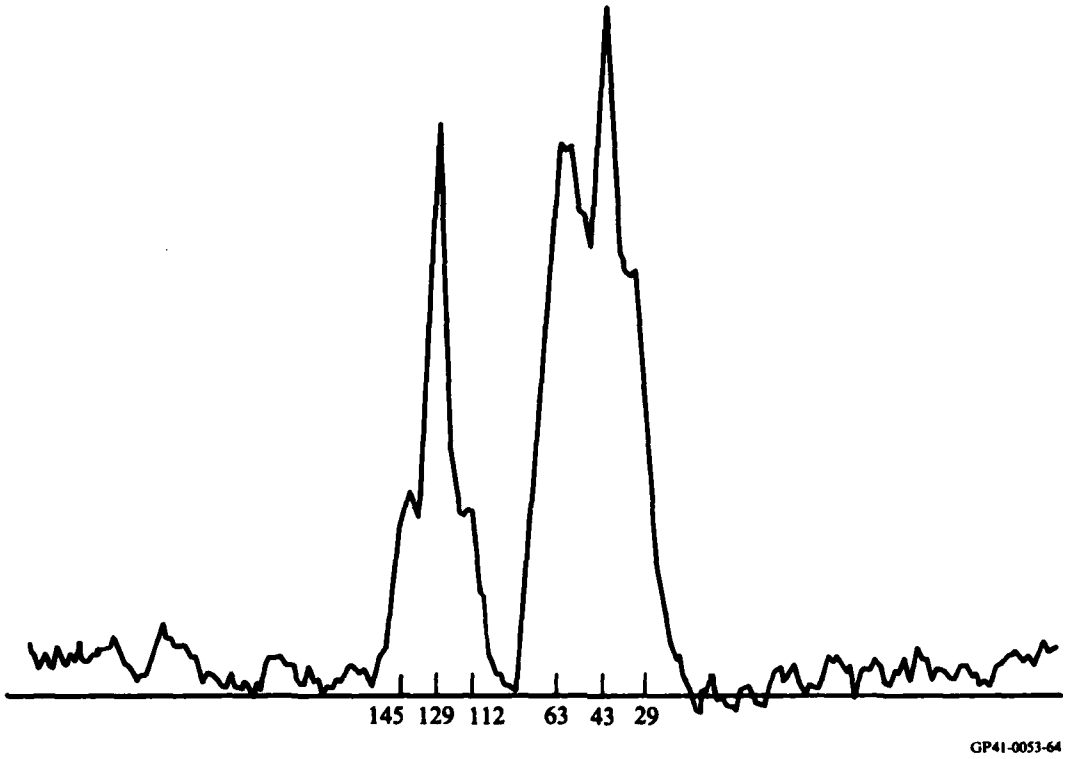

Figure 70. ^{13}C NMR spectrum of 5:0:5 sample.

The broad resonance at ~ 64 ppm, shown in Figures 67-70, results from carbon nuclei associated with the opened epoxy ring, which before opening is at ~ 50 ppm. The area beneath this peak could be used to monitor the epoxy curing reaction, although, as mentioned earlier, the relative area beneath this peak will be a function of the relaxation processes which also change during curing. Also, during the time required to produce a spectrum with an acceptable signal-to-noise ratio, additional curing will take place unless the probe temperature is low enough to effectively halt the curing process. Because our magic-angle spinning probe presently operates only at room temperature, these experiments have not yet been performed.

3.3 Investigation of Two-Dimensional Solid-State ^{13}C NMR for Characterizing Epoxies

The ^{13}C NMR spectra presented in Section 3.2 (Figures 67-70) of cured epoxy resins illustrates the relatively poor resolution that is obtained from solids, relative to the resolution obtained from liquids. For this reason,

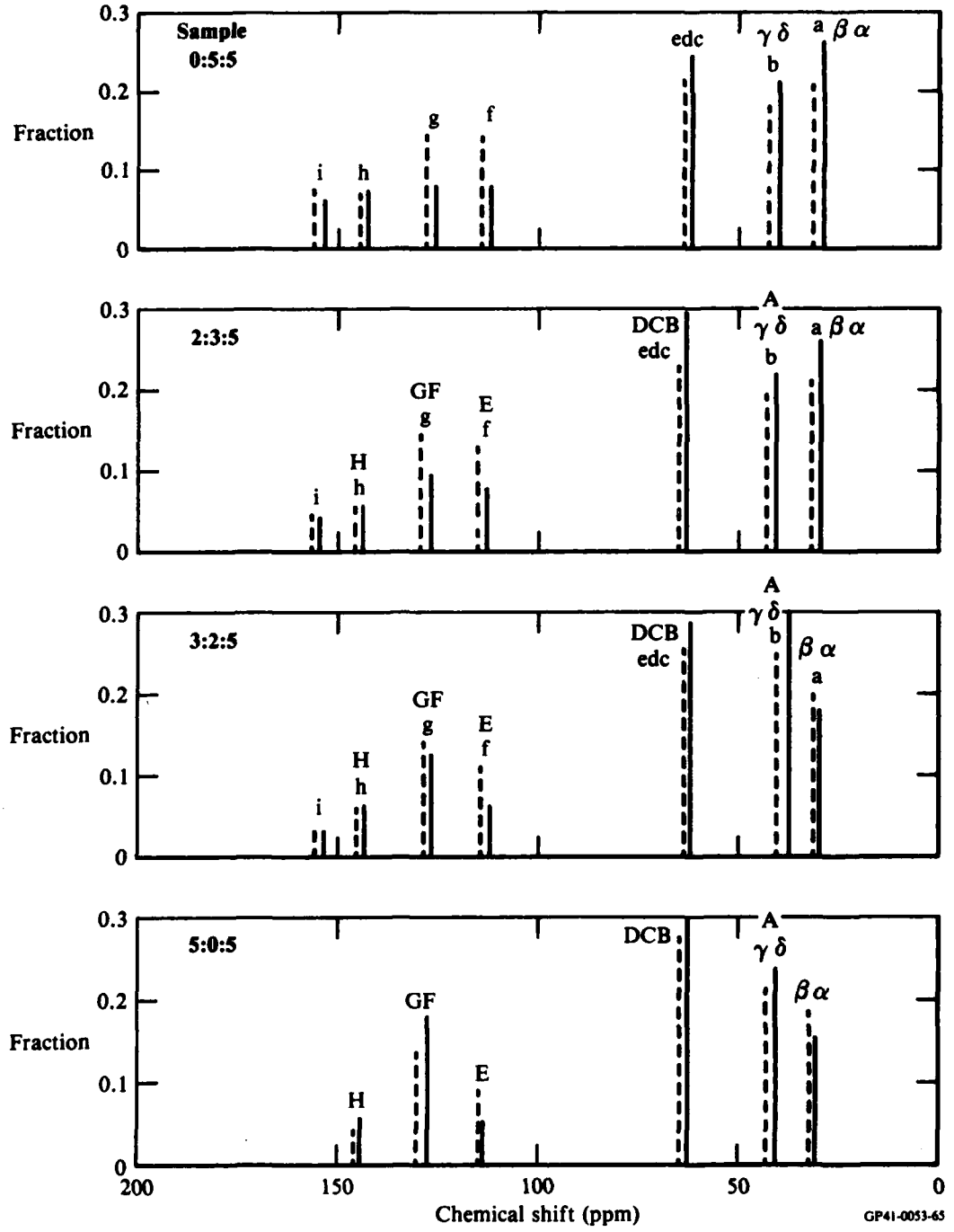

Figure 71. Stick spectra of the four epoxy samples. The height of a solid stick is equal to the measured fraction of the total area beneath the resonance peak, and the height of the dotted stick is equal to the fraction of the total number of carbon nuclei producing the resonance peak. The letters above the sticks identify the carbon nuclei producing the resonances.

two-dimensional NMR techniques were investigated for improving resolution and revealing chemical exchange phenomena. The 2-D technique that was investigated measured the chemical shift spectrum at one time and then again after a time interval of from 10 ms to 100 s. The time interval is called the mixing period. The spectrum after mixing is plotted against the spectrum before mixing, as in the example illustrated in Figure 72 for (a) a case in which exchange does not occur, and (b) a case in which exchange does occur.

In the example shown in Figure 72, it is supposed that the three resonances result from a single carbon atom at a particular location in a molecule having three conformations. The first resonance results from the molecule in the first conformation, the second resonance from the molecule in the second conformation, and the third resonance from the molecule in the third conformation. The nearly equal areas beneath the three resonances in case (a) indicate the three conformations are nearly equally populated, and the absence of off-diagonal resonances indicates that no conformational changes took place during the mixing period. In case (b) conformational changes took place during the mixing period, as evidenced by the off-diagonal resonances. In this example, the molecule experienced exchange between the first and second conformations during the mixing period, as evidenced by the resonance at frequency f_2 before mixing and at f_1 after mixing, and the resonance at frequecy f_1 before mixing and at f_2 after mixing. The lack of

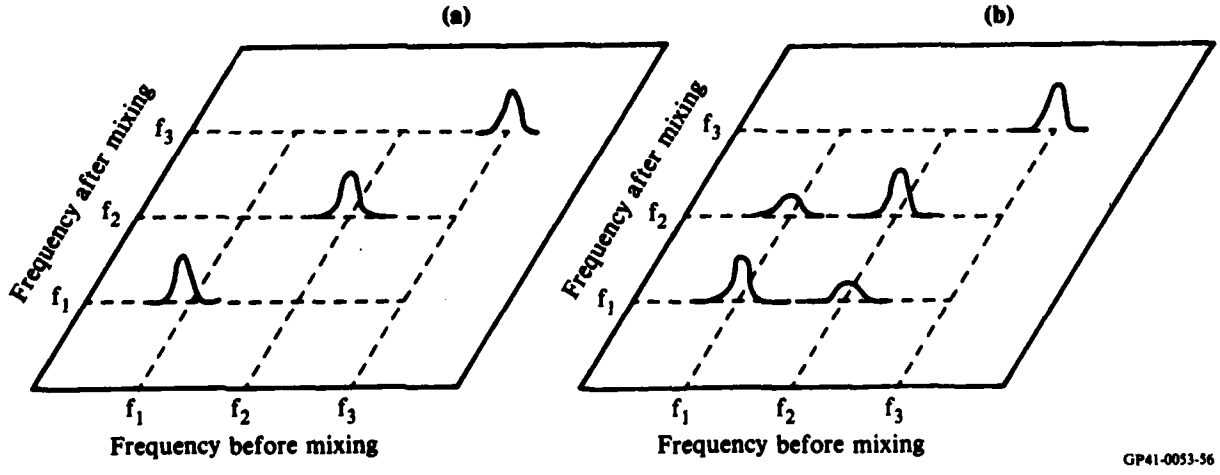

Figure 72. Sketch showing two-dimensional spectra when (a) no exchange occurs during the mixing period and (b) an exchange takes place between conformation during the mixing period.

cross-resonances between f_3 and either f_1 or f_2 indicates that molecules in the third conformation did not experience a conformational change during the mixing period. The areas beneath the off-diagonal resonances are a measure of the number of conformational changes that took place during the mixing period.

The pulse sequence[36] and parameters used to generate two-dimensional spectra are shown in Figure 73. The first part of the pulse sequence is identical to that shown in Figure 65 and is used to transfer polarization to the ^{13}C nuclei from the ^{1}H nuclei. The evolution time period t_1 allows the nonequivalent ^{13}C nuclei to process at their own resonance frequencies. A complete two-dimensional experiment consists of a 128 or more subexperiments in which t_1 is increased by Δt_1 between experiments. For each different t_1 a different phase relationship exists between the nonequivalent nuclei at the end of the evolution period. Therefore, the $\pi/2$ pulse acts differently on each of the nonequivalent nuclei and in a perfectly predictable manner depending upon t_1 and the resonant frequency of the nuclei, the nonequivalent nuclei after the $\pi/2$ pulse have different amounts of z-magnetization.

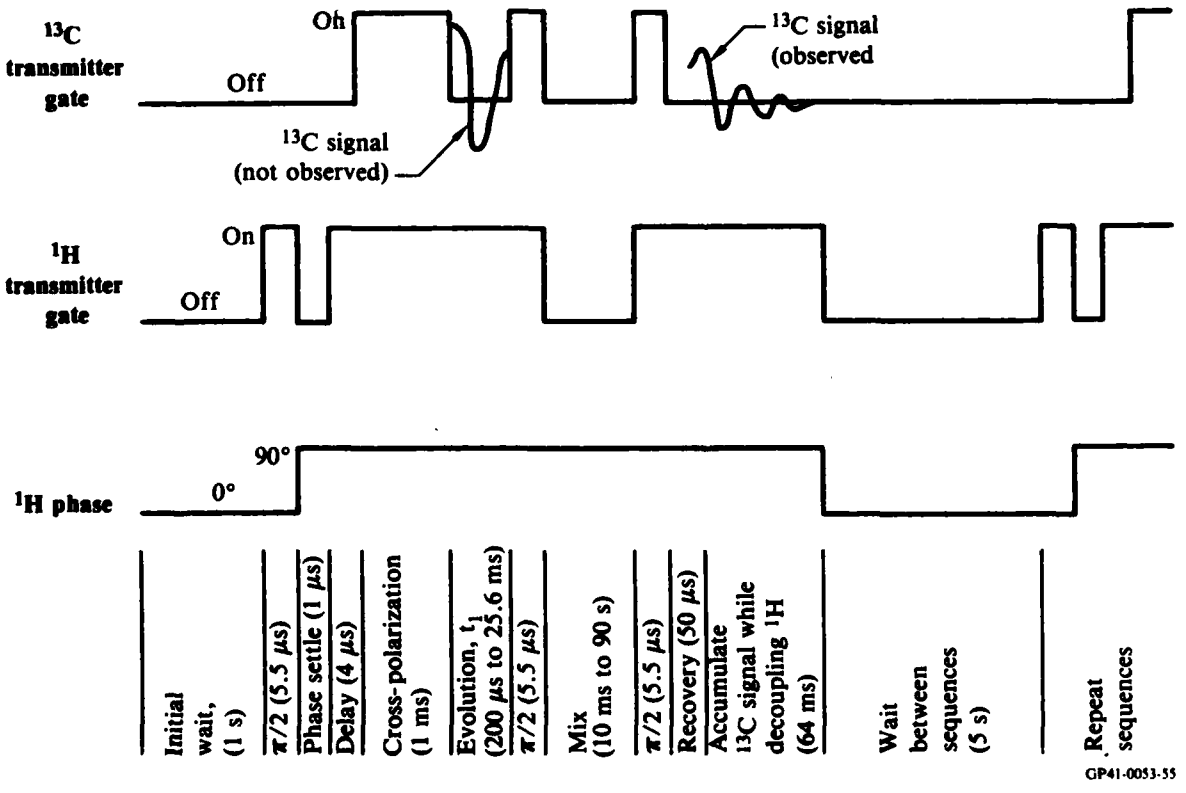

Figure 73. Pulse sequence for two-dimensional Fourier transformation of solids.

During the mixing period, the z-magnetization is exchanged between the ^{13}C nuclei. In general this exchange can occur in a number of ways. While it is highly unlikely, an exchange could occur if nonequivalent carbons exchanged places. A more likely occurrence would be a conformational change which produced a chemical shift change in one or more carbons. Also, the nuclei can undergo magnetic dipolar interactions in which nuclear polarization is exchanged between two ^{13}C nuclei while the nuclei remain in place. The effect of such exchanges between nonequivalent ^{13}C nuclei is that a ^{13}C nucleus having a particular chemical shift will contribute to the total z-magnetization at the end of the evolution period by an amount governed by its chemical shift (resonance frequency) and the time t_1; then after the $\pi/2$ pulse following the mixing period have this exchanged z-magnetization contribute to the NMR signal of a ^{13}C nucleus having a different chemical shift.

The two-dimensional Fourier transform consists of performing a conventional one-dimensional Fourier transform on each NMR signal following the second $\pi/2$ pulse. Typically there are 128 or more of these one-dimensional spectra, one for each value of t_1 used; they represent the amplitudes and resonance frequencies of the nuclei after a fixed mixing period and variable evolution period. The second Fourier transform of these spectra generates a two-dimensional array representing the amplitudes and chemical shifts (frequencies) of the nuclei before mixing along one direction, and the amplitude and chemical shift of the nuclei after mixing along the other direction. If no exchange occurs, the two-dimensional spectra appear as resonances along a diagonal as sketched in Figure 72a; and if exchange occurs, off-diagonal resonances appear as in Figure 72b.

The curing agent Eporal was used to develop our two-dimensional ^{13}C NMR techniques. Figure 74 shows the solid-state, one-dimensional spectrum of Eporal obtained with conventional cross-polarization, high-power decoupling, and magic-angle spinning. Below the spectrum are shown the chemical shifts of the nonequivalent carbons which were obtained from liquid ^{13}C NMR spectra of a 50% solution of Eporal in acetone-d.[35] In the solid-state spectrum, the carbon atoms labeled b and c appear unresolved as a single peak, carbon a is resolved, and carbon d is resolved but is of small amplitude, whereas in the liquid spectrum all four nonequivalent carbons are easily resolved. This lack of resolution illustrates the need for techniques to extract more information

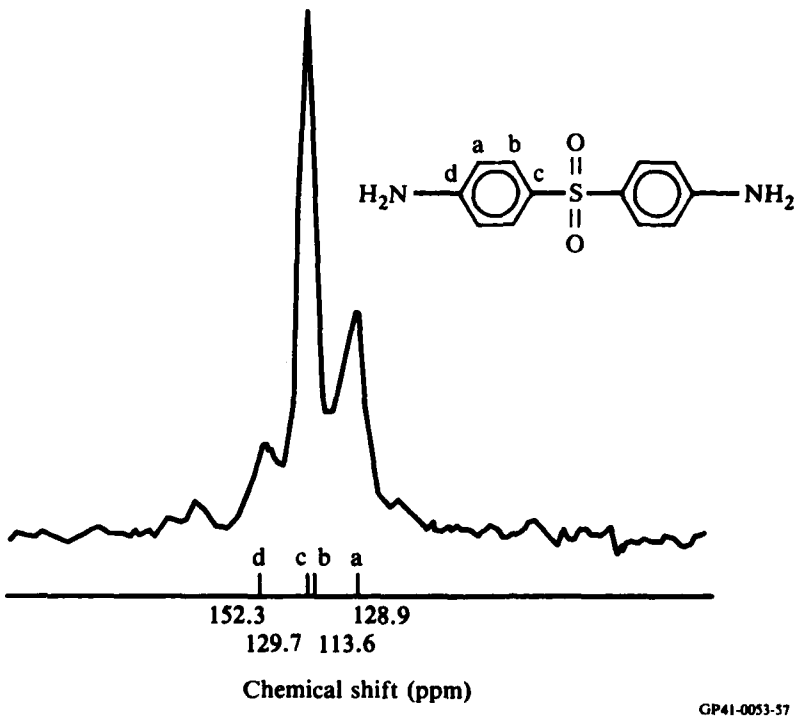

Figure 74. Magic angle, cross-polarization, high-power decoupling ^{13}C NMR spectrum of solid Eporal.

from solid-state ^{13}C NMR spectra; two-dimensional NMR is expected to be such a technique.

Figure 75 shows a two-dimensional ^{13}C NMR spectrum of Eporal. The parameters used to generate this spectrum have not yet been optimized. The optimization procedure is time consuming: to construct a two-dimensional spectrum of the type shown in Figure 75 requires 89 h for data accumulation and 4 h for plotting one view.

In Figure 75 one sees the existence of a set of mirror-image resonance peaks caused by the transform technique used. The mirror-image peaks allow observation of the back side of the resonance peaks. While the exchange peaks are not particularly clear in Figure 75, they can be seen; and it is expected that further optimization of the pulse parameters will lead to substantial improvements in the two-dimensional spectra.

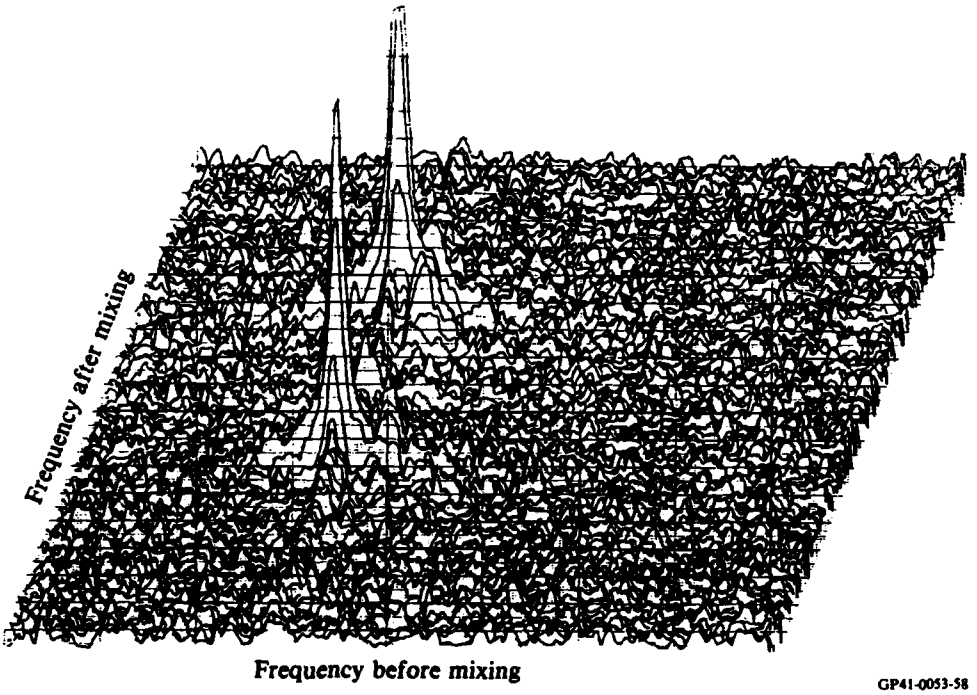

Figure 75. Two-dimensional Fourier transform spectrum of Eporal. Image resonances appear at the rear permitting the back side of the resonance peaks to be seen. Mixing time was 1 s.

4. SUMMARY OF CONCLUSIONS

4.1 EPR Conclusions

- The reaction rate for the initial step in the reactions of a secondary amine (METAMIN) and a tertiary amine (DIMETAMIN) obey pseudo-first-order kinetics at low nitroxide concentrations.

- The temperature dependence of the rate of the reaction for METAMIN in TGDDM is given by $k_1 = k_{01} \exp(-\Delta E/RT)$ where $\Delta E = 55$ kJ mol^{-1} and $k_{01} = 1.3 \times 10^4$ s^{-1}.

- For the rate of reaction of DIMETAMIN in TGDDM, the temperature dependence is given by $\Delta E = 55$ kJ mol^{-1}, $k_{02} = 4 \times 10^3$ s^{-1} at 333 K; and $\Delta E = 18.5$ kJ mol^{-1}, $k_{02} = 1.7 \times 10^{-2}$ s^{-1} at 373 K.

- The ratio of the frequency factors for METAMIN and DIMETAMIN in TGDDM at 333 K can be interpreted in terms of an entropy difference resulting from the steric hindrance around the quaternary nitrogen.

- The logarithm of the rotational correlation time for TEMPENE in the amine-cured epoxies is linearly dependent on the crosslink density.

- The rotational correlation time for TEMPENE in the amine-cured epoxies above T_g obeys the WLF equation.

- The decomposition rate for nitroxides in the TGDDM indicates there is more than one remnant impurity in the resin.

- The expression for the temperature dependence of the rotational correlation time for TEMPENE in amine-cured epoxy hosts contains a contribution from the free volume content (Doolittle term) and one from the explicit temperature dependence (Arrhenius term).

- Amine nitroxide diffused into plasticized amine-cured epoxy samples covalently bind to unreacted epoxy groups trapped in the polymer network.

- Glycidyl nitroxides diffused into plasticized amine-cured epoxy samples covalently bind to unreacted amine groups trapped in the polymer network.

- 0.95 wt% unreacted epoxy groups were detected in the presence of 3.0 wt% unreacted amine groups in the same sample of amine-cured TGDDM.

4.2 NMR Conclusions

- The activation energy for curing MY720 with Eporal was measured with ^{1}H NMR and was found to be 49.8 ± 3.7 kJ/mol.

- The activation energy for curing appeared to increase slightly (from 45 to 55 kJ/mol) as curing proceeded.

- The spin-lattice relaxation time experienced a minimum early in the curing process that appeared to be caused by molecular motion of the products of curing rather than by the motion of the reactants.

- Early in the cure two components were observed, one more mobile than the other, implying that an inhomogeneous structure develops early in the cure.

- The character of the time dependence of the mobile fraction during curing differed for different isothermal cure temperatures, suggesting that the nature of the crosslink structure formed during curing is a function of cure temperature.

- The mobile fraction is a sensitve parameter for monitoring the last stages of epoxy curing.

- ^{13}C NMR was used to measure the composition of cured epoxy resins.

- Preliminary two-dimensional ^{13}C NMR spectra of the curing agent Eporal were obtained.

REFERENCES

1. R. E. Cuthrell, Macrostructure and Environment Influenced Surface Layer in Epoxy Polymers, J. Appl. Polymer Sci. 11, 949 (1967).
2. J. L. Racich and J. A. Koutsky, Nodular Structure in Epoxy Resins, J. Appl. Polymer Sci. 20, 2111 (1976).
3. J. S. Mijovic and J. A. Koutsky, The Effect of Postcure Time on the Fracture Properties and Nodular Morphology of an Epoxy Resin, J. Appl. Polymer Sci. 23, 1037 (1979).
4. J. Mijovic and J. A. Koutsky, Correlation Between Nodular Morphology and Fracture Properties of Cured Epoxy Resins, Polymer 20, 1095 (1979).
5. R. J. Maty, D. R. Uhlmann, and J. A. Koutsky, Structure of Glassy Polymers: Small Angle X-Ray Scattering from Epoxy Resins, J. Polymer Sci. 18, 1053 (1980).
6. R. J. Morgan and J. E. O'Neal, The Microscopic Failure Processes and Their Relation to Structure of Amine-Cured Bisphenol A Diglycidyl Ether Epoxies, J. Mater. Sci. 12, 1966 (1977).
7. A. S. Kenyon and L. E. Nielsen, Characterization of Network Structure of Epoxy Resins by Dynamic Mechanical and Liquid Swelling Tests, J. Macromol. Sci. A3, 275 (1976).
8. L. J. Berliner, Ed., Spin Labeling: Theory and Applications, Volumes I and II (Academic Press, New York, 1976).
9. I. M. Brown, A. C. Lind, and T. C. Sandreczki, Magnetic Resonance Studies of Epoxy Resins, Technical Report MDC Q0721, 7 December 1980; Final Report, Naval Air Systems Command Contract N00019-79-C-0414.
10. I. M. Brown, A. C. Lind, and T. C. Sandreczki, Magnetic Resonance Studies of Epoxy Resins and Polyurethanes, Technical Report MDC Q0673, 3 May 1979; Final Report, Naval Air Systems Command Contract N00019-78-C-0031.
11. I. M. Brown and T. C. Sandreczki, Nitroxide Spin Label Studies in an Epoxy Resin, Chem. Phys. Letters 64, 85 (1979).
12. I. M. Brown and T. C. Sandreczki, Nitroxide Spin Labeling of Epoxy Resins, Macromolecules 16, 1890 (1983).
13. I. M. Brown, A. C. Lind, and T. C. Sandreczki, Magnetic Resonance Determinations of Structure and Reaction Kinetics of Epoxy/Amine Systems, Technical Report MDC 0759, 31 December 1981; Final Report, Naval Air Systems Command Contract N00019-80-C-0552.

14. I. M. Brown, Nitroxide Spin Probe Studies in a Block Copolymer, Macromolecules 14, 801 (1980).
15. L. Hagnauer, Army Material and Machanics Center, Boston, MA (private communication).
16. D. Katz, and A. V. Tobolsky, Rubber Elasticity in a Highly Crosslinked Epoxy System, Polymer 4, 417 (1963).
17. L. E. Nielsen, Mechanical Properties of Polymers and Composites, Vol. I (Marcel Dekker, New York, 1974).
18. D. Kivelson, Theory of ESR Linewidths of Free Radicals, J. Chem. Phys. 33, 1094 (1960).
19. A. L. Buchachenko, A. L. Kovarskii, and A. M. Vasserman, in Advances in Polymer Science, Z. A. Rogovin, ed., (Halsted Press, New York, 1974), p. 26.
20. J. D. Ferry, Viscoelastic Properties of Polymers, (John Wiley, New York, 1980).
21. A. L. Kovarskii, A. M. Wasserman, and A. L. Buchachenko, in Molecular Motion in Polymers by ESR, B. F. Boyer and S. E. Keinath, eds. (Harwood Academic Publishers, New York, 1980), p. 177.
22. P. J. Flory and J. Rehner, Statistical Mechanics of Crosslinked Polymer Networks, II Swelling, J. Chem. Phys. 11, 521 (1943).
23. I. T. Smith, The Mechanism of the Crosslinking of Epoxide Resins by Amines, Polymer 2, 95 (1961).
24. N. S. Isaacs and R. E. Parker, Mechanisms of Epoxide Reactions, Chem. Rev. 59, 737 (1959).
25. Y. Tanaka and T. F. Mika, Epoxide-Curing Reactions, in Epoxy Resins, C. May and Y. Tanaka, eds. (Marcel Dekker, New York, 1973), p. 76.
26. J. J. King and J. P. Bell, Reactions in a Typical Epoxy-Aliphatic Diamine System, Epoxy Resin Chemistry, R. S. Bauer, eds. (American Chemical Society Symposium Series Number 114, Washington, DC, 1979), p. 225.
27. S. Meiboom and D. Gill, Modified Spin-Echo Method for Measuring Nuclear Relaxation Times, Rev. Sci. Instrum. 29, 688 (1958).
28. H. Y. Carr and E. M. Purcell, Effects of Diffusion on Free Precession in Nuclear Magnetic Resonance Experiments, Phys. Rev. 94, 630 (1954).

29. D. W. Larsen and J. H. Strange, Diglycidyl Ether of Bisphenol A with 4,4′-Methylenediamine: A Pulsed NMR Study of the Curing Process, J. Polym. Sci. Phys. Ed. 11, 1453 (1973).

30. J. B. Enns and J. B. Gillham, Molecular Structure/Macroscopic Property Relationships of Epoxy/Amine Systems using Time-Temperature-Transition (TTT) Cure Diagrams, Org. Coat. Appl. Polym. Sci. Proc. 46, 592 (1982).

31. W. X. Zukas, W. J. MacKnight, and N. S. Schneider, Dynamic Mechnical and Dielectric Properties of an Epoxy Resin During Cure, ACS Symposium Series 227, 223 (1983).

32. A. Pines, M. G. Gibby, and J. S. Waugh, Proton Enhanced NMR of Dilute Spins in Solids, J. Chem. Phys. 59, 569 (1973).

33. J. Schaefer, E. O. Stejskal, and R. Buchdahl, ^{13}C Magic-Angle Spinning in Polymers, Macromolecules 12, 384 (1979).

34. S. R. Hartmann and E. L. Hahn, Nuclear Double Resonance in the Rotating Frame, Phys. Rev. 128, 2042 (1962).

35. C. F. Poranski, Jr., W. B. Moniz, D. L. Birkle, J.T. Kopfle, and S. A. Sojka, Carbon-13 and Proton NMR Spectra for Characterizing Thermosetting Polymer System, NRL Report 8092, June 20, 1977.

36. N. M. Szeverenyi, M. J. Sullivan, and G. E. Maciel, Observation of Spin Exchange by Two-Dimensional Fourier Transform ^{13}C Cross Polarization-Magic-Angle Spinning, J. Magn. Reson. 47, 462 (1982).

CONTRACT N00019-82-C-0244
DISTRIBUTION LIST

Commander
Naval Air Systems Command
ATTN: AIR-5304C2
AIR-7226 (8 copies)
AIR-310A
Washington, DC 20361

Commander
Naval Air Development Center
ATTN: Code 606
Warminster, PA 18974

Director
Naval Research Laboratory
ATTN: Codes 6383, 6654, 6120
Washington, DC 20375

Commander
Naval Sea Systems Command
ATTN: Codes 051, 05D23
Washington, DC 20360

Director
Naval Ship R&D Center
ATTN: Mr. M. Krenzke & Mr. A. Macander
Washington, DC 20034

Director
Naval Surface Weapons Center
ATTN: Dr. J. Augl (R-31)
White Oak
Silver Spring, MD 20350

Air Force Wright Aeronautical Laboratories
Materials Laboratory
ATTN: AFWAL
Wright-Patterson Air Force Base, OH 45433

Army Materials & Mechanics Research Center
Department of the Army
ATTN: Library
Watertown, MA 02171

NASA Headquarters
ATTN: Mr. C. F. Bersch
600 Independence Ave., S.W.
Washington, DC 20406

NASA
Langley Research Center
ATTN: Library
Hampton, VA 23665

NASA
Lewis Research Center
ATTN: Library
Cleveland, OH 44185

Defense Technical Information Center
Cameron Station, Bldg. #5
Alexandria, VA 22314

Director
Plastics Technical Evaluation Center
Picatinny Arsenal
Dover, NJ 07801

U.S. Applied Technology Laboratory
AVRADCOM
ATTN: DAVDL-ATL-ATS
Fort Eustis, VA 23604

Brunswick Corporation
Technical Products Division
325 Brunswick Lane
Marion, VA 24354

Celanese Research Company
Box 1000
ATTN: Mr. R. J. Leal
Summit, NJ 07901

E. I. DuPont de Nemours & Company
Textile Fibers Department
Wilmington, DE 19898

Fiber Materials, Inc.
ATTN: Mr. J. Herrick
Biddeford Industrial Park
Biddeford, ME 04005

General Dynamics
Convair Aerospace Division
ATTN: Technical Library
P. O. Box 748
Fort Worth, TX 76101

General Dynamics
Convair Division
ATTN: Mr. W. Scheck
Dept. 572-10
P. O. Box 1128
San Diego, CA 92138

General Electric
R&D Center
ATTN: Mr. W. Hillig
Box 8
Schnectady, NY 12301

General Electric Company
Valley Forge Space Center
Philadelphia, PA 19101

B. F. Goodrich Aerospace & Defense
Products
500 South Main St.
Akron, OH 44318

Graftex Division
EXXON Industries
2917 Highwoods Blvd.
Raleigh, NC 27604

Great Lakes Research Corporation
P. O. Box 1031
Elizabethton, TN 37643

Grumman Aerospace Corporation
ATTN: Mr. L. Poveromo
Bethpage, LI, NY 11714

Hercules Incorporated
ATTN: Mr. E. G. Crossland
Magua, UT 84044

HITCO
1600 W. 135th St.
Gardena, VA 90446

Illinois Institute of Technology
Research Center
10 West 35th St.
Chicago, IL 60616

Lear Fan Corporation
P. O. Box 60,000
Reno, NV 89506

Lockheed California Company
ATTN: Mr. J. H. Wooley
Box 551
Burbank, CA 91520

Lockheed-Georgia Company
ATTN: M. L. E. Meade
Marietta, GA 30063

Lockheed Missiles & Space Company
ATTN: Mr. H. H. Armstrong
Dept. 62-60
Sunnyvale, CA 94088

Material Sciences Corporation
1777 Walton Road
Blue Bell, PA 19422

McDonnell Douglas Corporation
McDonnell Aircraft Company
ATTN: Mr. R. J. Juergens
P. O. Box 516
St. Louis, MO 63166

McDonnell Douglas Corporation
Douglas Aircraft Company
ATTN: Mr. R. J. Palmer
3855 Lakewood Blvd.
Long Beach, CA 90801

North American Aviation
Columbus Division
4300 E. Fifth Ave.
Columbus, OH 43216

Northrop Corporation
3901 W. Broadway
ATTN: Mr. G. Grimes
Mail Code 3852-82
Hawthorne, CA 90250

Philco-Ford Corporation
Aeronutronic Division
Ford Road
Newport Beach, CA 92663

Rockwell International Corporation
ATTN: Mr. C. R. Rousseau
12214 Lakewood Blvd.
Downey, CA 90241

TBW, Inc.
Systems Group
One Space Park
Bldg. 01, Rm 2171
Redondo Beach, CA 90278

TRW, Inc.
23555 Euclid Ave.
Cleveland, OH 44117

Union Carbide Corporation
Chemicals & Plastics
One River Road
Bound Brook, NJ 08805

Union Carbide Corporation
Carbon Products Division
P. O. Box 6116
Cleveland, OH 44101

United Aircraft Corporation
United Aircraft Research Laboratories
E. Hartford, CT 06108

United Aircraft Corporation
Hamilton-Standard Division
ATTN: Mr. T. Zajac
Windsor Locks, CT 06096

United Aircraft Corporation
Sikorsky Aircraft Division
ATTN: Mr. J. Ray
Stratford, CT 06602

University of California
Lawrence Livermore Laboratory
ATTN: Mr. T. T. Chiao
P. O. Box 808
Livermore, CA 94550

University of Maryland
ATTN: Dr. W. J. Bailey
College Park, MD 20742

University of Wyoming
Mechanical Engineering Department
ATTN: Dr. D. F. Adams
Laramie, WY 82071

Westinghouse R&D Center
ATTN: Mr. Z. Sanjana
1310 Beulah Road
Churchill Boro
Pittsburgh, PA 15235

END

FILMED

3-85

DTIC